ANL-6569
Chemical Separations
Processes for Plutonium
and Uranium
(TID-4500, 17th Ed.)
AEC Research and
Development Report

ARGONNE NATIONAL LABORATORY
9700 South Cass Avenue
Argonne, Illinois

CHEMICAL ENGINEERING DIVISION SUMMARY REPORT

April, May, June, 1962

Stephen Lawroski, Division Director
R. C. Vogel, Associate Division Director
V. H. Munnecke, Assistant Division Director

August 1962

Preceding Quarterly Reports:

ANL-6543	January, February, March, 1962
ANL-6477	October, November, December, 1961
ANL-6413	July, August, September, 1961

Operated by The University of Chicago
under
Contract W-31-109-eng-38

DISCLAIMER

SUMMARY

CHEMICAL ENGINEERING DIVISION SUMMARY REPORT

I. Chemical-Metallurgical Processing (pages 25 to 92).

Two small-scale (7-g) experiments with highly irradiated uranium-5 weight percent fissium alloy were performed to investigate the behavior of condensable fission products volatilized during melt refining. In the first experiment, the fission products that were volatilized during melting for one hour at 1400 C were condensed on a nickel surface. In the second experiment, they were collected on a Fiberfrax bed which simulated the fume trap in the plant equipment. The only significant fission product activities collected were iodine and cesium. Over 90 percent of the iodine and 70 percent of the cesium recovered were in a zone between 450 and 700 C on the nickel collector. Over 99 percent of the iodine and cesium recovered in the second experiment were in the Fiberfrax, which had a temperature gradient from 1000 to 450 C. The amounts of barium, strontium, cerium, tellurium, zirconium, and ruthenium in the condensed volatiles were negligible.

Further experiments on the nitridation rates of irradiated uranium-fissium fuel pins in nitrogen-argon atmospheres have shown that prior exposure to air decreases the reactivity of the alloy toward nitrogen. Pins irradiated to 1.18 total atom percent burnup became completely unreactive to nitrogen at 650 C after 8 to 10 days of exposure to air at 30 C. The nitridation rate of a sodium-coated, irradiated uranium-fissium pin at 500 C in 100 percent nitrogen was identical with the rate observed earlier with an unirradiated pin under the same conditions.

The skull reclamation process is under development for recovery of skull material which remains in a crucible after melt refining. The process presently involves removal of a melt refining skull from a crucible by oxidation of the skull to convert it to a powder, selective extraction of noble metals into zinc from the skull oxides suspended in a molten chloride salt, reduction of uranium oxides by magnesium in a zinc solution, two uranium precipitations to enable removal of various fission products in supernatant solutions, and a retorting step to isolate a uranium metal product. The first demonstration run of the skull reclamation process has been completed in a recently completed inert atmosphere glove box, using a charge of 190 g of oxidized skull. An encouraging overall uranium recovery of about 90 percent was realized, with much of the remaining 10 percent residing in recoverable heels. The major components have been ordered for processing $2\frac{1}{2}$-kg-uranium batches of skull oxide in integrated equipment.

A beryllia crucible assembly (pressed-and-sintered beryllia crucible in a stainless steel secondary with annular space packed with beryllia powder) has shown no significant deterioration through four runs conducted to

date, each duplicating the sequence of precipitation steps in the skull reclamation process. The uranium product in two runs was carried through the retorting step and was recovered with essentially 100 percent yields.

A study was made of the fates of stainless steel constituents in the skull reclamation process and of possible modifications required to handle stainless steel-clad fuel pins in this process. Iron and nickel were readily separated from the uranium in the noble metal-extraction step. However, a substantial extraction of chromium along with uranium into the flux phase occurred during this extraction. To make this process usable, provision must be made for the separation of chromium from uranium.

Further data have been obtained on the distribution coefficients of uranium, plutonium, and rare earths between molten magnesium chloride and zinc-magnesium solution at 800 C. Distribution coefficients are now available for uranium, plutonium, yttrium, cerium, praseodymium, neodymium, and americium as a function of magnesium concentration in the metal phase. At 10 weight percent magnesium, distribution coefficients [w/o in flux/w/o in metal] are as follows: yttrium (1.9), cerium (0.91), neodymium (0.74), praseodymium (0.65), americium (0.31), plutonium (0.015), and uranium (0.0049).

Work was continued on the EBR-II blanket process in which plutonium and uranium are separated by utilizing the high solubility of plutonium in magnesium-rich solutions and the contrasting low solubility of uranium in such solutions. In the blanket process, blanket material is first dissolved in a zinc-rich alloy and then magnesium is added to effect precipitation of the uranium away from the plutonium. Direct dissolution of stainless steel-clad blanket elements would be allowable if the stainless steel elements did not affect plutonium recovery and if they could be separated from the plutonium. Results of a demonstration run indicated that stainless steel and fission elements, which were added in the appropriate amounts, would have no effect on plutonium behavior. A plutonium recovery of 96 percent was obtained by separation of the supernatant phase, and a total recovery of 99 percent was obtained with the use of a single magnesium wash. However, in another run in which plutonium was not present, it was determined that chromium and iron would be precipitated with the uranium and thus be separated from the plutonium, but that nickel would quantitatively follow the plutonium unless the process were modified.

An important step in the blanket process is the separation of the plutonium-bearing zinc-50 weight percent magnesium solution from the uranium which has been precipitated by magnesium addition and cooling to 400 C. In nine such phase separations with 500-g batches of uranium ($\frac{1}{20}$th of full scale), phase separations of 95 to 97 percent were obtained in conical-bottom crucibles with little entrainment of solid uranium. A phase separation of 95 percent would eliminate the necessity of a wash of the uranium precipitate.

Tungsten is one of the most promising materials for containment of flux and metal systems of the skull reclamation process. Tests continue to show good stability of uranium-zinc-magnesium solutions in tungsten crucibles in the concentration ranges of interest for fuel processing. Studies are beginning to determine the effects of flux and zinc-magnesium solutions on pressed beryllia crucibles (about 90 percent of theoretical density). In preliminary tests it was found that molten chloride fluxes of the type used in the skull reclamation process penetrated into the crucible walls.

The addition of uranium oxides to molten lithium chloride-magnesium chloride at 650 C produces a species believed to be uranium(V) in solution. The absorption spectra of uranium(III) and uranium(IV) in molten lithium chloride-magnesium chloride at 650 C were found to have the same general characteristics as the spectra in other molten chloride media. Approximate values for the molar absorptivities were determined.

Operation of a large cadmium-distillation unit was continued to gain experience on an engineering scale in the distillation operation and associated liquid metal-handling operations. In additional runs in the large-scale cadmium-distillation unit, the power input was gradually increased to determine the capability of the unit and to uncover problems associated with high distillation rates. The apparent rate of cadmium evaporation reached 102 kg/hr, but there was evidence of extensive entrainment of liquid in the vapor. A fundamental study has been started on the mechanisms of entrainment during boiling of liquid metals.

A dynamic loop for study of mass transfer in flowing metal systems has been completed. Preliminary testing of the loop components is underway. A series of runs for study of mass transfer in agitated metal systems has also been started.

The diffusivity of uranium in zinc has been determined and was found to range from 1.5×10^{-5} sq cm/sec at 625 C to 2.7×10^{-5} sq cm/sec at 800 C, with estimated accuracies of $\pm$ 15 percent.

Three additional experiments were completed on the preparation of uranium monocarbide by addition of carbon to uranium dissolved in molten zinc-magnesium alloy. The use of sodium as a wetting agent does not appear to be as effective in enhancing the reaction rate in the experiments on a larger scale as it is in small-scale studies. Degassing the activated charcoal used as the source of carbon appears to reduce the oxygen content of the product. Reduction of the carbon-to-uranium ratio in the charge has produced a corresponding reduction in the product, although the values are still high (C/U atomic ratios of 1.16, 1.20, and 1.12).

Confirmatory studies indicate that complete reductions of thorium oxide by zinc-five weight percent magnesium solution in 3 hr at 750 C are obtained with fluxes containing at least 50 mole percent magnesium chloride,

7 to 15 mole percent calcium fluoride, and the balance calcium chloride. Reproducible results are obtained when the reductions are carried out in tantalum equipment and under an argon atomosphere.

Work on the Fuel Cycle Facility this quarter was mainly of a corrective nature. During construction, voids formed in the fill under the Air Cell Floor. These have been filled by pressure grouting. Bearings on the cranes and manipulators were cleaned to remove abrasive particles. Bearings for the hanging bridge wheels of the cranes in the Argon Cell were redesigned to improve performance. The current collector assemblies on the cell cranes were modified to eliminate binding. The control circuits of the cell cranes and the crane and manipulator removal hoist were modified to reduce excessive voltage drop.

Equipment which has been installed includes two-thirds of the oil-filled tank units of the shielding windows, a jib crane which operates through the roof hatches of the process cells, and the major components of the locks used to transfer items between the Air and the Argon Cells. These locks were found to leak and are being repaired. Fifty-seven of the required 65 service feed throughs for the Argon Cell have been delivered and are being installed.

Two 20-ton fuel-transfer coffins are being designed; the designs differ in the method of removing heat from a circulating stream of gas coolant. The design of the sampling system for stack gas has been modified, two sampling nozzles having been replaced with a single nozzle. An improved stereo-optical depth perceptor has been designed for use in remote cell operation. Four radiation-resistant wide-angle viewers have been ordered and will be installed through the cell shield.

A manipulator tool rack and changer is being built and will be shipped to Idaho for testing. A new type of clutch for the operating manipulator has been procured and is being tested.

A gas-control system for the skull oxidation process is being designed. The system will keep the rate at which the skull is oxidized constant throughout the reaction period. The system also permits the oxidation of metal scrap.

When the melt refining furnace was previously used to distill magnesium-zinc, appreciable amounts of vapor apparently permeated through the zirconia crucible and graphite susceptor of the furnace. A liner of stainless steel was installed to eliminate this escape. Because of difficulties which were encountered in removing the crucible when the modified furnace assembly was used, this approach to overcoming the loss of magnesium-zinc vapor has been abandoned.

Inductive heating and mixing is being examined for use in the skull reclamation process. The present power supply proved inadequate, and possible modifications and replacements of this power supply are being investigated.

Fundamental studies of the chemistry of liquid metal systems are being made in connection with the Division's work in the field of pyrometallurgical fuel reprocessing. Basic to these practical processes is knowledge of the solubilities of fission product, fissionable, and structural elements in metallic solvents. The solubility of uranium in liquid gallium has been measured and may be represented by the empirical equation

(343 to 649 C) Uranium: $\log(\text{atom percent}) = 6.70 - 8840T^{-1} + 1.99 \times 10^{6} T^{-2}$.

Further information has been obtained on the phase boundaries in the uranium-zinc system. At 650 C the epsilon phase field extends from 24.1 to 28.0 weight percent uranium, and a two-phase (epsilon plus delta) field extends from 28.0 to 30.0 weight percent uranium. Previous studies have shown that a two-phase (delta plus uranium) field extends from 30 to about 100 weight percent uranium.

The solubility of zirconium in a liquid 48 weight percent zinc-52 weight percent magnesium solution has been measured as a function of temperature from 709 to 422 C. The solubility of zirconium was found to vary from about 0.5 weight percent at 709 C to 0.02 weight percent at 422 C. A break in the solubility curve suggests a different equilibrium solid phase above and below 610 C.

The solubility of uranium in liquid magnesium-zinc solutions has been measured as a function of magnesium concentration at 750, 700, and 650 C. At 750 C the uranium solubility varied from 9.7 weight percent at 17.7 weight percent magnesium to 0.09 weight percent at 66.7 weight percent magnesium. At 700 C the uranium solubility was 7.1 weight percent at 18.9 weight percent magnesium and 0.1 weight percent at 63.6 weight percent magnesium. At 650 C the uranium solubility varied from 3.2 weight percent at 25.0 weight percent magnesium to 0.05 weight percent at 65.2 weight percent magnesium.

The distribution of zirconium between the immiscible liquid metals lead and zinc has been measured in the presence of uranium, cerium, and ruthenium. The distribution coefficients (zirconium in zinc-rich layer/ zirconium in the lead-rich layer) were found to be 530 at 701 C, 350 at 732 C, and 110 at 757 C.

By means of analyses of samples of the two liquid layers in the lead-zinc system, the consolute temperature of the system has been found to lie between 784 and 789 C.

The cerium-cadmium system has been studied by means of the recording effusion balance. The following sequence of intermetallic phases was found: $CeCd_{11}$, $CeCd_{6.4-5.6}$, Ce_2Cd_7, $CeCd_{4.1-3.4}$, $CeCd_2$, and CeCd. Except for differences in the homogeneity ranges, the cerium-cadmium system is the same as the praseodymium-cadmium system.

II. Fuel Cycle Applications of Volatility and Fluidization Techniques (pages 93 to 128)

Development of the Direct Fluorination Process for the recovery of uranium and plutonium from oxide fuels continued. This process involves fluorination of uranium oxide fuels in a fluid-bed reactor. The heat produced is controlled by use of an inert bed material (Alundum is currently being used) as a medium for heat transfer. The development of fluorination techniques for the effective removal of plutonium from a solid solution of oxides of uranium and plutonium mixed with granulated Alundum is continuing. Experiments were carried out with an initial mild fluorination step employing 10 volume percent fluorine at 450 C. This initial step was followed by a second fluorination at 550 C and in some experiments at 650 C using 75 volume percent fluorine. The lowest plutonium concentration in the Alundum residue was obtained for experiments in which the second fluorination was performed at a temperature of 650 C for 5 hr. This procedure resulted in an average plutonium concentration in the residue of 0.016 weight percent, corresponding to a removal of 98.7 percent of the plutonium.

An important variable in the reaction scheme is the quantity of Alundum used as the inert solid. With an increase in Alundum from 0.9 to 1.5 g (3.42 g of uranium-plutonium oxides used) there was an increase in the retention of plutonium in the Alundum residues from 0.072 to 0.118 weight percent. Upon further increasing the amount of Alundum to 3 g, the plutonium content of the residue remained relatively constant at 0.107 weight percent. The plutonium removals from the mixtures containing 0.9, 1.5, and 3.0 g of Alundum were 94.9, 87.1, and 77.4 percent, respectively.

Two experiments were performed to determine the feasibility of using the same batch of Alundum as the inert solid for several fluorinations in which an addition of uranium-plutonium oxides was made prior to each fluorination. The recycle use of Alundum did not result in a greater removal of plutonium than that which would have resulted if three separate batches of Alundum had been used.

The direct fluorination of uranium dioxide pellet fuel is being studied on an engineering scale with the aim of optimizing production rate, fluorine efficiency, and fluidization quality.* The fluidization of inert, refractory

*Fluidization quality includes sufficient fluidization of the inert solids to maintain good heat transfer conditions in the reactor. It also includes the criterion that the bed be freely flowing at all times during and at the end of a run.

alumina in the voids of the pellet bed is used as an aid to heat removal. The current series of "deep-bed" runs has been concluded with two runs made during the present period in the 3-in.-diameter, air-cooled reactor. Both runs were made at 500 C with a total fluidization gas velocity of 1.3 ft/sec and an initial pellet bed of 18-in. depth. In these runs a partial recycle of process gas was employed to promote fluorine utilization efficiency, while maintaining a predetermined low concentration of oxygen entering the reactor. In one run made at a relatively low uranium hexafluoride production rate, 17 lb uranium hexafluoride/(hr)(sq ft), the fluorination was carried to completion in 44 hr with good fluidization and 78 percent overall fluorine efficiency. In another run made at a fluorination rate about 30 percent higher, operating instabilities developed with respect to channelling and caking. These results suggest that the 18-in.-deep charge can be practically fluorinated only at a relatively low rate, corresponding to about 40 hr. Since rates of up to 50 lb uranium hexafluoride/(hr)(sq ft) were successfully carried out with 6-in. pellet beds, further study will be given to the bed-height variables, both of the pellet and the inert, fluidized material.

Construction of a plutonium-handling facility for studying volatility processing techniques on a pilot-plant scale successfully developed in laboratory-scale fluorination experiments was continued. Initially, the installation is to be used for studies of the process variables in the fluorination of uranium-plutonium oxide pellets in a fluidized-bed reactor. Later, equipment will be added to study methods for the separation of the uranium from the plutonium. The facility consists of two alpha-containment boxes equipped with glass windows and gloves to allow direct manipulations as required, although the process is to be remotely monitored and controlled.

Additional development work was carried out on a fluidization-volatility scheme for reprocessing enriched uranium-zirconium alloy fuels. This scheme involves separation of volatile zirconium tetrachloride from uranium during chlorination with hydrogen chloride, followed by a fluorination step to volatilize the uranium as the hexafluoride. The reactions are carried out in a fluidized bed of inert solids (currently aluminum oxide) which serves as a heat transfer medium. Work included additional experiments in the $1\frac{1}{2}$-in.-diameter fluid-bed reactor in the chlorination-fluorination reaction sequence, additional studies in the 6-in.-diameter fluid-bed column on the conversion of zirconium tetrachloride to zirconium dioxide by reaction with steam, and additional detail work on the pilot-scale facility, the installation of which is planned for this Fall.

Studies on the chlorination-fluorination reaction sequence were concerned with the effect of hydrogen chloride excess and reaction temperatures on overall retention of uranium by the inert bed material (Norton Alundum, Type RR) used as a heat transfer medium during the alloy reaction. Also, exploratory work with phosgene as an auxiliary chlorinating agent was initiated.

Results showed the lowest residual uranium content was associated with the utilization of greater amounts of hydrogen chloride and higher temperatures, although the range of final uranium values extended from only 0.03 to 0.06 percent of the final bed. This was equivalent to a retention of from 0.8 to 1.9 percent of the initial uranium charged. Moreover, increased uranium removal was achieved by refluorination at a higher temperature (500 C). Extended fluorination at a uniform temperature did not give improved removal. The use of only four times the stoichiometric equivalent of hydrogen chloride is believed insufficient (unreacted metal probably remains), since residual zirconium concentrations were relatively high: 0.23 and 0.44 weight percent of the bed as compared with 0.04 weight percent when high hydrogen chloride excesses (11 to 25 times stoichiometric based on initial alloy charge) were used.

The use of a phosgene treatment after reaction with hydrogen chloride, both in a boat experiment and in an experiment conducted in the fluid-bed column, resulted in the lowest residual uranium values to date, less than 0.01 weight percent of the final bed (<0.2 percent of the charge). A spontaneous ignition of halogen gases in the cold traps used for uranium hexafluoride collection occurred in a subsequent run in which a mixture of hydrogen chloride and phosgene was used as the initial reactant gas. Causes for the ignition are being sought.

For future studies, an auxiliary "settling" chamber is being installed between the fluid-bed reactor and the static-bed filter section. Recent results indicated that such a unit may be of benefit in easing the load on the down-flow filter bed. Apparatus is also being installed for the continuous analysis (by thermal conductivity measurements) of off-gas streams during chlorination and fluorination in order to follow more closely the effects of process parameters.

Studies continued on the fluid-bed conversion of zirconium tetrachloride to zirconium dioxide by reaction with steam. This work is directed toward a scheme for disposal of the waste tetrachloride produced by chlorination of zirconium fuels. Efforts were directed at finding operating conditions which would be more favorable for the conversion reaction to occur on the surface of the bed particles. In this way, the problems associated with pressure buildup at the filters, which is believed to be caused by buildup of fines formed in the gas phase, might be eliminated.

Improved results have been obtained with lower bed temperatures (300 C as compared with 350 and 450 C), that is, a longer sustained period of operation without excessive pressure buildup was achieved. For example, after 3.5 hr at 300 C, the pressure rose to only about 0.4 in. Hg, whereas in a previous 3.0-hr run at 450 C, pressure rose to 10.3 in. Hg. The quantity of fines produced does not appear to be substantially reduced, but there is a positive growth trend (particle coating) indicated.

Essentially all of the equipment for the pilot-plant facility for the uranium-zirconium alloy fuel reprocessing is in the process of being fabricated or on order. Plant Engineering (ANL) will soon negotiate for an installation contract which will cover all the necessary service work, including installation of a new 100-KVA power transformer.

Process development studies were continued in a 3-in.-diameter column on a simple direct fluid-bed scheme for preparing high-density uranium dioxide particles. The scheme involves the simultaneous reaction of uranium hexafluoride with steam and hydrogen ($UF_6 + H_2 + 2H_2O \rightarrow UO_2 + 6HF$). Additional exploratory studies were made this quarter in which the quantity of steam used ranged from 10 to 320 percent of the stoichiometric requirement. A value of 9.5 g/cc (86 percent of theoretical density) was obtained for the density of the uranium dioxide. Density measurements on similar material in xylene gave values of 10.5 to 10.7 g/cc, which indicate that the solid material is near theoretical density and that the pore structure is primarily open but not penetrable by mercury under atmospheric pressure. (Pores smaller than 17 μ are not penetrated by mercury in the density determinations by mercury displacement.)

Residual fluoride contents in the recent products have been reduced to 200 to 300 ppm in most cases. Nickel content has been found to range from 17 to 30 ppm, thereby indicating that corrosion of the reactor is low. Fines carryover from the reactor section to the filter section has ranged from two to nine percent by weight of the hexafluoride feed input.

Development studies involving fluid-bed calcination in small-diameter columns were continued. The technique involves vertical upward injection of the aqueous feed into a conical-bottom reactor such that the feed atomizing and decomposition gases make up the fluidizing medium. This technique permits a substantial reduction in overall gas volumes normally associated with calciners, and also allows the consideration of nuclear-critical applications, for which size is important. Current work investigated the effect of bed depth (or, in effect, particle-residence time) on overall particle size effects, such as particle growth or fines formation. Bed depths of 10 and 15 in. were used, giving residence times of 5.2 and 7.8 hr.

An increase in the amount of fines as well as of particle growth was evident in the shallow-bed runs, whereas both effects appeared to be halted in the runs utilizing deeper beds. A problem remains in that the fines entrained and deposited on the filters do not appear to be returned to the bed uniformly upon blowback. From time to time, "excessive" return of fines has caused column upset and run termination. Further efforts to optimize the blowback cycle (varying pulse length and frequency) will be made in order to relieve this "fines" problem. Future work will also be aimed at demonstrating reliability of the unit during continuous operations.

III. Calorimetry (pages 129 to 135.)

Two calorimetric series of combustions have been completed: one is a series of nine combustions of cadmium in fluorine; the other is a series of ten combustions of magnesium in fluorine. However, the calculation of heats of formation from the results of these two series awaits several additional calibration experiments.

The determinations of the heats of formation of the tetrafluorides of titanium and hafnium have been completed. Titanium tetrafluoride has been definitely characterized as the product of combustion of the titanium combustions in fluorine.

Exploratory noncalorimetric experiments are being carried out to develop techniques for calorimetric studies with fluorine on several substances. Adequate techniques have been developed for the study of fluorination of niobium and tantalum. The same techniques as used with silicon appear to be satisfactory with sulfur. Considerable additional exploratory work will be necessary for zirconium diboride and carbon.

The study of the heat of formation of uranium hexafluoride has developed into a complex problem of chemical analysis. If the problem is not solved soon, it may be necessary to settle for results considerably less precise than originally anticipated.

Work is continuing on the assembly of the 1500 C high-temperature enthalpy calorimeter. Vacuum systems for the calorimeter have been assembled and tested. Circuits for the dropping mechanisms are being tested.

IV. Reactor Safety (pages 136 to 155.)

The oxidation, ignition, and combustion processes of uranium and zirconium are being studied to provide information to aid in minimizing the hazards associated with handling these materials.

The program of theoretical studies designed to relate quantitatively ignition results to isothermal oxidation data is continuing. The results of isothermal oxidation studies of uranium in the temperature range from 300 to 700 C (see ANL-6543, page 168) were expressed in the form of empirical equations. These equations were used in conjunction with a simple heat balance to simulate mathematically burning-curve ignition experiments. In a burning-curve ignition experiment, the uranium sample is heated uniformly (usually 10 degrees per minute) in a flowing, oxidizing atmosphere. The temperature at which the sample begins to self-heat rapidly and finally ignite is then determined by a graphical method.

The mathematical procedure involved a stepwise computation of the amount of reaction occurring during a small time interval. The amount of self-heating and the heat exchange by convection and thermal radiation between the sample and the program furnace were also computed. By extension of the calculations over a series of time intervals it was possible to generate the temperature-time history of the metal specimen. The ignition temperatures of uranium samples having specific areas of 0.5, 5, and 50 sq cm/g were computed in this manner. As part of the calculations, the assumption was made that the metal followed an accelerating rate law up to a temperature of 450 C and a decelerating rate law above 450 C in accordance with the isothermal oxidation results reported in the previous quarterly report. The demonstration that there was no protective oxide formed in the 300 to 450 C temperature range allowed the assumption that no protective oxide was involved when the sample reached 450 C. The calculations above 450 C were therefore carried out as if one were starting out with unoxidized metal at this temperature.

The computed ignition temperatures were in excellent agreement with experimental values for samples having specific areas of 0.5 sq cm/g (theoretical temperature 608, experimental temperature 575 C) and 5 sq cm/g (theoretical temperature 390, experimental temperature 410 C). Calculated values for samples having a specific area of 50 sq cm/g, however, were 50 C higher than experimental values, and further attention will be given to this problem. The general agreement between calculated and experimental ignition temperatures indicates that uranium ignitions are purely thermal ignitions.

A mathematical theory has been developed to compute the velocity of burning propagation along foil strips of uranium and zirconium. Computed results compare favorably with previously reported experimental values. The theory is similar to one used to describe gaseous flame propagation. The rate of oxygen uptake by foils burning in air is determined by the rate of gaseous diffusion of oxygen through a barrier of nitrogen. Propagation occurs by heat conduction ahead of the burning zone.

Studies of the ignition of spherical zirconium powder are continuing. The effects of specific area and sample size and shape are being studied. Ignition temperatures were found to decrease uniformly with increasing specific area. Ignition temperature was determined as a function of sample depth in 1-cm-diameter copper crucibles for powders of -140 + 170 and -325 + 400 mesh size. Increasing the sample depth from 0.02 to 0.5 cm decreased the ignition temperature over 200 C.

The experimental program to determine rates of reaction of molten reactor fuel and cladding metals with water is continuing. Further results of studies of the reaction of uranium with steam are reported. In these studies, steam at one atm is passed over one-cm uranium cubes. Hydrogen

generated by metal-water reaction is collected over water in a graduated vessel. The sample is heated by an external induction coil and temperature is controlled and measured by means of a very small thermocouple located in a hole at the center of the specimen cube. The reaction was found to obey the parabolic rate law from 500 to 1200 C (the highest temperature studied). The experimental results were adequately described by the following rate law between 600 and 1200 C:

$$V^2 = 1.95 \times 10^5 t \exp\left[-\frac{18,600}{RT}\right] , \qquad (10)$$

where V is the volume of hydrogen generated in cc H_2 STP/(sq cm), T is temperature, K, and t is time in min. The reaction rate at 500 C was too high to be described by the above equation.

The uranium-steam reaction at 400 C was entirely different in character. The reaction occurred in two stages; the initial slow reaction was followed by a rapid linear reaction. The initial reaction or induction period lasted for about 10 min. The rapid second-stage reaction continued for as long as the reaction was followed. A very finely divided oxide separated from the sample continuously during the second-stage reaction at 400 C. At higher temperatures, at which the parabolic rate law applied, the oxide adhered to the sample and retained the glossy appearance of the original metal.

In-pile studies of metal-water reactions in TREAT are continuing. In these studies, small fuel pins are placed under water in a high-pressure autoclave located at the center of the TREAT reactor in Idaho. They are then subjected to a vigorous neutron burst. In-pile studies were conducted with unclad 89.4 weight percent zirconium, 10.6 weight percent uranium alloy fuel-plate specimens. The three transients resulted in 4.0, 7.7, and 8.5 percent metal-water reaction for reactor energies of 251, 372, and 458 Mw-sec, respectively, on a reactor period of 80 msec (analytical data are not yet available to convert the megawatt-seconds figures to the energy absorbed in calories per gram of sample). The fuel plates formed molten pools of metal which eventually solidified in the alumina retaining crucibles in the autoclaves. No pressure spikes were recorded.

V. Energy Conversion (pages 156 to 159.)

Operation of a regenerative lithium hydride fuel cell system for converting nuclear energy to electricity is being studied. This thermally regenerative emf cell system is one in which heat is used to disassociate lithium hydride which is then re-formed in an electrochemical cell with the production of electric power. The apparatus for these experiments is being moved into the new laboratory wing. Systems are being installed for fused salt purification, for studies of hydrogen diffusion through metals,

for control and recording of heating and cooling of an inert atmosphere box-furnace combination, and for purification of helium.

Thermoelectric methods for direct conversion of nuclear reactor heat energy into electrical power are being investigated. Measurements are being made in the areas of liquid thermocouple systems and refractory solid thermocouple systems. Studies on the indium-bismuth liquid system have continued. Data taken to date indicate the indium-bismuth system shows regions of linear relation between the Seebeck coefficient and composition. Room-temperature Hall coefficient measurements made on a sintered plate of the refractory solid uranium monosulfide gave a value for the Hall coefficient R of about 6.2×10^{-3} cc/coulomb; for resistivity ρ of about 530×10^{-6} ohm-cm; for Hall mobility U of about 11.7 sq cm/(volt)(sec); and for carrier density n of about 1.0×10^{21}/cc. Measurements of the Seebeck coefficient as a function of temperature (150 to 1200 C) were also made on the sintered plate of uranium monosulfide.

VI. Determination of Nuclear Constants (pages 160 to 165.)

The total cross section of dysprosium for capture of neutrons is being measured in the kev energy range for neutrons. The cross sections range from 15 to 10 b in the energy range from 10 to 200 kev. Neutron-energy spreads seen by a sample 1.0 cm in diameter placed 2.0 cm from a lithium-7 target have been calculated for proton energies between 2.1 and 3.0 Mev. The ratio of the capture to fission cross sections, alpha, has been determined for uranium-233 irradiated in the third loading of EBR-I. The results are given as a function of position in the reactor. Alpha varies from 0.06 to 0.13 from core to outer blanket.

VII. Routine Operations (page 166.)

The operation of the radioactive waste-processing facility and the gamma-irradiation facility continued without incident.

TABLE OF CONTENTS

TABLE OF CONTENTS

LIST OF TABLES

LIST OF TABLES

LIST OF TABLES

LIST OF FIGURES

LIST OF FIGURES

LIST OF FIGURES

LIST OF FIGURES

CHEMICAL ENGINEERING DIVISION
SUMMARY REPORT

April, May, June, 1962

I. CHEMICAL-METALLURGICAL PROCESSING*

Pyrometallurgical processes for the recovery of fissionable material from discharged reactor fuels offer promise of achieving a reduction in the reprocessing costs associated with nuclear power. The principal characteristics of pyrometallurgical processes which are likely to result in reduced costs are their simplicity, compactness, low-volume dry wastes, and capability for handling short-cooled fuels, with an attendant reduction in fuel inventories. Among the pyrometallurgical processes under development are melt refining (a simple melting procedure for metallic fuels) and various processes for core and blanket materials which utilize liquid metal solvents as processing media. Pyrometallurgical techniques also show promise for the preparation of various reactor-fuel materials, including metals and carbides. The melt refining process is presently in the most advanced state of development and will be used for recovery of enriched uranium from the first core loading of the second Experimental Breeder Reactor (EBR-II).

A. Pyrometallurgical Development

1. Melt Refining

(R. K. Steunenberg, L. Burris, Jr.)

The melt refining process will be used to recover uranium from the first core loading of EBR-II. The fuel consists of approximately 50 percent enriched uranium alloyed with about five weight percent noble metal fission product elements. The fuel pins are clad with stainless steel, thermally bonded by a small amount of sodium. The pins are declad mechanically, chopped, and charged to a lime-stabilized zirconia crucible in which they are melted and maintained in a liquid state at 1400 C for a period of 3 to 4 hr. Approximately two-thirds of the fission products are removed in this procedure through volatilization and selective oxidation. The purified metal product is poured to form an ingot from which new pins are prepared by injection casting. A mixture of oxidized and unpoured metal remaining in the crucible as a skull is recovered by a separate process employing liquid metal solvents. Experimental results for the quarter are reported on (1) the behavior of condensable fission products volatilized during melt refining, and (2) the nitridation rates of irradiated fuel pins in argon-nitrogen mixtures simulating the atmosphere anticipated in the EBR-II Fuel Cycle Facility.

*A summary of this section is given on pages 1 to 6.

a. Fission Product Volatilization Studies
(N. R. Chellew, C. C. Honesty, W. H. Spicer)

The volatilization of fission product elements during melt refining was originally investigated in experiments with inactive and low-activity synthetic fissium alloys.[1] Subsequently, results were obtained from small-scale (300 to 400 g) melt refining experiments with highly irradiated EBR-II prototype fuel alloy (ANL-6413, pages 34 to 39; ANL-6477, pages 30 to 33). The principal fission product elements removed through volatilization during melt refining are xenon, krypton, iodine, cesium, and cadmium. The evolution of krypton and xenon was investigated in detail in special supplementary experiments with highly irradiated fuel pins (ANL-6287, pages 38 to 42; ANL-6379, pages 37 to 40). The present report is concerned mainly with additional studies of cesium and iodine volatilization, along with confirmatory information on the behavior of several typical nonvolatile fission product elements. No further work has been done on cadmium, since it appears to present no particular handling problem and is a relatively minor fission product.

Two additional small-scale experiments, each involving about 7 g of highly irradiated uranium-fissium alloy, have been completed. In the first, Experiment A, the type and amount of condensable activity that volatilized from the melt refined charge and collected on a nickel condenser were determined. In the second, Experiment B, the amounts of volatilized fission products that were retained by a Fiberfrax* trap were determined. The temperature gradient of the trap (450 to 1000 C) simulated that which is found in the Fiberfrax fume trap of the plant melt refining equipment.

The fuel pins that were used in the experiments were identical with those prepared for the first EBR-II core loading except for a lower uranium enrichment (9.44 vs 45.7 percent uranium-235). The fuel was irradiated in the Materials Testing Reactor to 1.18 ± 0.13 total atom percent burnup, as determined by mass-spectrometric analysis. The cooling time of the fuel was 25 days. Prior to use, the pin sections were polished lightly with emery paper to remove surface reaction products formed during irradiation and decanning.

The experiments utilized an induction-heated furnace which was located in a cave. The assemblies that were used for the

---

[1] Burris, L., et al., The Melt Refining of Irradiated Uranium: Application to EBR-II Fast Reactor Fuel. I. Introduction, Nuclear Sci. and Eng. 6, 493 (1959) et seq.

*Fiberfrax is a molded product of the Carborundum Corporation, prepared from amorphous fibers and colloidal silica binder. The reported composition of the fibers in weight percent is: Al_2O_3 (51.2), SiO_2 (47.4), B_2O_3 (0.7), and Na_2O (0.7).

collection of volatile fission products in the two experiments are shown in Figure 1. In Experiment A, Assembly A was used for determining the deposition of volatilized activity at various temperature zones along a nickel tube. In Experiment B, Assembly B was employed. This assembly utilized a 3.3-cm-deep Fiberfrax bed for the collection of the volatile fission products. Sodium was vaporized to the fume trap during this experiment, since it will comprise the largest part of condensable volatiles in a plant charge. The temperature profile of each assembly was determined prior to the experiment.

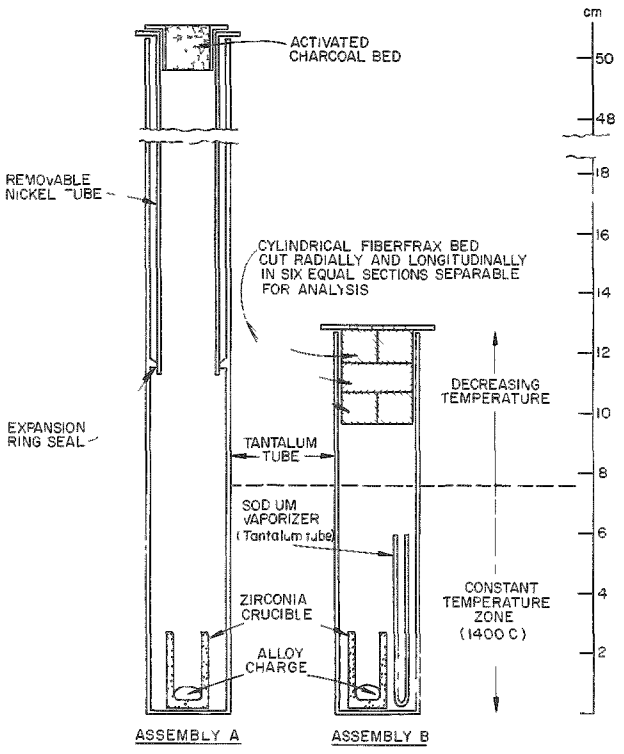

Figure 1

EXPERIMENTAL ASSEMBLIES FOR COLLECTION OF VOLATILIZED MATERIAL

In each experiment, the fuel (about 7 g) was charged to a lime-stabilized zirconia crucible which was inserted in a fission product collector assembly, outgassed at 200 C for 10 min, then heated under argon at one atmosphere to 1400 C for one hour. When the furnace had cooled after the experiment, the argon atmosphere was replaced by air, and the assemblies were dismantled for inspection and analysis. In both experiments, the fuel alloy melted completely and formed a button in the shape of a sessile drop.

Analytical samples were obtained by dissolving various portions of the assemblies in acid, or by leaching when dissolution was impractical. Standard radiochemical methods were used to separate and analyze the activities. Iodine, cerium, tellurium, and strontium were counted as beta activities, and barium, cesium, zirconium, and ruthenium as gamma activities. A control sample was analyzed similarly and counted

at approximately the same time. When necessary, appropriate decay corrections were made. For the uranium analyses, a fluorophotometric technique was used.

Analytical results from the two experiments are presented in Tables 1 and 2. The distribution data for the volatilized activities are given in Table 3 on a gram-atom basis. On the basis of these data, the following comments can be made regarding the fates of individual fission products.

Iodine and Cesium. In Experiment A (Table 1), cesium and iodine accounted for nearly all of the gamma activity volatilized. However, only about 51 percent of the cesium and 55 percent of the iodine in the charge material were accounted for. These low material balances probably resulted from losses that were incurred during remote handling of the nickel collection tube. Of the amounts recovered, about 90 percent of the iodine and 70 percent of the cesium had collected in a zone that had been at temperatures between 450 and 700 C. A dark gray material had deposited in the same zone, forming a band about one inch wide on the nickel collector. The small amount of iodine found in the charcoal trap and deposition of the bulk of this activity at temperatures exceeding 450 C are evidence that iodine was not volatilized in elemental form. Comparison of condensate fractions (on a gram-atom basis) from the first experiment (Table 3) shows that the amount of cesium present in the individual fractions was well in excess of the quantity necessary to account for the presence of iodine as cesium iodide (melting point, 621 C; boiling point, 1280 C).

Table 1

DISTRIBUTION OF MATERIAL DURING MELT REFINING OF EBR-II PROTOTYPE FUEL: EXPERIMENT A

Crucible: Lime-stabilized zirconia

Charge: 7.196 g U - about 5 w/o fissium alloy pins; burnup, 1.18 ± 0.13 percent of total atoms; cooling time, 25 days

Apparatus: See Figure 1, Assembly A

Conditions: Alloy heating, one hour at 1400 C; atmosphere, argon[a]

		Initial Element Concentration (mg)[b]							
		U	Ru	Zr	Te	Ce	Ba-Sr	Cs	I
Charge (prior to heating)		6790	170	17	0.9	8.5	6.5	9	0.5
		Percent of Starting Material							
Fraction	Temperature (C)	U	Ru	Zr	Te	Ce	Ba-Sr	Cs	I
Ingot plus Skull Material[c]	1400	-	-	-		94	1.3	0.5	1.3
Crucible	1400	-	-	-	-	1.2	75[d]	2.5	1.5
Volatilized[e] to									
Charcoal Trap	~ 200	-	-	-	-	-	-	<0.1	0.1
Nickel Collector	200-450	1×10^{-3}	1×10^{-5}	1×10^{-4}	1×10^{-4}	1×10^{-5}	1×10^{-3}	0.3	0.3
Nickel Collector	450-700	1×10^{-3}	3×10^{-5}	2×10^{-4}	4×10^{-3}	1×10^{-4}	1.5×10^{-3}	37	49
Nickel Collector	700-900	1.5×10^{-3}	1×10^{-5}	1×10^{-3}	1×10^{-3}	2×10^{-5}	7×10^{-3}	10	2.1
Tantalum Collector	900-1400	5×10^{-4}	2×10^{-5}	5×10^{-4}	1×10^{-3}	8×10^{-5}	4×10^{-3}	1.0	0.4

[a] After the furnace had cooled, the argon pressure in the system was reduced from about one atmosphere to 10 mm twice and these gases stored. Prior to removal of the collector assembly, one atmosphere of air was admitted to the furnace.

[b] Calculated from irradiation data and analysis of constituents of the unirradiated alloy.

[c] Unpoured ingot and adhering skull material physically separated from crucible.

[d] Separate individual analyses of barium and strontium activities showed their distribution to this fraction to be 74 and 79 percent of starting material, respectively.

[e] Values reported are considered maximum because of probable cross-contamination effects during radiochemical separation; uranium concentrations in volatilized fractions were near the limits of detection for the fluorophotometric analytical method employed.

Table 2

DISTRIBUTION OF MATERIAL DURING MELT REFINING OF EBR-II PROTOTYPE FUEL EXPERIMENT B

Crucible: Lime-stabilized zirconia

Charge: 6.662 g U - about 5 w/o fissium alloy pins plus 0.43 g Na; burnup, 1.18 ± 0.13 percent of total atoms; cooling time, 35 days

Apparatus: See Figure 1, Assembly B; Fiberfrax outgassed at 1000 C prior to use.

Conditions: Alloy heating, one hour at 1400 C; atmosphere, argon[a]

		Initial Element Concentration (mg)[b]				
		Ce	Sr	Ba	Cs	I
Charge (prior to heating)		7.9	3.2	2.8	8.3	0.46
		Percent of Starting Material				
Fraction	Temperature (C)	Ce	Sr	Ba	Cs	I
Ingot plus Skull Material, Oxidized[c]	1400	102	2.6	0.9	-	0.25
Crucible	1400	1.6	96	96	0.8	-
Volatilized to						
Fiberfrax Bed Section[d]	450-600	e	-	e	10.0	8.0
Fiberfrax Bed Section[d]	600-800	e	-	e	38.0	15.0
Fiberfrax Bed Section[d]	800-1000	e	-	e	40.1	8.3
Tantalum Collector	1000-1400	-	-	-	0.6	0.3

[a]After the furnace had cooled, the argon pressure in the system was reduced from about one atmosphere to 10 mm twice and these gases stored. Prior to removal of the collector assembly, one atmosphere of air was admitted to the furnace.

[b]Calculated from irradiation data.

[c]Unpoured ingot and skull material separated from crucible by oxidation at 700 C for 9 hr in an argon-25 volume percent oxygen atmosphere.

[d]Total bed depth, 3.3 cm.

[e]Activities not detectable in gamma-spectrometric scan of samples leached from bed sections.

Table 3

MATERIAL VOLATILIZED DURING HEATING OF EBR-II PROTOTYPE FUEL IN STABILIZED ZIRCONIA AT 1400 C

Conditions: Experiment A, see Table 1
Experiment B, see Table 2

Expt	Collector	Temperature (C)	Gram Atoms x 10^{10} U	Ru	Zr	Te	Ce	Sr[a]	Ba[a]	Cs	I
A	Charcoal Trap	~200	-	-	-	-	-	-	-	<700	40
	Nickel Tube	200-450	<2900	2	2	0.1	0.1	2	1	2,030	120
	Nickel Tube	450-700	<2600	5	4	3	0.6	3	2	250,000	19,300
	Nickel Tube	700-900	<3800	2	19	0.7	0.1	13	8	68,000	830
	Tantalum Tube	900-1400	<1350	3	9	0.7	0.5	8	4	6,800	160
B	Fiberfrax Bed Section	450-600	-	b	b	b	b	-	b	62,400	2,900
	Fiberfrax Bed Section	600-800	-	b	b	b	b	-	b	237,000	5,400
	Fiberfrax Bed Section	800-1000	-	b	b	b	b	-	b	250,000	3,000
	Tantalum Tube	1000-1400	-	-	-	-	-	-	-	3,800	100

[a]Identical distribution of activities in condensate fractions assumed in calculation of gram atoms from distribution data reported in Table 1.

[b]Activities not detectable in gamma spectrometric scan of samples leached from bed sections.

Previous studies[2] had indicated that reactions with crucible constituents, particularly calcium, played a role in the vaporization of iodine when uranium-fissium alloy spiked with uranium triiodide and/or lightly irradiated uranium was melted in zirconia crucibles stabilized with five weight percent calcium oxide. However, cesium was either absent or present in trace amounts (< 0.02 ppm) in these experimental charges. For the experiments with high-activity level, it was not possible to determine accurately the amounts of inactive crucible constituents volatilized.

In Experiment B (Table 2), over 99 percent of the cesium and iodine recovered was found in the Fiberfrax bed, under conditions which approximate those anticipated in the fume trap of the plant melt refining equipment. In this experiment, a 3.3-cm bed with a temperature gradient from approximately 1000 to 450 C was exposed to sodium vapor. The material balances for cesium and iodine, however, were about 90 and 30 percent, respectively. In view of the low material balance for iodine, further work is considered necessary.

As in Experiment A, the amount of cesium in each bed section was in excess of the quantity required to account for volatilization of the iodine as cesium iodide. The absence of a definite collection pattern of the activities suggests that additional effects may lead to incomplete retention of iodine by Fiberfrax during or after melt refining. Iodine analysis of the Fiberfrax bed sections as a function of storage time in air indicated that a loss of iodine from the Fiberfrax does occur with time. The data shown in Table 4 indicate that, of the iodine initially collected on the Fiberfrax, about 50 percent is lost in about 6 weeks. This loss may result from the oxidation of iodine by air or from radiodecomposition. The greater retention shown by the bed section heated to the highest temperature during the experiment very likely results from entrapment of the iodine in glassy material formed by the reaction of sodium with Fiberfrax.

The experiments also provided an indication of the extent of iodine retention by a melt refining skull when it is oxidized to separate it from the zirconia crucible. In the first experiment, 1.3 percent of the iodine charged to the system was found in the unoxidized ingot and skull, whereas in the second experiment only 0.25 percent was found in the skull and ingot after oxidation in an oxygen-argon atmosphere at 700 C. On the basis of these results, it appears that a small, but significant, quantity of iodine will be present in the skull oxides entering the skull reclamation process.

Barium, Strontium, and Cerium. Barium and strontium were both incorporated preferentially into the zirconia crucible used for melt refining. The concentrations of barium and strontium in the condensed

---

[2]Chellew, N. R., and Ader, M., The Melt Refining of Irradiated Uranium; Application to EBR-II Fast Reactor Fuel. XI. Behavior of Iodine in Melt Refining, Nuclear Sci. and Eng., 9, 82 (1961).

volatile material were small. Their combined concentrations would account for less than one percent of the iodine present if it were assumed that the iodine volatilized as barium iodide or strontium iodide.

Table 4

EFFECT OF TIME ON IODINE-131 RETENTION IN FIBERFRAX BED SECTIONS
EXPERIMENT B

Experimental Conditions: See Table 2

Bed Section	Temperature during Experiment (C)	Iodine Retention[a] (percent of starting material) Initial Analysis (samples stored 1 day)[b]	Final Analysis (samples stored 42 days)[b]	Percent Released
Top	450-600	8.0	2.0	75
Middle	600-800	15.0	5.0	67
Bottom	800-1000	8.3	7.3	12
	Total	31.3	14.3	

[a]Iodine leached from one-half sections of Fiberfrax beds (see Assembly B, Figure 1) after the indicated storage times; activity retention in each section determined by weighing amount in analytical samples according to total weight of bed in temperature zone of interest.

[b]Samples stored in air in separate containers prior to analysis.

Less than two percent of the cerium was found in the crucible. The remainder appeared in the ingot plus skull fraction, presumably as a constituent of the skull.

Tellurium, Zirconium, Ruthenium, and Uranium. Negligible volatilization of these elements occurred in both of the experiments.

In summary, it appears that the iodine activity volatilized during melt refining is largely collected on surfaces between 450 and 700 C, either as cesium iodide or as the iodide of an inactive element. Cesium is also volatilized in the melt refining process and is condensed in the same temperature region. Barium and strontium are found mainly in the crucible, and cerium appears in the skull. Volatilization of tellurium, zirconium, ruthenium, and uranium is negligible.

b. Nitridation Rates of Irradiated Fuel Pins
(J. P. LaPlante, C. C. Honesty)

Some nitridation of irradiated fuel pins is expected to occur in the Argon Cell of the EBR-II Fuel Cycle Facility, since the argon atmosphere of the Cell may contain up to five percent nitrogen and fission product decay heat is expected to raise the temperature of the declad fuel

pins. Since excessive nitride formation might have an adverse effect on the melt refining process, the nitridation rates of irradiated fuel pins under conditions simulating those expected in the plant are being investigated.

Several additional experiments were performed at various temperatures and nitrogen concentrations in argon, using the procedure outlined previously in ANL-6543, page 30. Experimental results were lower than those obtained earlier, but this discrepancy was explained when it was noted that a correlation exists between nitridation rate and the number of days that irradiated pins had been stored in the air atmosphere of the cave facility. This effect is shown by the data in Table 5. The uranium-fissium alloy fuel pins that were irradiated to 1.18 total atom percent burnup became completely unreactive to nitrogen after exposure to air for approximately 8 days, although they had been polished with emery paper immediately before the nitridation experiments. The correlation between nitridation rate and number of days of prior exposure to air appears to be affected by the percent of burnup and the specific activity of the fuel pins.

Table 5

EFFECT OF PRIOR AIR EXPOSURE ON THE NITRIDATION RATES OF IRRADIATED URANIUM-FISSIUM FUEL PINS

Fuel Pins: 95 w/o uranium (10% enriched)-5 w/o fissium alloy pins irradiated and cooled as indicated

Temperature: 300 C

Atmosphere: 100% nitrogen at one atmosphere pressure

Burnup (a/o)	Cooling Time (days)	Specific Activity (c/g)	Prior Air Exposure[a] (days)	Nitridation Rate (% of original)
0.87	100	4.3	0	100
			12	84
			14	73
			18	50
1.20	90	4.8	0	100
			7	20
1.18	20	14.3	0	100
			8	0
			13	0
			14	0

[a]At ambient temperature of the cave facility (~30 C).

The nitridation rate of a sodium-coated uranium-five percent fissium pin irradiated to 1.18 total atom percent burnup and cooled 80 days was determined in a single experiment at 500 C in a 100 percent nitrogen atmosphere. Exposure of the pin to air prior to the experiment was limited to less than one hour. Previous experience had shown that exposure under these conditions does not affect the nitridation rates at temperatures from 300 to 650 C. The result is compared in Figure 2 with data obtained previously for an unirradiated sodium-coated uranium-fissium pin in a five percent nitrogen atmosphere at 300 C (ANL-6287, page 42). Since it has been shown that the same nitridation rates are obtained in five percent and 100 percent nitrogen atmospheres (ANL-6333, page 38), it appears that irradiation has little, if any, effect on the nitridation rate of the sodium-coated fuel pins.

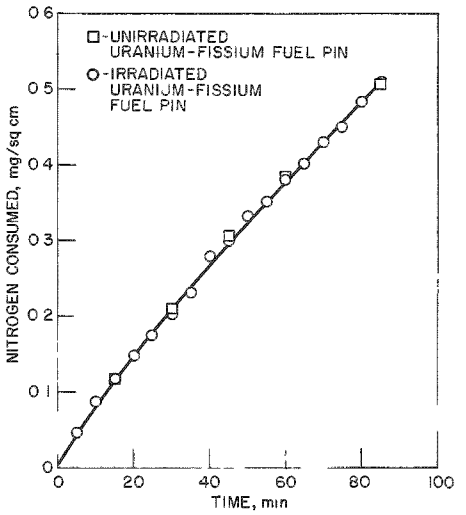

Figure 2

NITRIDATION RATE OF SODIUM-COATED URANIUM-FISSIUM FUEL PINS

Atmosphere:	Nitrogen
Temperature:	500 C
Burnup (%):	1.18
Cooling Time:	80 days
Specific Activity (c/g):	5.37

In general, the nitridation rate data for uranium-fissium alloy fuel pins indicate that irradiation has no large effect on the rate at temperatures below about 500 C. It does appear, however, that, in order to prevent difficulty with nitride shells on the pins in the melt refining process, it may be necessary (1) to limit the exposure of fuel pins to the cell atmosphere, (2) to prevent the pin temperatures from rising above about 300 C, or (3) to lower the nitrogen content of the cell atmosphere significantly.

2. Processes Utilizing Liquid Metal Solvents
(L. Burris, Jr., R. K. Steunenberg)

Engineering and laboratory development of liquid metal processes for recovering the fissionable material remaining as a skull in the melt refining crucible and for the isolation of plutonium bred in the EBR-II blanket material was continued. Laboratory work is in progress to develop processes for other fuel materials, especially future EBR-II

cores, which will contain plutonium as a fissionable material. In progress, also, are fundamental studies in which molten salt and metal media are utilized and studies of various unit operations (distillation, mass transfer, and mixing) in liquid metal systems.

a. Demonstration of Skull Recovery Process
(R. D. Pierce, K. R. Tobias)

An experimental program is underway to demonstrate the process for recovering melt refining crucible residues (skull material) on a 130-g-uranium scale in the recently completed inert atmosphere glovebox described in ANL-6543, page 32. These experiments are intended to test process variables and to determine optimum process conditions prior to the operation of larger, integrated process equipment.

During this reporting period, equipment shakedown was completed and the first demonstration run was made in accordance with the flowsheet presented in ANL-6477, page 36. Generally, the equipment operated satisfactorily, but minor changes in both equipment and operating technique were shown to be necessary. A pressed-and-sintered tungsten crucible was utilized for noble metal extraction and uranium oxide reduction; a beryllia crucible was used for the uranium precipitations and for the retorting step.

Only data relating to uranium recovery are available; analyses are still to be made to determine the behavior of fission product elements. The results of this experiment will be reported when the analytical data become available.

The design of integrated equipment for large-scale recovery of fissionable material ($2\frac{1}{2}$ kg of skull oxide) is nearing completion. Many of the major equipment items have been ordered.

b. Retorting of Uranium Concentrates
(J. F. Lenc, M. A. Bowden)

A final retorting step is required in the current skull reclamation process (flowsheet previously given in ANL-6477, page 36) to isolate the uranium precipitated in the intermetallic-compound-decomposition step from residual zinc and magnesium. Experimental work on the retorting operation has been directed at achieving easy, high-yield removal of the isolated uranium product from the retorting crucible in a form suitable for remote recycle to the melt-refining process.

The feasibility of utilizing the uranium concentrate from the magnesium decomposition step (i.e., precipitated uranium enveloped in the zinc-magnesium alloy) as the end product of the skull reclamation

process is also being investigated. The success of this process modification is dependent upon two conditions: (1) the ability to remove the uranium concentrate from the decomposition crucible, and (2) the ability to handle such a product in subsequent process steps; for example, in subsequent melt refining operations, it would be necessary to make suitable provisions for the collection of zinc and magnesium vapors.

Performance of a Metal-jacketed Beryllia Crucible. To date, retorting experiments have been conducted in a variety of crucible materials. However, easy removal of the uranium in high yield, either as an isolated product after retorting or as a concentrate after the intermetallic-decomposition step, has been accomplished only in beryllia crucibles (isostatically pressed and sintered). Similar results may be realized with other ceramic crucibles, but beryllia offers the following three advantages: (1) high thermal conductivity (consequently, low susceptibility to thermal shock), (2) high chemical stability, and (3) nonwetting by zinc-magnesium-uranium systems. Regardless of the method (pressing and sintering, thixotropic casting, or assembly from blocks - see ANL-6543, page 44) that eventually will be selected for fabrication of beryllia crucibles, metal jacketing is considered necessary to minimize the consequences of any metal leakage through cracks in the crucible.

Testing of a metal-jacketed beryllia crucible assembly was begun during the past quarter. Beryllia powder was packed in the annulus between the beryllia crucible and the stainless steel secondary crucible. Four 120-g-uranium scale runs were conducted in the stainless steel-jacketed, isostatically pressed beryllia crucible assembly (4-in. OD by $9\frac{7}{16}$ in. high) in accordance with the "three-step" procedure* described in ANL-6379, page 62. The uranium concentrate (uranium enveloped in zinc and magnesium) did not adhere to the beryllia crucible after the intermetallic decomposition step in any of the four runs. The retorting step for distilling off the residual zinc and magnesium was carried out in only two of the runs. Nearly 100 percent of the uranium present in the crucible was easily removed from the crucible in each of these. The uranium concentrates recovered from the other two runs will be used in future experiments to determine whether the uranium can be satisfactorily melted under conditions in which the zinc and magnesium are boiled off at pressures near atmospheric. No visible deterioration of the stainless steel-jacketed beryllia crucible assembly was detected after any of the above tests.

Experiments will be continued in this same assembly to determine its useful life. On the basis of tests performed to date, no serious problems are anticipated in using a metal-jacketed ceramic crucible assembly for full-scale process application.

*The three steps are the last three steps of the skull reclamation process, all of which are conducted in the same crucible. The steps are: (1) precipitation of uranium-zinc intermetallic compound and removal of the supernatant liquid, (2) decomposition of this compound with magnesium to precipitate uranium, and, following removal of the supernatant liquid, (3) retorting to drive off residual zinc and magnesium.

c. Application of the Skull Reclamation Process to the Recovery of Uranium from Stainless Steel-clad Fuel Pins (V. Trice, W. Spicer)

The first core loading of the EBR-II reactor will be processed by the melt refining process. The procedure for preparing the fuel pins for melt refining includes the mechanical removal of the stainless steel cladding. There exists the possibility that some of the fuel pins will be too badly distorted or otherwise unsuitable for decladding. To provide for this contingency, a study is being made to determine whether the noble metal extraction step of the skull reclamation process can be adapted to the recovery of uranium from clad fuel.

The noble metal extraction step in the skull reclamation process provides for the removal of elements more electropositive than zinc from skull oxide by contacting a suspension of skull oxide in flux with molten zinc. To accommodate clad fuel, the noble metal extraction step was modified by the addition of sufficient zinc chloride to the flux to oxidize uranium and thereby to provide for its extraction into the flux as uranium trichloride. It is likely that a small percentage of zinc chloride, perhaps about two mole percent, will be added as a precautionary measure to the flux phase in the noble metal-extraction step to oxidize any uranium metal which might not have been oxidized in the skull-oxidation step. This quantity of zinc chloride is, of course, considerably less than that required to oxidize all of the uranium as would be necessary for fuel pins which cannot be declad.

Two-step experiments were conducted to determine the behavior of uranium and the stainless steel constituents (iron, nickel, and chromium) in the modified noble metal-extraction step and in the subsequent uranium-reduction step of the skull reclamation process. One experiment was made with each of the two fluxes currently under consideration for the skull recovery process, namely, flux A which contains 47.5 mole percent calcium chloride, 47.5 mole percent magnesium chloride and 5.0 mole percent of magnesium fluoride and which was used in Experiment A, and flux B which contains 47.5 mole percent lithium chloride, 47.5 mole percent magnesium chloride, and 5.0 mole percent of magnesium fluoride and which was used in Experiment B.

In the first step of the experiments, uranium and the stainless steel constituents were dissolved in zinc and at the same time, the uranium was oxidized by zinc chloride to uranium trichloride which transferred to the flux phase. Essentially equal weights of flux and zinc were used. The extraction step was carried out under an argon atmosphere for 3 hr at 800 C. Moderate stirring (450 rpm) was used. Preliminary experiments had shown that these conditions sufficed to provide a virtually equilibrium distribution of uranium between metal and salt phases. The metal phase consisted of the following substances which were charged separately: 200 g zinc, 21 g uranium-5 percent fissium alloy, and

3.2 g 304 stainless steel. The flux phase contained 200 g flux (Type A or B) and 30 g zinc chloride. The flux and zinc chloride were melted together in air before use. After the uranium-bearing salt phase and the metal phase had solidified, they were separated mechanically.

In the second step, the uranium-bearing salt was contacted at 800 C with an equal weight of zinc-10 weight percent magnesium which reduced and dissolved the uranium. Experimental conditions for the reduction step were moderate stirring (450 rpm) under argon atmosphere for 3 hr at 800 C. Preliminary experiments showed that these conditions were adequate to attain an essentially equilibrium distribution of uranium.

Experimental conditions and results are summarized in Figure 3.

Figure 3

BEHAVIOR OF URANIUM AND STAINLESS STEEL CONSTITUENTS IN NOBLE METAL EXTRACTION STEP (MODIFIED) AND REDUCTION STEP OF SKULL RECLAMATION PROCESS

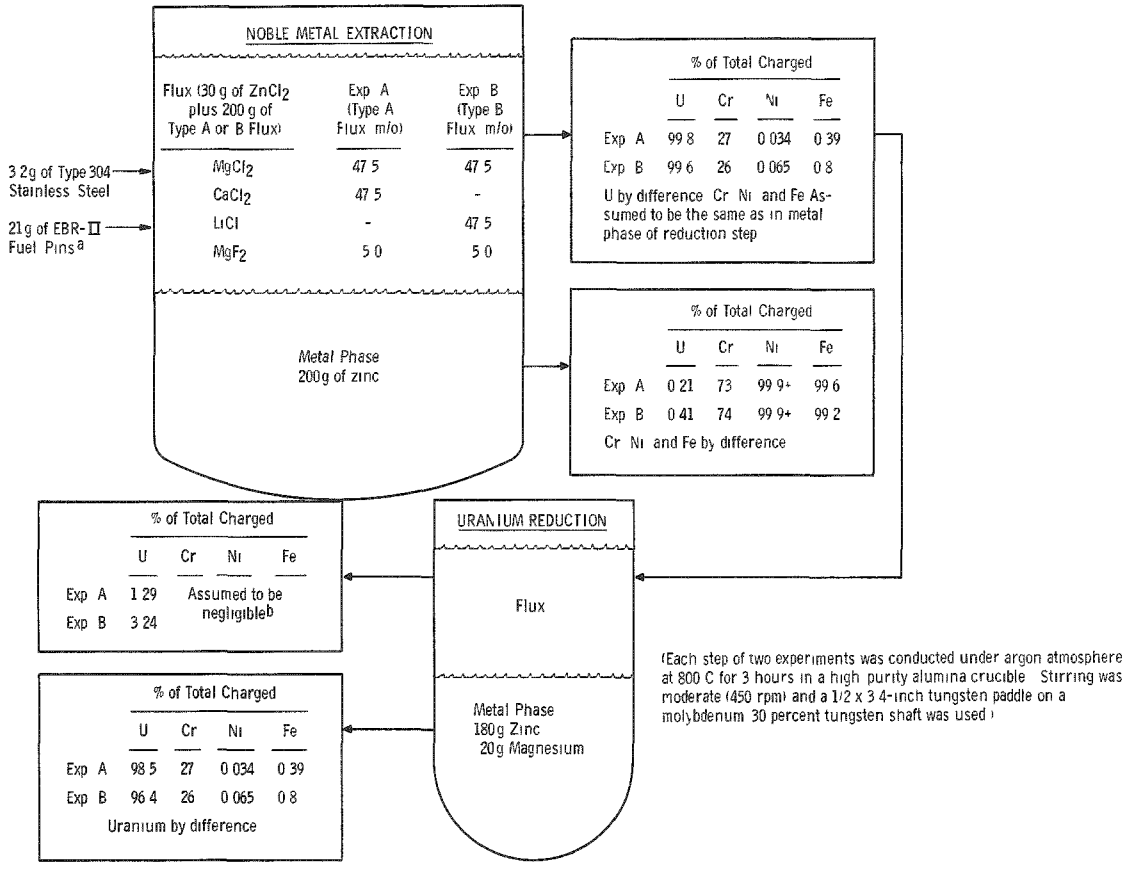

[a] The nominal composition of EBR-II fuel is 95 weight percent uranium 2 46 weight percent molybdenum 1 95 weight percent ruthenium 0 28 weight per cent rhodium 0 18 weight percent palladium 0 10 weight percent zirconium and 0 01 weight percent niobium

[b] This is a reasonable assumption in view of the large excess of magnesium employed

The behavior of uranium, iron, nickel, and chromium was determined by comparing the amounts charged to the modified noble metal-extraction step with the amounts of these elements found upon complete dissolution and analysis of the metal phase from the reduction step. The coefficients of distribution of the various elements between the salt and metal phases in the noble metal-extraction or oxidation step were calculated on the assumption that reductions were essentially complete in the reduction step. Uranium losses were determined by analyses of the metal phase from the oxidation step after complete dissolution in aqua regia and by aqua regia leaching of water-insoluble components of the salt phase from the reduction step. The absence of color in the water-soluble portion of the salt phase showed that residual uranium present in the flux phase was in the form of water-insoluble uranium compounds.

Comparisons of both uranium losses and the distribution coefficients of uranium and stainless steel constituents shown in Table 6 indicate Flux A, containing calcium chloride, to be somewhat superior to Flux B, containing lithium chloride. In the oxidation step, the uranium distribution coefficient (flux to metal on a weight basis) was 475 for Flux A and 240 for Flux B. In these experiments, iron and nickel were largely retained in the metal phase with distribution coefficients of 3.4×10^{-4} and 3.9×10^{-3}, respectively. However, substantial extraction of chromium occurred with both fluxes. Based on the distribution coefficients observed with Flux A, and assuming no subsequent separation of stainless steel constituents, the uranium recovered by processing clad fuel under the conditions employed in this experiment would contain approximately 40 ppm of iron, 500 ppm of nickel, and 8000 ppm of chromium.

Table 6

DISTRIBUTION COEFFICIENTS OF URANIUM AND STAINLESS STEEL CONSTITUENTS IN MODIFIED NOBLE METAL EXTRACTION STEP

(see conditions and procedure in Figure 3)

	Distribution Coefficient in Noble Metal-extraction Step (w/o in flux/w/o in metal)	
Constituent	Flux A	Flux B
Uranium	475	240
Iron	3.4×10^{-4}	6.5×10^{-4}
Nickel	3.9×10^{-3}	8.0×10^{-3}
Chromium	0.37	0.36

The amount of uranium retained in the flux phase after reduction was 1.3 percent with Flux A and 3.2 percent with Flux B. In preliminary studies of the reduction step with zinc-10 weight percent magnesium or zinc-5 weight percent magnesium as the reducing agents at contact times of up to 13 hr, some uranium in the form of a precipitate was retained in the salt phase in every case. In all cases, the solidified salt phase from the oxidation step also contained a settled zone of reddish brown precipitate. This material, which was separable by water leaching, was identified by X-ray spectrographic analysis as uranium dioxide. The presence of a small amount of moisture or zinc oxide in the system during the oxidation step would explain the formation of uranium dioxide. It is postulated, therefore, that the recovery of uranium in the reduction step was limited by the amount of uranium dioxide formed. The only relevant data available concerning the reduction of uranium dioxide were obtained with the use of Flux B at 750 C under an air atmosphere. These data, reported in ANL-6477, page 40, show the rate of reduction of uranium oxide to be relatively slow.

d. Processes for Plutonium Reactor Fuels
(R. K. Steunenberg)

The second core loading of EBR-II is expected to be a plutonium alloy of approximately the following composition: uranium, 70 percent; plutonium, 20 percent; fissium elements, 10 percent. One of the principal problems encountered in processing irradiated material of this type is to achieve an adequate separation of rare earth fission products from the plutonium. Two promising methods for accomplishing this separation are being investigated. One involves selective extraction of the rare earths from a zinc-magnesium solution of plutonium and uranium by a molten halide flux. The other entails the use of a calcium-zinc solution in which the rare earths are soluble whereas the plutonium and uranium are relatively insoluble. Additional information has been obtained on the technique of molten salt extraction during the past quarter.

Separation of Rare Earths from Uranium and Plutonium by Molten Salt Extraction
(J. B. Knighton, J. D. Schilb, J. W. Walsh)

The objective of this program is to investigate the possibility of separating the various elements present in spent reactor fuels by equilibration of the constituents of the fuel between a liquid metal, such as molten magnesium-zinc alloy, and a molten salt flux, such as magnesium chloride. Distribution coefficients for yttrium, cerium, and praseodymium in this system have been shown previously to be dependent on the magnesium concentration in the metal phase and the magnesium chloride concentration in the flux phase (ANL-6379, page 61; ANL-6543, page 49). Additional distribution data have been obtained for plutonium, americium,

Figure 4

DISTRIBUTION OF SELECTED ELEMENTS BETWEEN ZINC-MAGNESIUM ALLOY AND MAGNESIUM CHLORIDE

Temperature: 800 C
Mixing Rate: 300-350 rpm
Crucible: tantalum
Atmosphere: argon

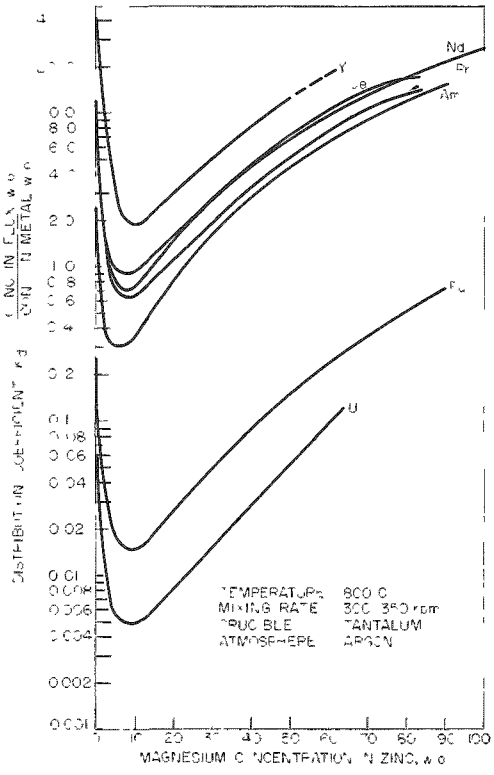

neodymium, and uranium. The present status of the program is summarized in Figure 4, where the distribution coefficients [K_d = (w/o in flux)/(w/o in metal)] are presented as functions of the magnesium concentration in the zinc phase. Details of the individual experiments are as follows:

Plutonium

The distribution data for plutonium are given in Figure 5. These results are from three separate experiments in which the equilibrium as approached from the zinc-rich side and from the magnesium-rich side. When a material balance determination was made at 50 weight percent magnesium, the plutonium material balance was 93.3 percent. Each point on the distribution curve is based on analyses of the metal and flux for plutonium and analysis of the metal for magnesium. The plutonium concentrations were determined by alpha counting the dissolved flux and metal samples.

Figure 5

DISTRIBUTION OF PLUTONIUM BETWEEN ZINC-MAGNESIUM ALLOYS AND MAGNESIUM CHLORIDE

Temperature: 800 C
Mixing Rate: ~300 rpm
Crucible: tantalum
Atmosphere: argon

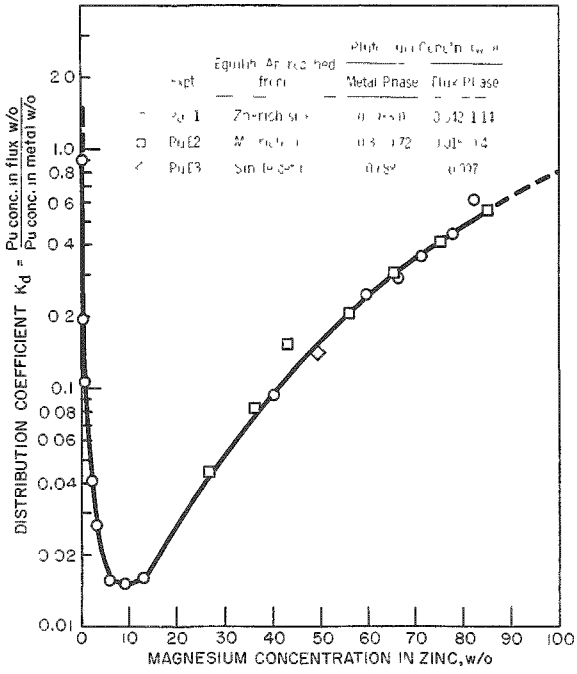

The plutonium distribution curve, like that of uranium (see Figure 4), is displaced downward from the curves for the rare earths, indicating that a plutonium-rare earth separation is possible. Further work on the plutonium system will consist of determining the distribution coefficient at 100 weight percent magnesium concentration and establishing whether the distribution coefficient is dependent on the plutonium concentration.

Americium

The distribution curve for americium has also been determined, with the samples obtained in the plutonium experiments. The americium was separated by standard radiochemical methods and was determined by gamma counting.

Figure 6

DISTRIBUTION OF AMERICIUM BETWEEN ZINC-MAGNESIUM ALLOYS AND MAGNESIUM CHLORIDE

Temperature: 800 C
Mixing Rate: ~300 rpm
Crucible: tantalum
Atmosphere: argon

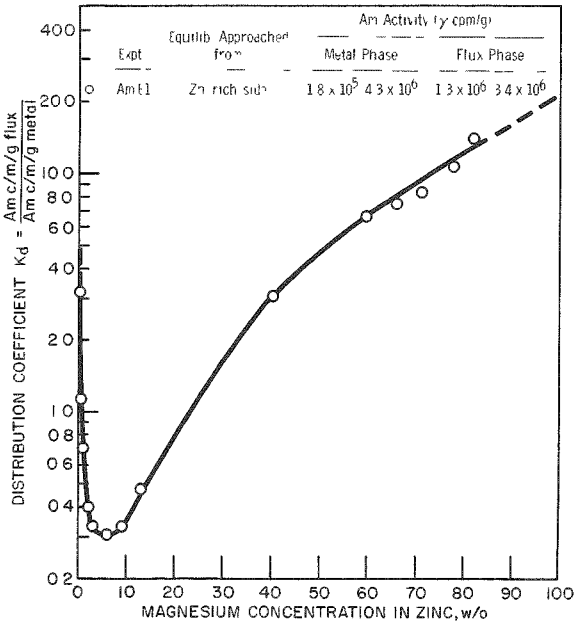

The results, shown in Figure 6, indicate that americium behaves in much the same way as the rare earth elements and should be removed from plutonium by a separations procedure capable of a plutonium-rare earth separation. In order to complete the curve, a determination is being made at 100 percent magnesium concentration. The curve is also being verified by experiments in which the equilibrium is approached from the magnesium-rich side.

Neodymium

The distribution data for neodymium from zero to 100 percent magnesium in the metal phase are shown in Figure 7. These results were obtained from two experiments in which the equilibrium was approached from both the zinc-rich and magnesium-rich sides. Inactive neodymium was used in one of the experiments and activated neodymium was used in the other (NdE-2). The concentrations of neodymium added to the system differed by a factor of about ten. The agreement of the data at different neodymium concentrations shows the distribution coefficient to be independent of concentration. The distribution coefficient curve for neodymium falls between the curves for cerium and praseodymium.

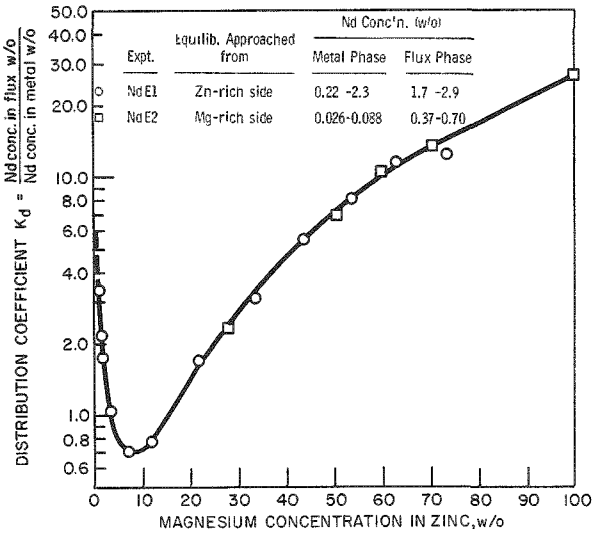

Figure 7

DISTRIBUTION OF NEODYMIUM BETWEEN ZINC-MAGNESIUM ALLOYS AND MAGNESIUM CHLORIDE

Temperature: 800 C
Mixing Rate: ~300 rpm
Crucible: tantalum
Atmosphere: argon

Uranium

The distribution of uranium between zinc-magnesium alloys and magnesium chloride at magnesium concentrations ranging from zero to 60 weight percent magnesium is shown in Figure 8. The distribution coefficient curve for uranium lies considerably below the curves for the rare earths and americium (see Figure 4). This work is being continued in order to complete the curve in the magnesium-rich region of the metal phase. In considering the separations obtainable in these systems, it is necessary to take into account the very low uranium solubility in the magnesium-rich regions. Preliminary results have indicated that the distribution coefficient is sensitive to the uranium concentration at low uranium concentrations (less than two weight percent in the metal phase). Additional data on this effect are being obtained.

Figure 8

DISTRIBUTION OF URANIUM BETWEEN ZINC-MAGNESIUM ALLOYS AND MAGNESIUM CHLORIDE

Temperature: 800 C
Mixing Rate: ~300 rpm
Crucible: tantalum
Atmosphere: argon

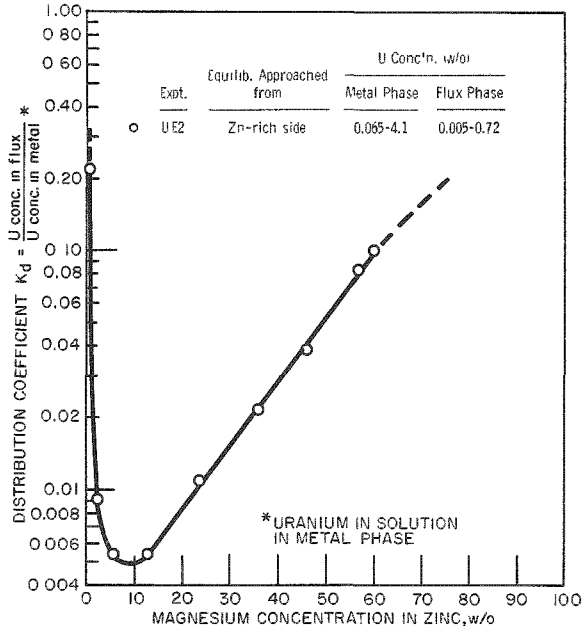

On the basis of the data available thus far, it appears that a practical separation of uranium and plutonium from yttrium and the rare earths may be possible

by this technique, although multiple-stage contacting would very likely be necessary. Present plans call for extending the study to include other important fission product elements, fuel cladding materials of interest, and other actinide elements.

e. Recovery of Plutonium from EBR-II Blanket Material
(I. O. Winsch, T. F. Cannon, J. D. Arntzen, P. J. Mack)

Plutonium will be generated in the depleted uranium blanket material of the EBR-II reactor to a concentration of about one percent before the blanket material is discharged for processing. The blanket processes under investigation for the separation of plutonium from uranium by a pyrometallurgical method are based on the high solubility of plutonium in magnesium-rich zinc alloys and the contrasting low solubility of uranium in these alloys.

(1) Blanket-process Demonstration Runs

The fourth blanket-process demonstration run* was completed during the past quarter. As usual, the blanket material was dissolved in a 12 to 15 weight percent magnesium-zinc alloy to produce an approximately 13 weight percent uranium solution, the uranium was precipitated from solution by adding magnesium to a 50 weight percent concentration, and then the supernatant phase containing the soluble plutonium was separated from the precipitated uranium. In this demonstration run, direct dissolution of stainless steel-clad uranium blanket material and plutonium was carried out to ascertain the effects of the stainless steel constituents. A number of the major fission product elements (inactive) which would be present in blanket material were also added to the original charge, as shown in Table 7. Results have been summarized for each step of the process in Table 8.

Table 7

MATERIALS CHARGED TO BLANKET-PROCESS DEMONSTRATION RUN 4

Element	Weight (g)	% of Blanket Material	% of Total Charge	Element	Weight (g)	% of Blanket Material	% of Total Charge
U	504	91.51	12.87	Rh	0.075	0.014	1.92×10^{-3}
Pu	4.74	0.865	0.12	Pd	0.025	0.005	7.00×10^{-4}
Cr[a]	6.67	1.23	0.17	Te	0.031	0.006	7.97×10^{-4}
Ni[a]	2.96	0.55	0.076	Ba	0.10	0.020	2.55×10^{-3}
Fe[a]	27.43	5.00	0.70	La	0.10	0.020	2.55×10^{-3}
Na	2.94	0.543	0.071	Ce	0.235	0.045	6.00×10^{-3}
Sr	0.085	0.018	2.17×10^{-3}	Nd	0.275	0.050	7.0×10^{-3}
Zr	0.23	0.046	5.87×10^{-3}	Mg	465	-	11.88
Mo	0.245	0.048	6.26×10^{-3}	Zn	2900	-	74.07
Ru	0.160	0.030	4.09×10^{-3}				

[a]Constituent of 304 stainless steel cladding.

* The results of previous blanket-process demonstration runs are reported in ANL-6379, page 76, ANL-6413, page 56, and ANL-6477, page 47.

Table 8

SUMMARY OF BLANKET-PROCESS DEMONSTRATION RUN 4

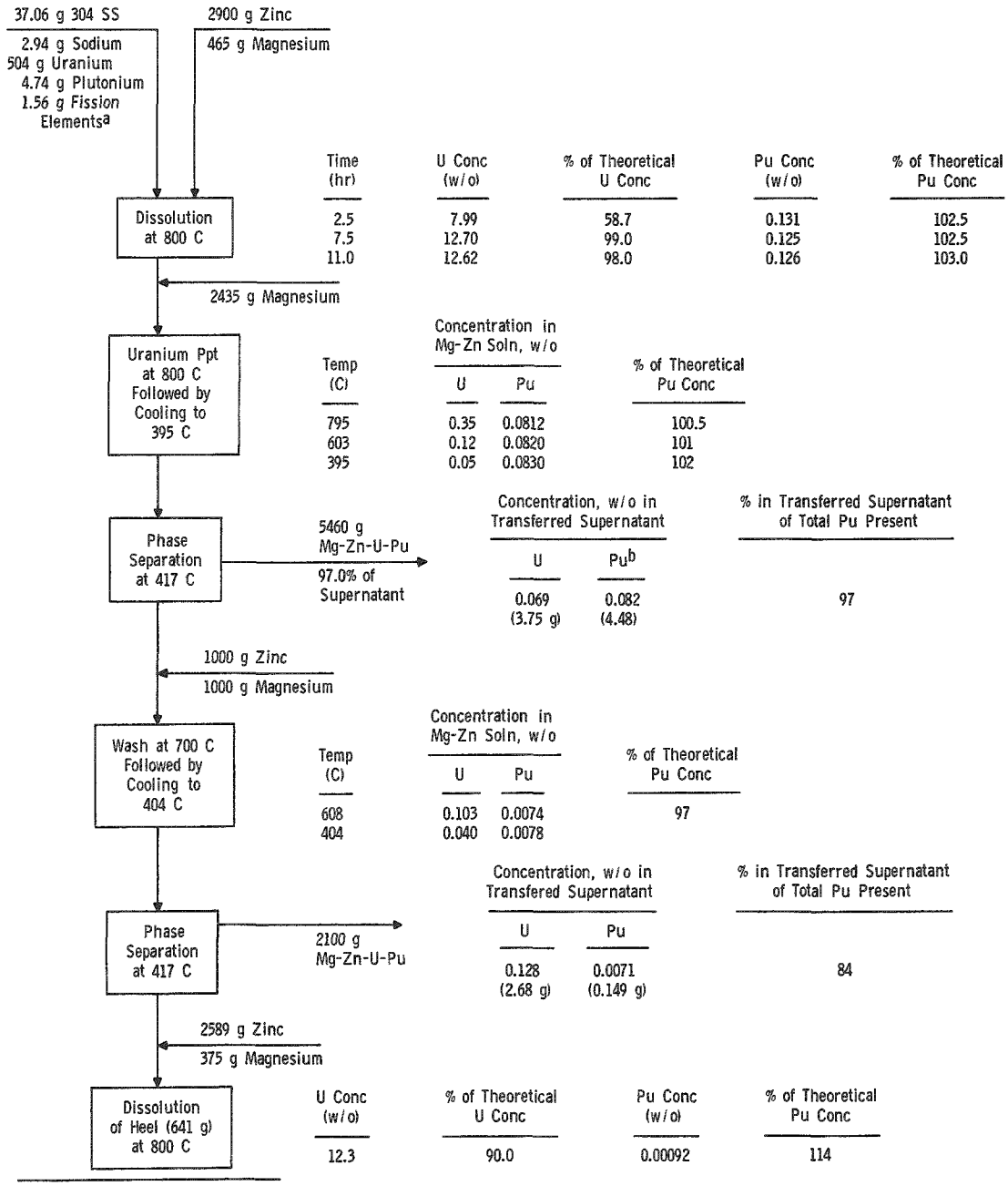

[a] See Table 7 for the amounts of each fission element added.

[b] The plutonium concentration in the transferred supernatant was taken to be the average of the three plutonium concentrations in the supernatant phase obtained prior to transfer. An actual analysis of a sample of the transferred supernatant phase gave a value of 0.0735 weight percent plutonium. This apparent loss of plutonium is considered to be an abnormal result, since it has not been encountered in either previous or subsequent demonstration runs. Possibly some precipitation of plutonium occurred in the receiver by impurities present in the receiver.

No significant retardation of uranium dissolution was caused by the presence of stainless steel, which is itself rapidly attacked by zinc-rich solutions at 800 C. At the end of 7.5 hr, all of the uranium and plutonium was in solution. As indicated by a sodium deposit on the upper wall of the reaction vessel, the sodium present in the annulus between the stainless steel jacket and the depleted uranium was volatilized during the dissolution step.

Following uranium dissolution, the bulk of the uranium was precipitated at 800 C by adding magnesium to a 50 weight percent concentration, after which the uranium concentration was further decreased from 0.35 to 0.05 percent by cooling to 395 C. The plutonium concentration in the zinc-magnesium solution remained in the vicinity of 100 percent. In all four demonstration runs, good plutonium recovery and separation from uranium were demonstrated in the precipitation step.

A 97 percent removal of the supernatant phase was realized in this run, as compared with 70, 87, and 72 percent in the previous three runs. This increase in efficiency of phase separation was attributed to the use of a new transfer line similar to that shown in ANL-6543, page 57. The separated plutonium-magnesium-zinc supernatant had a uranium concentration of 0.069 percent which, in comparison with the solubility value of 0.04 to 0.06 weight percent, indicates a slight physical carryover of uranium.

Analyses of samples of the transferred supernatant showed the plutonium concentration to be about 0.0735 percent, which is lower than several values of about 0.082 percent obtained before transfer of the supernatant phase. It is thought that possibly some plutonium was precipitated from solution by impurities present in the receiver crucible. The precipitation of the amount of plutonium represented by the concentration decrease could be caused by carbon in an amount of only 0.02 g. In a subsequent run, the plutonium product receiver was one which had been used several times to contain plutonium-magnesium solutions. With this receiver, no decrease in the concentration of the plutonium solution transferred into it occurred.

The uranium precipitate was washed with a 50 weight percent magnesium-zinc solution at 700 C, followed by cooling of the solution to 417 C and separation of the solution from the uranium precipitate by pressure siphoning. An additional 3 percent of the plutonium was recovered in this step to give a total recovery of 100 percent of the available plutonium. The uranium concentration of the transferred wash phase was 0.128 percent, which is a considerably higher uranium carryover than generally experienced in the transfer of the supernatant phases (see Table 10, p. 48). As shown by phase-transfer studies which are described on page 47, a shield placed over the open end of the transfer line should prevent carryover of uranium in transferred supernatant solutions.

The uranium-plutonium heel which remained after the wash step was dissolved in a 12 weight percent magnesium-zinc solution at 800 C. Samples of the melt showed a uranium concentration of 12.3 percent and a plutonium concentration of 9.2×10^{-4} percent which, respectively, are 90 and 105 percent of the expected concentrations. Overall material balances were 99 percent for plutonium and 91 percent for uranium. The plutonium recovery of 99 percent may be compared with recoveries of 92, 95, and 93 percent obtained in the three previous runs. The overall plutonium-uranium separation factor in this run was 77.5 as compared with values of 169 and 157 in the second and third demonstration runs. The low separation factor in this run is the result of the unusually high physical carryover of uranium in the magnesium wash solution.

The presence of sodium, chromium, iron, nickel, and fission product elements appeared to have no effect on the behavior of plutonium. The behaviors of iron, chromium, and nickel were studied in a separate experiment, reported in the following section.

A few additional demonstration runs will be made to complete this phase of the work. Work will then be concentrated on scaling up the process and possibly on investigating alternative blanket processes.

(2) Behavior of Stainless Steel in the Blanket Process

In order to determine the fate of the nickel, chromium, and iron which make up the 304 stainless steel cladding of the depleted uranium blanket material, a clad blanket rod was dissolved in a 14 weight percent magnesium-zinc solution at 800 C. The uranium was then precipitated from solution by addition of magnesium to form a 50 weight percent magnesium-zinc solution and by cooling to 400 C.

As shown in Table 9, dissolution of the uranium and stainless steel constituents was complete in about 7.5 hr. No significant problem of uranium dissolution is imposed by the presence of the stainless steel cladding.

Table 9

DIRECT DISSOLUTION OF STAINLESS STEEL-CLAD BLANKET URANIUM

504 g Uranium
25.96 g Iron
5.9 g Chromium
3.2 g Nickel
2.9 g Sodium

430 g Magnesium
2638 g Zinc

Dissolution at 800 C

Time (hr)	Concentration, w/o U	Fe	Cr	Ni	% of Charge in Solution U	Fe	Cr	Ni
3	4.5	0.51	0.145	0.097	29.1	64	79	99
7.5	13.8	0.69	0.154	0.095	99.5	96	94	106

2200 g Magnesium

Ppt at 800 C Followed by Cooling to 400 C

Temp (C)	Concentration, w/o U	Fe	Cr	Ni	% of Charge in Solution U	Fe	Cr	Ni
795	0.333	0.007	0.022	0.067	3.5	1.4	19.5	109
605	0.128	0.0028	0.011	0.064	1.3	0.57	9.8	105
400	0.056	0.0014	0.0015	0.063	0.59	0.011	1.33	103

In the subsequent uranium-precipitation step, the iron and chromium precipitated or coprecipitated almost completely with the uranium while the nickel remained in solution. Figure 9 shows the approximate concentrations of the uranium, chromium, nickel, and iron in zinc-50 weight percent magnesium after precipitation of the uranium with magnesium at 800 C and subsequent cooling to 400 C. It is apparent that if clad blanket material were dissolved directly in the blanket process, all of the nickel would accompany the plutonium. The resulting nickel content of the plutonium product would be intolerably high, since the amount of nickel involved is comparable to that of plutonium. Therefore, direct dissolution of EBR-II blanket elements cannot be considered unless the process can be modified to provide adequate removal of the nickel.

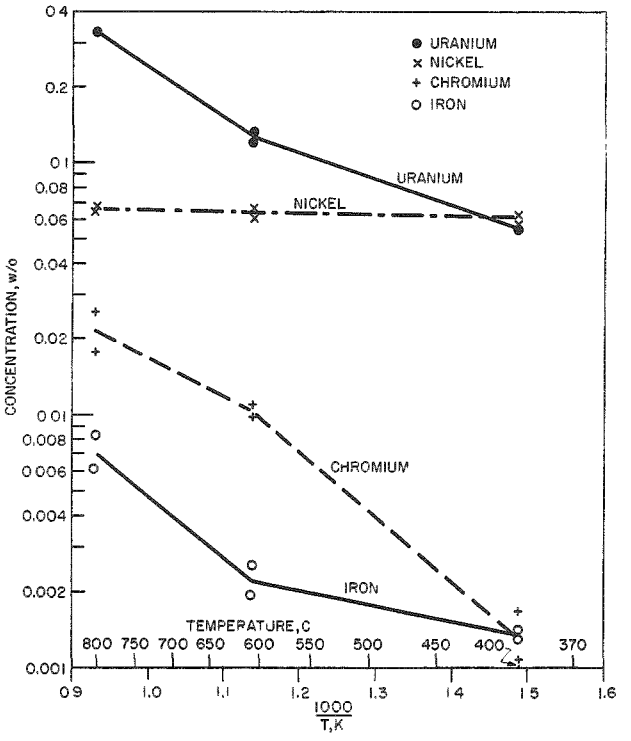

Figure 9

CONCENTRATION OF URANIUM, CHROMIUM, IRON, AND NICKEL IN ZINC-50 WEIGHT PERCENT MAGNESIUM AFTER PRECIPITATION BY MAGNESIUM ADDITION TO ZINC-10 WEIGHT PERCENT MAGNESIUM-14 WEIGHT PERCENT URANIUM SOLUTION

(3) Separation of Magnesium-Zinc Supernatant Solutions

Seven additional phase-separation runs have been completed in studying the separation of the magnesium-zinc supernatant from the precipitated uranium phase. In all of these runs, which were conducted on a 500-g-uranium scale, the removal of the supernatant solution followed dissolution of uranium in a 12 weight percent magnesium solution to give a 13 weight percent uranium concentration and subsequent precipitation of the uranium by addition of magnesium to about a 50 weight percent concentration. Supernatant solution removals which were effected in the temperature range of 405 to 415 C are given in Table 10. The equipment used in these studies and the results of four previous runs are described in ANL-6543, pages 56 to 58.

Table 10

PHASE SEPARATION OF MAGNESIUM-ZINC SUPERNATANT SOLUTIONS FROM PRECIPITATED URANIUM METAL

Scale: 5.2 to 5.7 kg of 46-50 weight percent magnesium-zinc and 500 g of uranium

Beginning with Run 4, a shield having the same cross-sectional area as the tube was placed about 1/16 in. from the open end of the tube.

Run No.	Phase Sepn Temp, C	Mg Conc in Supernatant, w/o	Uranium Conc, w/o			Percent of Supernatant Phase Transferred	Percent of Total Uranium Transferred[a]
			Solubility at Transfer Temperature	Transferred Phase[a]	Precipitated Phase		
1	415	50	0.04-0.06	0.126	72.5	97.3	1.25
2	405	50	0.04-0.06	0.045	71.6	97.5	0.50
3	415	50	0.04-0.06	0.069	69.0	97.5	0.76
4	415	50	0.04-0.06	0.052	58.5	93.5	0.49
5	415	46	0.06-0.09	0.102	70.5	97.3	1.13
6	417	46	0.06-0.09	0.094	71.5	97.0	0.92
7	415	46	0.06-0.09	0.077	72.5	97.0	0.84
8[b]	410	46	0.06-0.09	0.073	51.6	92.0	0.77
9	416	46	0.06-0.09	0.090	60.9	95.0	0.97
10[b]	410	50	0.04-0.06	0.043	54.0	91.5	0.50
11	410	50	0.04-0.06	0.066	53.5	92.5	0.69

[a]Value obtained by resampling of transferred supernatant at 800 C and includes uranium in solution at transfer temperature.

[b]Flat-bottom crucible - all other runs in conical-bottom crucible.

In Runs 1 through 4 and Runs 10 and 11, the uranium was precipitated from a 50 weight percent magnesium-zinc solution, whereas in Runs 5 through 9 the uranium was precipitated from a 46 weight percent magnesium-zinc solution. The results of the first run indicated the possibility that precipitated uranium was jammed into the open end of the downleg transfer line as it was moved toward the bottom of the crucible. Subsequently, any uranium particles trapped in the transfer line were transferred with the magnesium-zinc supernatant during the pressure-siphoning operation. Therefore, beginning with Run 4, a shield having approximately the same cross-sectional area as the transfer line was placed over the open downleg end of the transfer line, at a distance of $\frac{1}{16}$ in. from the tube end, to lessen the possibility of precipitated uranium being trapped in the line.

With the exception of one or two runs (No. 1 and possibly No. 5), the amount of solid uranium entrained in the supernatant phase was essentially negligible in comparison with the amount of uranium in solution. In the runs in which a conical-bottom crucible was used (all runs except 8 and 10), about 92.5 to 97.5 percent of the supernatant phase was transferred from the precipitated uranium by pressure siphoning at about 415 C. Somewhat lower transfer efficiencies (about 92 percent) were realized with a flat-bottom crucible (Runs 8 and 10).

It is interesting to note that in some runs the uranium precipitated to form a cake, as shown in Figure 10, whereas in other runs a uranium ball, as shown in Figure 11, was formed in the precipitation step. A cross-sectional view of the ball is shown in Figure 12. No explanation for this difference in uranium behavior can be given at this time.

Figure 10

CROSS SECTION OF PRECIPITATED URANIUM CAKE

(Obtained in Run 4 of a series of runs shown in Table 10 for studying the phase separation step of the EBR-II blanket process. The calculated uranium content of the cake is 59 weight percent.)

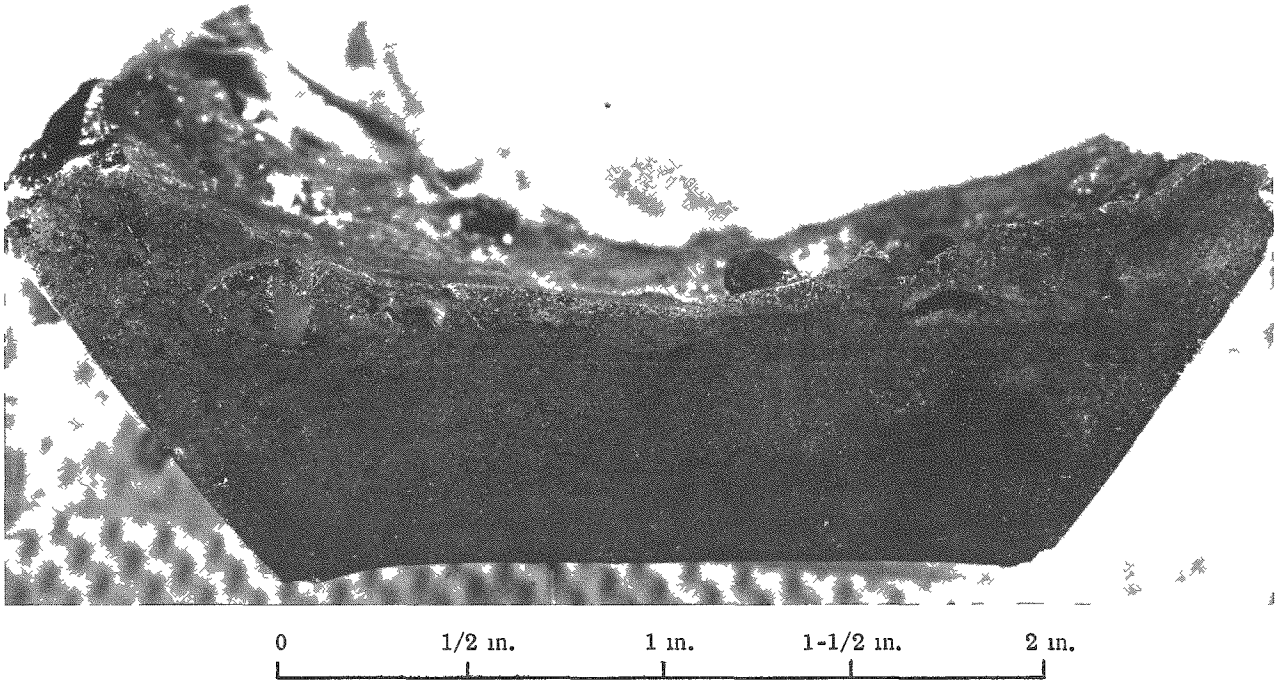

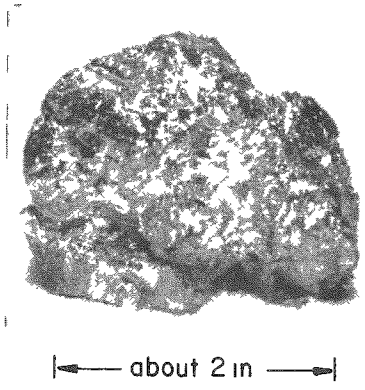

Figure 11

PRECIPITATED URANIUM BALL

(Obtained in Run 6 of a series of runs shown in Table 10 for studying the phase separation step of the EBR-II blanket process. The uranium content of the ball is about 70 percent.)

It is believed that the efficiency of the phase separations of 92.5 to 97.5 percent, obtained in the above 1/20th-scale runs, would be equalled or surpassed in full-scale operations. The minimum desired recovery of 90 percent of the plutonium in the blanket process should be easily provided by phase-separation efficiencies of about 95 percent. Such efficiencies would eliminate the necessity of washing the uranium precipitate to recover additional plutonium.

Equipment has been fabricated for the purpose of demonstrating the phase-separation operation on one-half scale (5 kg of uranium). Phase-transfer studies will begin as soon as equipment is assembled.

Figure 12

ENLARGED CROSS-SECTIONAL VIEW OF
PRECIPITATED URANIUM BALL

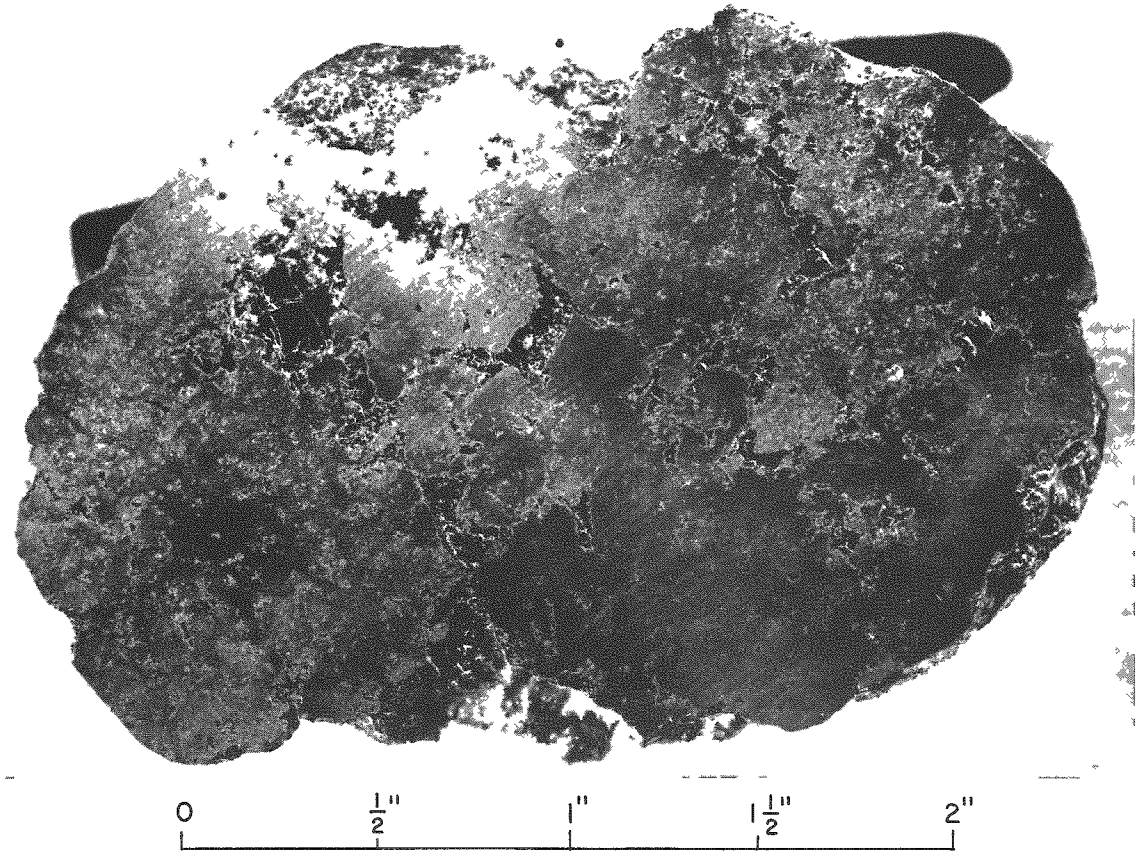

f. Materials and Equipment Evaluation
(P. A. Nelson)

Studies are in progress to evaluate the compatibility of various materials with liquid metal systems of the types contemplated for reprocessing reactor fuels. The selection of materials for EBR-II processing equipment is the main objective, but data of more general interest are also being accumulated. Corrosion tests with metal coupons and runs in agitated crucibles under processing conditions are being used to evaluate materials. Methods of fabrication of process equipment from materials which have proved to be corrosion resistant to process solutions are being investigated and compared. Investigations on the wettability of beryllia by molten salt fluxes and on solution stability are reported below.

(1) Corrosion by Molten Metal and Flux Systems
(M. Kyle, M. Deerwester)

Wettability of Beryllia by Molten Halide Flux

Beryllia is of interest as a container material for fuel processes because of its chemical inertness to flux and metal-process solutions, and because it is not wetted by uranium precipitated from zinc-rich solutions, as evidenced by successful removal of retorted uranium from beryllia crucibles (see ANL-6477, page 44). Future requirements for large vessels might surpass the capability of one-piece construction methods for either refractory metals or beryllia. The use of bricks would thus become necessary. This would favor the use of beryllia rather than refractory metals. For these reasons, consideration is being given to beryllia in materials tests which are designed to measure the performance of beryllia under typical fuel-processing conditions.

In order to determine whether the surface of a beryllia crucible is wetted by a typical processing flux, a run was conducted at 800 C for 100 hr in which beryllia was contacted with molten flux of the following composition (in mole ratios): 47.5 magnesium chloride, 47.5 lithium chloride, 5 magnesium fluoride, and 2 zinc chloride. The beryllia piece used in this experiment was cut from the top of an isostatically pressed crucible (92 percent theoretical density) which had been previously used in a retorting operation. After contacting the beryllia piece with flux under the conditions described above, the surface layers were removed, the interior region was leached, and the resulting solution was analyzed for lithium ion. From this analysis and the knowledge of the flux density and beryllia porosity, it was determined that the voids had been nearly completely filled with flux.

Examination of the crucible material after exposure to the flux revealed that the inside surface of the crucible was generally not wetted. The outside surface of the crucible was well wetted by the flux. The apparent difference in wettability between inside and outside walls of the crucible has also been noted by the supplier, who ascribes this difference to the fact that the as-fired crucible surface usually is protected by a surface film. In order to meet dimensional tolerances, the outside crucible wall is quite often ground to a depth sufficient to remove the protective coating produced by firing. Moreover, the manufacturing procedure of isostatic pressing results in a density variation in the crucible wall, with the inside of the crucible being most dense, but no quantitative data on the variation of wall density are available. This difference in density also could contribute to the difference in wettability of the inside and outside crucible surfaces.

(2) Solution Stability Studies
(G. A. Bennett, L. F. Dorsey, W. A. Pehl)

An important factor in determining the loss of fissionable material in liquid metal processes is the susceptibility of dissolved fissionable material to reactions with the container material or with impurities present in solution. That uranium is inert to a tungsten crucible under the conditions of the reduction step in the skull reclamation process has been demonstrated in long runs in which no significant change in uranium concentration was noted (ANL-6477, page 57). However, the concentrations obtained in some of these experiments were slightly below the values calculated from the charged materials. This discrepancy could have been caused by the reaction of uranium with impurities in solution, by sampling difficulties, or by analytical bias.

In an attempt to resolve this question, a run was made in which the stability of a zinc-magnesium-uranium and flux system was tested under the various operating conditions which would affect the reactivity of the dissolved uranium to impurities in the materials. These conditions were as follows:

1) low uranium concentration, low uranium activity coefficient;
2) low uranium concentration, moderate uranium activity coefficient;
3) high uranium concentration, moderate uranium activity coefficient;
4) high uranium concentration, high uranium activity coefficient.

The variations in the uranium activity coefficient in a magnesium-zinc solution at a given uranium concentration were obtained by changing the magnesium concentration. Approximate calculations showed that the uranium activity coefficient varied by a factor of 50 over the magnesium concentration range employed.

The run was carried out in a pressed-and-sintered tungsten crucible with a tungsten heat-shield assembly and with an agitator made of a molybdenum-30 weight percent tungsten alloy. The temperature was maintained at 800 C for a period of 3 hr at each of the first three uranium conditions (see Items 1, 2, and 3 above), and for a period of 7 hr at the last uranium condition.

A summary of the main experimental results is given in Table 11. These data show that in all parts of this run the average value of the uranium concentrations agreed with the theoretical (calculated) value within the estimated analytical accuracy (± 5 percent). A few unfiltered samples were taken, and these had the same uranium concentration, within

analytical accuracy, as the filtered samples. Thus, no significant reaction of dissolved uranium with impurities or the container materials occurred. Carbon, the most likely reactant with uranium, was found by analysis to be present in the starting material to the extent of 94 ppm. Analyses made during the run show that the average carbon concentration in the metal solution did not drop. No great significance is attached to this observation, however, because of the difficulty in obtaining representative samples for carbon analysis. It is concluded that uranium in magnesium-zinc solutions in the concentration ranges of interest for the skull reclamation process possesses good stability at temperatures up to 800 C.

Table 11

STABILITY OF SOLUTIONS OF URANIUM IN ZINC-MAGNESIUM ALLOYS AT 800 C

Charge: Metal Phase: Uranium-magnesium-zinc alloy of indicated composition with constant zinc weight of 3000 g

Flux Phase: 47.5 m/o $MgCl_2$, 47.5 m/o LiCl, 5.0 m/o MgF_2; weight of flux equalled four times weight of magnesium

Equipment: Pressed-and-sintered tungsten crucible; agitator of molybdenum-30 weight percent tungsten alloy. Agitator speed, 360 rpm.

Uranium Condition	Charge Composition (w/o)[a]		Uranium Concentration[b] (% of Theoretical)		
	Uranium	Magnesium	Initial[c]	Final	Average
Low U Conc; Low Activity Coefficient	0.20	0.50	101.5	99.5	100.0
Low U Conc; Moderate Activity Coefficient	0.19	5.08	103.7	99.5	98.4
High U Conc; Moderate Activity Coefficient	4.12	4.88	101.5	103.6	100.5
High U Conc; High Activity Coefficient	3.88	10.31	d	99.7	97.7

[a]Remainder zinc.

[b]By colorimetric analyses of samples taken with sample tubes fitted with tantalum filter tips; estimated accuracy ±5 percent.

[c]After 10-min agitation.

[d]Solution not thoroughly mixed after 10-min agitation.

In the earlier experiments a slight decrease in the uranium concentration near the beginning of the run had been noted. It is probable that this apparent decrease in uranium concentration was the result of unrecognized sampling difficulties which have now been corrected.

g. Supporting Chemical Investigations
(R. K. Steunenberg)

Both liquid metal and molten salt media are used extensively in the pyrometallurgical processing of EBR-II fuel. Consequently, fundamental chemical studies of these systems are needed to supply data for process use and to develop background information necessary for a sufficient understanding of the process variables. Work during the quarter has been devoted primarily to the reactions of uranium oxides in molten salts and to spectrophotometric studies of uranium species in molten chloride solutions.

(1) Reactions of Uranium Oxides in Molten Chloride Media
(M. D. Adams)

Reactions of the three common uranium oxides, uranium dioxide, uranium trioxide, and U_3O_8, with molten lithium chloride-magnesium chloride mixtures are being investigated. The objective of this study is to contribute to the understanding of the reactions of uranium oxides in molten salt systems. The work is an outgrowth of recent fuel-processing investigations which have shown the rate and extent of reduction of uranium oxides in molten salt suspension by zinc-magnesium alloy to be highly dependent on the composition of the salt (ANL-6287, page 51).

The uranium oxides were added to the molten salt, and the resulting mixtures were held for about 30 min at 650 C, then filtered to separate the solid and liquid phases. The solid phases were examined by means of X-ray diffraction. Spectrophotometric techniques were used to investigate the oxidation state of the uranium in the liquid phase.

During the course of the experiments, a new spectrum of uranium was found in molten lithium chloride-magnesium chloride solution. It is suspected that this spectrum represents a uranium(V) species, probably existing in solution as UO_2^+ ion. This species has been found in most of the filtrates from uranium oxide-molten chloride mixtures. It is also observed when magnesium uranate (see ANL-6543, page 48) or uranyl chloride is dissolved in the molten salt. On exposure to air, this species is oxidized rapidly to uranyl ion. There is a possibility that this species results from the thermal decomposition of uranyl chloride. At 850 C, the thermal decomposition of uranyl chloride in molten sodium chloride-potassium chloride eutectic has been shown to produce U_3O_8 and sodium diuranate.[3] The characteristic orange color of this species at high temperatures has been observed repeatedly on addition of uranium oxides to molten salt solutions.

---

[3]Wilks, R. S., A Study of the Mechanism of the Electrolysis of UO_2Cl_2 in Molten NaCl-KCl Eutectic, AERE-R3833 (1961).

Observations of the solid and liquid products of the reactions between uranium oxides and molten chlorides are summarized in Table 12. Since the uranyl ion has no characteristic absorption peaks in the visible and near-infrared spectral range, this species could not be identified by spectrophotometry. The distinctive yellow color of uranyl ion, however, gives a qualitative indication of its presence. It is believed that the uranium(V) species found in the uranium dioxide reaction is a result of traces of uranium(VI) impurity in the starting material.

Table 12

PRODUCTS OF THE REACTIONS BETWEEN URANIUM OXIDES AND MOLTEN LITHIUM CHLORIDE-MAGNESIUM CHLORIDE

Temperature: 650 C
Reaction Time: ~30 min

Solid and liquid phases separated by filtration in quartz apparatus under dry helium atmosphere.

Uranium Oxide	Solid Product[a]	Uranium Species in Solution
UO_3	$MgUO_4$	U(V);[b] traces of U(VI)[c]
U_3O_8	U_3O_{8-x}; $MgUO_4$	U(V)[b]
UO_2	UO_2	traces of U(IV),[c] U(V)[b]

[a]Identification by X-ray diffraction.

[b]Identification by spectrophotometry.

[c]Qualitative identification by color.

Further experimental work has been planned in which an attempt will be made to obtain more information concerning the origin and nature of the species believed to be uranium(V). An effort is also being made to determine the stoichiometry of the uranium oxide reactions implied by the results presented in Table 12.

(2) Molten Salt Spectrophotometry
(D. A. Wenz)

Spectrophotometric measurements in the visible and near-infrared regions are being exploited as a method of observing the reactions of uranium oxides and halides in molten chloride media. A high-temperature furnace assembly, patterned after a unit developed at

Oak Ridge National Laboratory,[4] is used with a Cary Model 14 recording spectrophotometer and is capable of operation at temperatures up to about 900 C. Normal 1-cm, fused quartz square cells are used in the furnace assembly.

Absorption curves for uranium trichloride and uranium tetrachloride in equimolar lithium chloride-magnesium chloride at 650 C have been determined. Reagent-grade lithium chloride was used, and the magnesium chloride was purified by sublimation. The two salts were mixed in a quartz apparatus, melted, sparged with hydrogen chloride at 700 C, evacuated, and filtered through a sintered quartz disc into ampoules. A uranium salt and the purified lithium chloride-magnesium chloride solvent were placed in an apparatus in which they were melted and filtered into an absorption cell, which was then sealed under vacuum. At the completion of the measurements, the salt was analyzed for uranium.

The results are shown in Figure 13. The ordinate is given in arbitrary absorbance units and the values in parentheses represent approximate molar absorptivities. These spectra show the same general features as those reported by Gruen and McBeth[5] for uranium trichloride and uranium tetrachloride in lithium chloride-potassium chloride eutectic at 400 C over the range from 360 to 1300 mμ. A slight irregularity in the shape of the uranium tetrachloride spectrum at 890 mμ in Figure 13 appears to be the result of traces of uranium trichloride impurity. Preliminary measurements indicate that the spectra are affected to a small extent by variations in the ratio of lithium chloride to magnesium chloride in the molten salt solution, and to a much greater extent by changes in the temperature.

Figure 13

ABSORPTION SPECTRA OF URANIUM TRICHLORIDE AND URANIUM TETRACHLORIDE IN EQUIMOLAR LITHIUM CHLORIDE-MAGNESIUM CHLORIDE AT 650 C

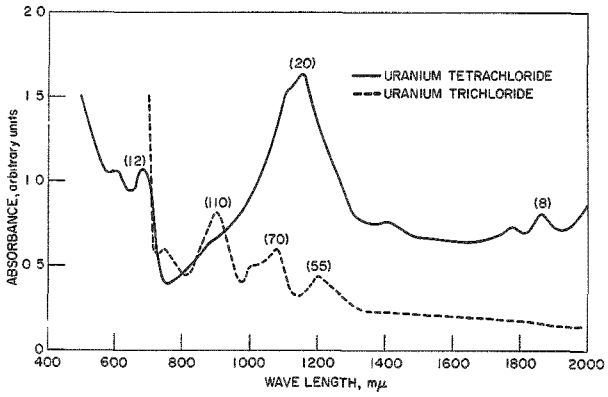

Temp: 650 C

Medium: 1:1 (molar basis) Lithium Chloride-Magnesium Chloride

(Values in parentheses represent approximate molar absorptivities.)

[4] Young, J. P., and White, J. C., A High-temperature Cell Assembly for Spectrophotometric Studies of Molten Fluoride Salts, Anal. Chem., 31, 1892-1895 (1959).

[5] Gruen, D. M., and McBeth, R. L., Oxidation States and Complex Ions of Uranium in Fused Chlorides and Nitrates, J. Inorg. Nucl. Chem., 9, 290-301 (1959).

h. Supporting Engineering Studies
(L. Burris, Jr.)

Engineering studies of liquid metal systems are in progress, principally in the areas of distillation, heat transfer, and mass transfer.

(1) Metal Distillation Studies

(a) Performance of Large-scale Cadmium-distillation Unit
(J. F. Lenc, P. A. Nelson, R. Paul, J. Arntzen)

Operation of the large-scale cadmium-distillation unit (for description, see ANL-6379, page 95) with a pure cadmium feed was continued in order to investigate problems associated with obtaining high distillation rates which may be necessary in future processes. At high distillation rates, the radiation-cooled induction coil will operate at high temperatures (700 to 800 C). In the past, the crucible has been thermally insulated from the induction coil by a Fiberfrax sleeve. In a recent set of runs, the results of which are shown in Table 13, this sleeve was removed, thus permitting the coil to radiate heat to the crucible. It was hoped that this change would increase the power efficiency and also reduce the operating temperatures of the coil. However, little change in power efficiency resulted at power inputs of 20 kw, although the coil temperature was reduced somewhat (from 700 to 655 C).

Table 13

EVAPORATION OF CADMIUM IN LARGE-SCALE DISTILLATION UNIT

Run No.	Distillation Pressure (mm)	Temperature (C)		Power (kw) Calculated from			Evaporator Rate (kg/hr)	Weight of Cadmium Evaporated (kg)	Power Efficiency (%)
		Distillation[a]	Coil	Input	Rate of Evaporation	Losses			
				Induction Coil No. 2 with Fiberfrax Liner					
19	30	555	725	22	8.3	13.7	38.6	264	46.2
20	30	557	700	20	10.1	9.9	36.5	102	48.0
18	60	587	705	20	9.6	10.4	31.4	274	41.5
				Induction Coil No. 2 without Fiberfrax Liner					
21	30	558	655	20	9.1	10.9	34.6	297	45.5
23	30	559	680	25	13.8	11.2	52.7	228	55.4
			710	30	17.6	12.4	68.2		59.5
24	30	559	706	30	17.1	12.9	65.5	224	57.2
25	30	561	760	35	26.8	8.2	102.2	226	76.6
22	60	592	615	19.3	9.0	10.3	34.2	188	45.6

[a] Measured about 8 in. below liquid-metal surface.

As the power input was increased the efficiency of power input also increased. However, the magnitude of the increase in power efficiency resulting from increasing the power input from 30 to 35 kw

Figure 14

EVAPORATION RATE AS A FUNCTION OF POWER INPUT LARGE-SCALE CADMIUM DISTILLATION UNIT

(Induction Coil No. 2 without Fiberfrax Liner. Distillation Pressure, 30 mm Hg abs.)

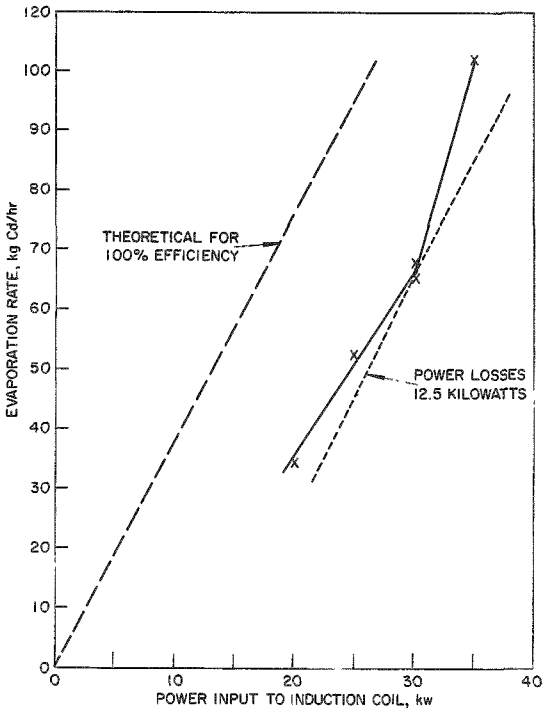

is questionable. This change in power input resulted in a decrease in the calculated power losses from 12.9 to 8.4 kw despite the increase in coil temperature from 706 to 760 C. Figure 14, a plot of the results of Runs 21 through 25, graphically illustrates the abrupt change in the slope of the curve of evaporation rate versus power input which takes place at 30-kw power input. The fact that the curve is approaching 100 percent efficiency more closely as the power input is increased illustrates the decrease in calculated power losses. A more plausible explanation of the relatively low power losses at the highest power input (in Run 25) is that the measured rate of cadmium evaporated included a significant amount of cadmium entrained as a liquid.

In order to determine whether liquid cadmium is being entrained, an experiment is planned in which a known amount of tin will be added directly to the distillation crucible. Since the vapor pressure of tin is extremely low at the distillation temperature (555 to 560 C) to be used, tin will be transferred from the distillation crucible to the distillate receiver only by entrainment in cadmium vapors. From periodic analyses of the distillate for tin, it will be possible to ascertain the magnitude of any entrainment which might occur. Suitable de-entrainment devices may then be designed and tested.

(b) Study of Mechanisms of Liquid Metal Boiling and Entrainment
(J. Wolkoff, R. E. Nowak)

The formation and entrainment of droplets by the vapor phase during the boiling of liquid metals has received little or no fundamental study. Aqueous systems have been studied and their entrainment mechanisms are reasonably well understood. Because of large differences in physical properties between liquid metals and water, e.g., thermal conductivity and surface tension, the nature and magnitude of the boiling and entrainment phenomena in liquid metals may differ significantly from those of water.

Since entrainment is intimately connected with the mode of boiling, the phenomenon of nonturbulent boiling (vaporization from the surface without bubble formation) is initially under study. Pure mercury is being boiled, condensed, and recirculated in a closed, all-glass system. The boiling surface is visible for study and photography.

From condensation-rate measurements, vaporization rates at the top surface of the mercury pool up to 55,000 Btu/(hr)(sq ft) [2.1 lb-moles of mercury/(hr)(sq ft)] have been attained with resistance heating under low pressure (less than 1 mm). This value is higher than data reported for normal boiling of mercury from nonwetted surfaces.[6]

The nonturbulent vaporization changed to irregular bumping when the heating rate was further increased. Other methods of heating the boiler and the effect of agitation will be investigated.

(2) Studies of Mass Transfer in Liquid Metal Systems

(a) Mass Transfer from Solids in Agitated Liquid Metal Systems

(R. D. Pierce, S. A. Miller,* D. R. Armstrong,** and M. R. Cusick**)

A fundamental investigation of mass transfer in agitated liquid metals is underway. This program was planned to provide data on mass transfer in agitated liquid metals comparable with existing data for more conventional liquids. It is hoped that general correlations of the data can be made in a form suitable for scale-up and extrapolation to other systems. Initially, the factors influencing the rate of dissolution of small cylinders of uranium in cadmium is being determined. During the past quarter, a brief preliminary study was made of the mixing of solid particles of various densities in water, methanol, and carbon tetrachloride to provide guidance in the selection of agitator and vessel designs for the liquid metal studies. With a number of different agitators and baffling arrangements, the stirring speeds at which solids began to be suspended and at which suspension was complete were recorded.

For a particular impeller speed and a particular system, a cylindrical, flat-bottom, baffled vessel with a downward-deflecting marine propeller was the most efficient geometry investigated

---

[6]R. E. Lyon, A. S. Faust, and D. L. Katz, Chem. Eng. Prog. Symp. Series, 51, No. 17 (1955).

*Consultant and summer professor from Rochester University.

**Temporary student employees.

for suspending particles. The optimum propeller diameter was found to be about one-half the vessel diameter. The agitator speed which provided corresponding results, i.e., the same degree of particle suspension in different systems, was found to be proportional to

$$\left(\frac{\rho_{solid} - \rho_{liquid}}{\rho_{liquid}}\right)^{1/2} ,$$

where ρ represents density.

Equipment is now being prepared for measurements of the rates of dissolution of $\frac{1}{4}$-in. uranium cylinders in cadmium under various agitation conditions. Cylinders were selected because of their simple geometry as well as ease of fabrication. Small uranium spheres will also be employed in later runs. The uranium cylinders have been prewetted with zinc to insure an oxide-free surface for dissolution. Zinc was found to wet uranium readily (inconsistent wetting was obtained with cadmium) and to dissolve quickly when immersed in molten cadmium.

A dynamometer has also been built to determine the mixing power input to liquid metals. Since the instrument is sufficiently sensitive to be used with conventional fluids, it will be used also with aqueous systems to permit checking against the established correlations.

(3) Determination of Uranium Diffusivity in Liquid Zinc
(J. C. Hesson, H. Hootman, G. Rogers)

The capillary-bath technique has been used to determine the diffusivity of uranium in liquid zinc. The diffusivity was found to range from 1.5×10^{-5} sq cm/sec at 625 C to 2.7×10^{-5} sq cm/sec at 800 C, with estimated accuracies of ±15 percent.

The capillary-bath technique used in this study consists of immersing a capillary tube filled with a uranium-zinc solution in a molten bath of zinc containing a negligible amount of uranium. The capillary is closed at its lower end and open at its upper end. During the immersion period, the uranium diffuses from the open upper end of the capillary into the bath. After a predetermined time period, the capillary is removed from the bath and cooled. The diffusivity is calculated from the initial and final uranium contents of the capillary and the bath, the length of the capillary, and the diffusion time. The unsteady-state diffusion equation used to correlate the data was

$$\frac{C_0 - \overline{C}}{C_0 - C_s} = 1 - \frac{8}{\pi^2}\left[e^{-\theta} + \frac{1}{9}e^{-9\theta} + \frac{1}{25}e^{-25\theta} + \ldots\right] ,$$

where

C_0 = initial capillary uranium concentration

$\overline{C}$ = final capillary uranium concentration

C_s = uranium concentration in bath

$\theta = \frac{\pi^2}{4} \frac{Dt}{L^2}$

D = diffusivity

L = length of capillary

t = time of the diffusion.

For values of Dt/L^2 less than 0.25, the above equation simplifies to:

$$\frac{C_0 - \overline{C}}{C_0 - C_s} = \left(\frac{4}{\pi} \frac{Dt}{L^2}\right)^{1/2} .$$

The experiments were conducted in a vertical $2\frac{1}{2}$-in.-ID by 24-in.-long stainless steel bomb which was previously described in ANL-6477, page 69. The flanged cover of the bomb contained openings for a thermowell, a sampling port, and the capillary-support rod. The bomb was heated by a 13-in.-long resistance furnace. The upper section of the bomb was water cooled by means of an external copper coil. The primary crucible material was recrystallized alumina, and the secondary crucible was made of stainless steel.

The capillary tubes were made of $\frac{3}{16}$-in.-OD tantalum tubing with a 0.01-in. wall thickness. Each tube was filled by fitting a graphite filter to a 6-in. length of tubing, immersing the end fitted with a filter into a molten uranium-zinc solution, and forcing the melt into the tube by pressurization. The filled tube was then quickly withdrawn and cooled. The tubing was cut into alternate sections which were one inch and $\frac{3}{8}$ in. long. The one-inch length was faced and used as the capillary tube after a tantalum cap had been force-fitted over the bottom end. The zinc and uranium in the $\frac{3}{8}$-in. sections were dissolved and analyzed to determine the uniformity of uranium concentration in the capillary sections.

During a diffusion run, the capillary was repositioned in the bath by rotating the holder slightly every 2 min to avoid "end effect," a localized concentration of uranium at the end of the capillary due to diffusion of uranium from the capillary.

The results of the experiments are shown in Table 14 and Figure 15. In the region of values of Dt/L^2 employed in these experiments, the errors in uranium analysis cause errors which are three or four times greater in the diffusivity values. The overall accuracy of the diffusivity values is estimated to be ±15 percent.

Table 14

DIFFUSION OF URANIUM IN LIQUID ZINC, CAPILLARY-BATH METHOD

Temp (C)	Length[a] of $\frac{3}{16}$-in.-OD capillary (cm)	Time (sec)	Uranium Concentration (w/o)			Computed Values	
			C_0	C_s	$\overline{C}$	Dt/L^2	$D \times 10^5$ (sq cm/sec)
625	2.52	86,400	0.261	0.000	0.134	0.190	1.41
625	2.56	86,400	0.245	0.001	0.122	0.200	1.53
700	2.49	86,400	0.660	0.042	0.289	0.285	2.04
700	2.52	64,800	0.896	0.000	0.432	0.210	2.07
700	2.57	64,800	0.694	0.002	0.374	0.165	1.70
800	2.61	64,800	0.968	0.000	0.396	0.280	2.95
800	2.50	57,600	0.657	0.004	0.298	0.240	2.61
800	2.56	57,600	1.200	0.008	0.506	0.265	3.01

[a] At run temperature.

The experimental values of diffusivity, plotted in Figure 15 appear to be lower than would be expected from the Einstein-Stokes equation if 2.842 Å is used for the diameter of the uranium atom. A similar relationship was found between the predicted and experimental values in the uranium-cadmium system (ANL-6477, page 73).

Figure 15

DIFFUSIVITY OF URANIUM IN ZINC AS A FUNCTION OF TEMPERATURE

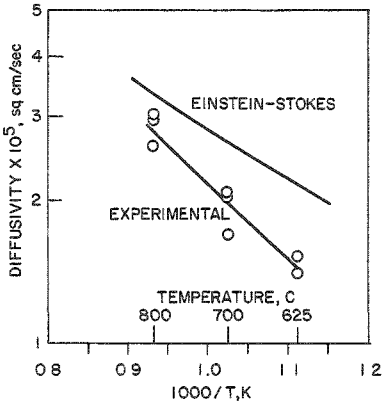

Uranium diffusivities will be measured in other metal solvents: bismuth, aluminum, and magnesium.

3. Reactor Materials
(R. K. Steunenberg)

Pyrometallurgical procedures offer considerable promise as simple, low-cost methods for producing nuclear fuel materials. Refractory compounds of interest as high-performance reactor fuels are conveniently synthesized by adding carbon, silicon, or other elements to liquid metal solutions of the actinide metals. The product precipitates from the solution and is recovered by appropriate phase-separation and retorting techniques. An effective method for the preparation of metallic fuel materials is the direct reduction of actinide oxides and fluorides suspended in a molten halide flux by liquid metal solutions containing magnesium. The present work is concerned with the preparation of uranium monocarbide and the production of thorium metal directly from the oxide.

a. Preparation of Uranium Monocarbide

(T. R. Johnson, R. D. Pierce, J. F. Lenc, R. L. Christensen, J. R. Pavlik, M. A. Bowden)

The Chemical Engineering and Metallurgy Divisions are cooperating in the development of liquid metal techniques for the preparation of uranium monocarbide and in the evaluation of the sinterability and utility of the product as a potential high-performance reactor fuel.

Three additional runs, P-10, P-11 and P-12, have been completed. (Results of eight of the preceding runs were reported in ANL-6543, page 62.) The reaction conditions and analytical data on the product are summarized in Table 15. Besides the use of sodium as a wetting agent for carbon in two of the runs, the major differences between the last three runs and the nine previous runs in the series were: (1) the activated charcoal used as a carbon source was degassed more thoroughly to reduce the possibility of oxygen contamination, (2) the uranium-zinc-magnesium alloy was prepared in a separate step to eliminate a possible reaction of carbon with the solid uranium, (3) the reaction temperatures were lowered to reduce the volatilization of sodium from the system, and (4) the carbon-to-uranium ratios in the charges were decreased in order to reduce the free carbon content of the product. In the previous runs the activated charcoal, uranium, zinc, and magnesium were charged directly to the furnace. The charcoal had not been degassed previously, but was heated to about 400 C under vacuum immediately prior to the reaction.

Table 15

SUMMARY OF URANIUM CARBIDE PRODUCTION RUNS. EXPERIMENTAL CONDITIONS AND PRODUCT ANALYSES

		Run No.		
		P-10	P-11	P-12
Charge	Uranium (g)	300	302	306
	Magnesium (g)	549	540	533
	Zinc (g)	2159	2165	2155
	Sodium (g)	39	-	35
	Carbon[a] (g)	19.4	18.9	17.0
	C/U (atom ratio)	1.28	1.24	1.10
Reaction Conditions	Temperature (C)	750[b]	750	760
	Time (hr)	5.5[b]	7.5	4.5
	Stirring (rpm)	500	550	600
	Charge to Retort (g)	1605	1516	2124
	Weight of Recovered Product (g)	305.7	320.5	320
Analytical Results on Product	C (w/o)	5.3 ± 0.1[c]	5.52 ± 0.02[c]	5.2 ± 0.2[c]
	O (w/o)	1.58	0.94	0.59
	C/U[d] (atom ratio)	1.18	1.18	1.11

[a]Degassed activated charcoal used.

[b]After 5.5 hr at 750 C, the melt temperature was raised to 820 C for 2 hr. During this period the stirring rate was 320 rpm.

[c]Average of two analyses.

[d]Based on an estimated uranium content.

In the last three runs, the activated charcoal was first degassed at 800 C under vacuum for 2 to 3 hr. The uranium-zinc-magnesium alloy was prepared in a separate step in a baffled tantalum crucible and was allowed to freeze in place. In preparation for the reaction step, the degassed charcoal and a freshly cut piece of sodium were transferred to the crucible with argon blanketing and were placed on top of the solid ingot. The crucible was placed in a furnace and the reaction was carried out in an argon atmosphere at 750 C. Stirring was accomplished by a flat tantalum paddle which was $\frac{7}{8}$ in. high and $1\frac{3}{4}$ in. wide. At the end of the reaction time the melt temperature was lowered to about 580 C. At this temperature solid $MgZn_2$ precipitates from this system, and it appears to carry down the suspended particles of uranium carbide product. The supernatant liquid was then removed by pressure siphoning, and a mixture of $MgZn_2$ and uranium carbide was left in the crucible.

The crucible was removed from the furnace and placed in the retort. Retorting consisted of gradually lowering the pressure to about 0.001 mm Hg and raising the temperature to about 830 C. The retorting operation usually required 6 hr. After retorting, the furnace was opened and the tantalum crucible containing the uranium monocarbide as a loose cake was removed and transferred with argon blanketing to a helium-filled glove box.

Since the retorting equipment must eventually be exposed to air after removal of the uranium carbide product, the presence of sodium in the magnesium-zinc distillate was considered to be a potential hazard. For this reason the melt temperature in Run P-10 was raised to 820 C after 5.5 hr of reaction time at 750 C in an attempt to distill off some of the sodium. This procedure, however, proved to be both ineffective and unnecessary, and no attempt was made to remove the sodium prior to retorting in Run P-12.

Runs P-10 and P-11 were made under similar conditions except for the variation described above and the 1.3 percent sodium added in Run P-10. No sodium was used in Run P-11. The times required for the reaction were quite similar, as shown by the uranium contents of filtered samples of the liquid metal taken periodically during the runs. Thus, it appears that sodium had little or no effect on the reaction rates, whereas in earlier, smaller-scale experiments, sodium accelerated the reaction (ANL-6543, page 59).

Analytical results on the products of the three runs are shown in Table 15. The higher oxygen content of the product from Run P-10 is very likely a result of difficulties in removing the crucible from the retort. The crucible was noticeably warm when it was removed from the cool retort, suggesting that the relatively long time required for the operation resulted in serious air contamination of the argon blanket. The

product from Run P-12 is the best material produced to date. It had the lowest oxygen content and the closest to stoichiometric carbon-to-uranium ratio of any material made from activated charcoal on this scale. One batch of carbide prepared from powdered graphite in an earlier run (Run P-8, ANL-6543, page 62) contained only 0.39 weight percent oxygen, but it had a high carbon content and could not be sintered. On a smaller scale (30 g uranium), a carbon-to-uranium ratio of 1.01 has been achieved.

Although further work is needed to develop a satisfactory procedure for process use, several tentative conclusions can be drawn from the results obtained to date:

(1) Although the results of Run P-11 cast doubt on the beneficial effects of sodium, the smaller-scale studies have indicated that it enhances the reaction rate and permits a closer control of the carbon-to-uranium ratio of the product. Further investigation of the use of sodium is considered desirable.

(2) The reaction conditions used in Run P-12 are believed to be close to optimum for this method of uranium carbide preparation. Somewhat longer reaction times may be required for lower carbon-to-uranium ratios in the charge.

(3) Of the various methods for separating the excess zinc and magnesium from the system, the technique of freezing part of the melt to hold the uranium carbide during siphoning seems to be the most satisfactory. This method separates the carbide effectively from the bulk of the metal and results in excellent product yields. It is not effective, however, in separating the carbide from unreacted carbon. The desired carbon-to-uranium ratio of the product must be controlled by the composition of the charge.

(4) Free carbon and oxygen are the most serious contaminants in the product, since they interfere with the formation of dense sintered bodies. It is believed that both of these impurities can be reduced to acceptable levels through refinements of the procedure. Although argon-blanketing techniques have been used in handling and transferring the product, they appear to be inadequate for the finely divided, highly pyrophoric material. Equipment is being obtained in which the operations can be conducted in high-purity inert gas atmospheres. Techniques are also being developed to reduce the oxygen content of the starting materials to the lowest possible levels. It appears that contamination with free carbon can be controlled by the carbon-to-uranium ratio in the charge. The addition of sodium also appears to aid in obtaining the desired carbon content in the product.

b. Reduction of Thorium Dioxide
(A. V. Hariharan,* J. B. Knighton)

The objective of this program is to develop a practical method for the direct reduction of thorium dioxide to the metal, by means of the liquid metal-flux technique. Previous investigations (ANL-6543, page 46) have established the optimum region of flux composition in the system, calcium chloride-magnesium chloride-calcium fluoride, for effective reduction of thorium dioxide by a zinc-five weight percent magnesium solution. The data indicated that a minimum magnesium chloride concentration of about 50 mole percent and a calcium fluoride concentration between 7 and 15 mole percent are necessary to achieve complete reductions in 3 to 4 hr at 750 C.

Some difficulty has been experienced with lowered yields and erratic results. The factors suspected of causing the difficulty were (1) the source of the thorium dioxide, (2) the materials used in the apparatus, and (3) impurities in the flux, including moisture in the air. No detectable difference in the reducibility of calcined and uncalcined thorium dioxide was found. The use of Vycor instead of quartz stirrers led to corrosion and considerable scatter of results, which was probably caused by the formation of a thorium-silicon compound. Quartz is not attacked and, when used, yields consistent results. The possible effect of flux impurities was examined by using analytical reagent-grade materials from various sources. It is strongly suspected, but not proved experimentally, that the humidity in the ambient air was the factor causing the low yields and erratic results. Successful reductions had been obtained consistently during the fall and winter when the absolute humidity was low.

The use of an inert atmosphere and tantalum equipment has eliminated the inconsistencies in the results, and it is believed that these precautions should be taken in production applications of the process.

In four confirmatory experiments with selected flux compositions in the optimum region, the anticipated complete reduction of thorium dioxide was obtained. The flux compositions used were as follows:

40 m/o $CaCl_2$-50 m/o $MgCl_2$-10 m/o CaF_2

37 m/o $CaCl_2$-50 m/o $MgCl_2$-13 m/o CaF_2

26 m/o $CaCl_2$-60 m/o $MgCl_2$-14 m/o CaF_2

27 m/o $CaCl_2$-65 m/o $MgCl_2$-8 m/o CaF_2.

These experiments utilized an argon-atmosphere, tilt-pour furnace with a baffled tantalum crucible and a tantalum stirrer. In all four experiments, the thorium dioxide was completely reduced to the metal in 3 hr at 750 C with a mixing rate of 800 rpm.

*Affiliate, International Institute of Nuclear Science and Engineering.

Following optimization and confirmation of the flux composition, a study of the process variables will be made: temperature, mixing rate, thorium dioxide loading in the flux, thorium loading in the metal, magnesium oxide loading in the flux, and magnesium concentration in the metal.

B. Fuel Processing Facilities for EBR-II

A direct-cycle fuel reprocessing plant based on pyrometallurgical procedures was designed and is being constructed as part of the Experimental Breeder Reactor No. II (EBR-II) Project. A Laboratory and Service Building is also included. Melt refining, liquid metal extraction, and processes involving fractional crystallization from liquid metal systems are methods being examined for the recovery and purification of EBR-II fuels. Based on these studies, process equipment is being designed and tested.

1. Design and Construction
(J. H. Schraidt, M. Levenson)

a. Status of Fuel Cycle Facility Building Design and Construction
(E. J. Petkus, H. L. Stethers, J. H. Schraidt)

The remaining construction work for the Fuel Cycle Facility and the equipment installation work are being done by the J. F. Pritchard Company under a cost-plus-fixed-fee contract (see ANL-6543, page 77). An exception to this is the correction of voids under the Air Cell floor, which the original construction contractor, Diversified Builders, Incorporated, chose to do with his own labor. These voids, which were as much as 42 in. deep, are believed to have been caused by water washing the earth fill into porous lava, the basic substratum in the area. A water main broken during construction was the probable source of the water. These voids, if not corrected, would have caused a serious loss of radiation shielding, structural uncertainty, and increased probability of corrosion damage to buried piping. The voids have been filled by Diversified Builders, Incorporated. The method of filling consisted, first. of pumping silica sand and grout into the voids and then pumping grout.

No special precautions were taken to prevent corrosion of the black iron-pipe storage pits beneath the Air Cell floor because compacted backfill of controlled moisture content was specified for this location. As a result of the prolonged contact of the pipes with the moisture associated with the void formation, however, extensive corrosion has occurred in the storage-pit system. Efforts are being made by Argonne National Laboratory to minimize this corrosion by the use of buried magnesium anodes to provide galvanic protection.

Cleaning and relubrication of the Argon Cell cranes and manipulators (ANL-6543, page 80) has been completed. One manipulator has been placed in operation in the Argon Cell and is being used to train operators and for installation of "in-cell" equipment.

The hanging bridge wheels installed on the cranes in the Argon Cell were not suitable for traveling on the circular rail because of the spherical, self-aligning roller bearings with which the wheels were provided. When the bridges of the cranes were moved, these hanging wheels locked. The wheels have been redesigned, using a double-row, deep-groove ball bearing in each wheel. The design has been approved and the wheel assemblies have been sent to the crane manufacturer for required alterations.

The electrical, sliding collector assemblies for the cell cranes have been modified and returned to Idaho. These collectors supply power to the crane bridges from slip rings mounted around the center of the Argon Cell. Similar assemblies supply power to the trolleys from bus bars mounted on the bridges. The collector brushes are spring loaded and each brush is guided by two pins. The brushes, as originally furnished, would bind when subjected to the slightest side pressures rather than adjust to the inaccuracies in alignment of the bus bars and the rails. The binding increased the load between collector brushes and bus bars, particularly when a trolley was placed on a bridge.

The collector assemblies as made by the fabricator did not conform to the drawings. Holes were not drilled parallel, plates were warped, and loose fits between guide pins and backup plates made the assembly faulty and contributed to the binding tendencies. The assemblies have been modified and made to conform with the drawings. Collector assemblies should now be interchangeable. Modifications made to the collector assemblies were as follows:

(1) Brass guide sleeves, $2\frac{1}{4}$ in. long, were pressed into the support plates. This changed the guiding length from $\frac{3}{4}$ to $2\frac{1}{4}$ in.

(2) Springs and backup plates were replaced with new ones.

(3) The collector brush clevises were ground flat where they are supported on the ceramic insulators.

(4) The guide pins were coated with molybdenum disulfide before assembly.

These modifications, as well as the changes made so that the assemblies conform to the drawings, have greatly improved the operation of the collector assemblies.

The control circuits for the cell cranes and the crane and manipulator removal hoist have been modified. In the original installation the voltage drop in the control wires was excessive, which made the relays in the control cabinets inoperable. A review of the control system revealed, also, that the transformers that supply the control currents were too small. The wiring system was copied to some extent from the system used for the manipulators. The current required for the relay coils for the crane and removal hoist controls is much greater than the current required for manipulator controls. The required control current is about 8 amp for the hoist and about 11 amp for the cranes, whereas the control current for the manipulator is about 1.5 amp. The length of cable between the control relay and the most distant operator control station is 220 ft. The 220-ft control cable has a resistance of 2.85 ohms (wires are 18 AWG) and, therefore, the required control currents would cause the following voltage drops:

Manipulators	4.3 v
Cranes	31 v
Removal Hoist	23 v

The supply voltage in each case is only 24 v. On the basis of the above analysis it was decided that the manipulator circuits were adequate, but that the circuits of the removal hoist and the cranes required modifications.

Corrective measures to the four control circuits involved consisted of the following changes:

(1) The 100-VA control transformers were replaced with 300-VA transformers.

(2) The existing circuit breakers were replaced with breakers with a higher rating.

(3) In each control circuit a relay was added and a few wiring changes made so that the current for most of the relay coils bypasses the control cables to the operator's control stations. This change reduces the current requirements for individual control cable wires to a maximum of 0.8 amp for the removal hoist and 1.5 amp for the cranes.

In addition to the above changes, errors in wiring made by the installation contractor have been corrected, and the control system is now operating satisfactorily.

The oil-filled tank units for the shielding windows are being repaired to correct oil leaks (see ANL-6543, page 83). The R. V. Harty Company, a subcontractor of the window supplier, has repaired and installed

approximately two-thirds of these units. None of the remotely removable glass sections have been installed, because it is desirable for training purposes and for compliance purposes to install these sections under remote operating conditions by means of cranes and manipulators.

The furnace for degassing of process materials has been installed, successfully leak tested, and released to the operations group.

Installation of a jib crane on the roof of the Argon Cell has been completed. This crane is being used to move heavy equipment through roof hatches into the Air and Argon Cells.

Steel shielding is being constructed around the off-gas delay tank. Radioactive gases from the melt refining and skull oxidation furnaces will be stored in this tank until meteorological conditions permit the discharge of the gases through the stack provided at the EBR-II site. One thousand pounds of National Grade ACC* activated charcoal was added to the tank as an additional iodine and a xenon trap.

Preparations are being made for the installation of two argon compressors on the service floor. Each compressor can deliver 60 scfm at 120 psig. These machines will be used to compress cell argon for re-use with pneumatic equipment, such as drive cylinders and ring gauges in the Argon Cell.

Installation of transfer lock equipment and components is underway. There are two types of locks used to transfer materials between the Air Cell and the Argon Cell, a single large transfer lock mounted vertically in the Argon Cell floor, and two small transfer locks mounted horizontally between the Air Cell and the Argon Cell.

The large transfer lock is basically a 6-ft-diameter cylinder, 8 ft long. It is composed of three major sections. The upper section consists of a spool piece with a counterbalanced hinged lid which is sealed by a lead gasket. This section is bolted to the middle section, which penetrates the 4-ft-thick cell floor. A steel ring gasket is used to seal the upper to the middle section. The bottom of the lock is a steel platform which can be elevated by a hydraulic ram and seals to the lower flange of the center lock section with a rubber O-ring. The load capacity of the lift is 5 tons. The platform and ram are part of the Transfer Cell equipment on the service floor which moves material from an opening in the Air Cell floor to the large transfer lock. Other components of this equipment are the transfer cart, which carries the platform between the two loading points, and a second ram, which raises the platform into the Air Cell.

*A product of the National Carbon Company.

The small transfer locks consist of two horizontal rectangular tubes which pass through the 4-ft shielding wall between the Air Cell and the Argon Cell. Material is transferred in small carts which ride on rails mounted inside the locks. Direction of travel is determined by the slope of the rails, which can be changed remotely with the operating manipulator. Items 2 ft high and 1 ft in diameter may be transferred. Special end fittings are bolted to each end of the locks to permit loading and unloading the carts. Hinged lids sealed by rubber gaskets are used to close the openings in the lock ends.

Defects have been discovered on most of the gasket surfaces of the above components, and these are now being repaired. Leaks in welds in the small lock end pieces have been discovered, and these welds are also being repaired.

All of the covers on the locks are opened by means of small motor-driven winches mounted on the cell walls. These motors are currently being installed.

b. Fuel Cycle Facility Equipment
(G. Bernstein, A. Chilenskas, L. Coleman, J. Graae, T. Eckels, M. Slawecki, H. Stethers)

Two 20-ton fuel-transfer coffins are being designed for use in transporting fuel subassemblies between the Reactor Building and the Fuel Cycle Facility. Both designs provide for removal of fission product heat from the subassembly by means of a circulating stream of argon. In one coffin, which is to be designed and supplied by O. G. Kelley and Company of Boston, Massachusetts, the argon stream is cooled by passing it through a gas-to-air heat exchanger. The design under development by the Chemical Engineering Division of Argonne National Laboratory provides for transferring the heat from the argon stream into the lead body of the coffin.

Crucibles and fume traps will be brought into the Argon Cell in batches. It is planned to store these on racks placed next to the outside walls between the shielding windows. Racks with slides and portable shelves are being developed for this purpose. Figure 16 shows a prototype rack with a single shelf. The shelf, loaded with six crucibles, is being rolled out of the rack on suspension slides by means of a tool grasped in the double hook of the prototype operating manipulator. When in the "out" position, the shelf can be lifted from the slide by the manipulator.

Services are brought into the Argon Cell by means of removable feed throughs installed and sealed in sleeves which penetrate the

Figure 16

PROTOTYPE RACK WITH CRUCIBLE STORAGE SHELF

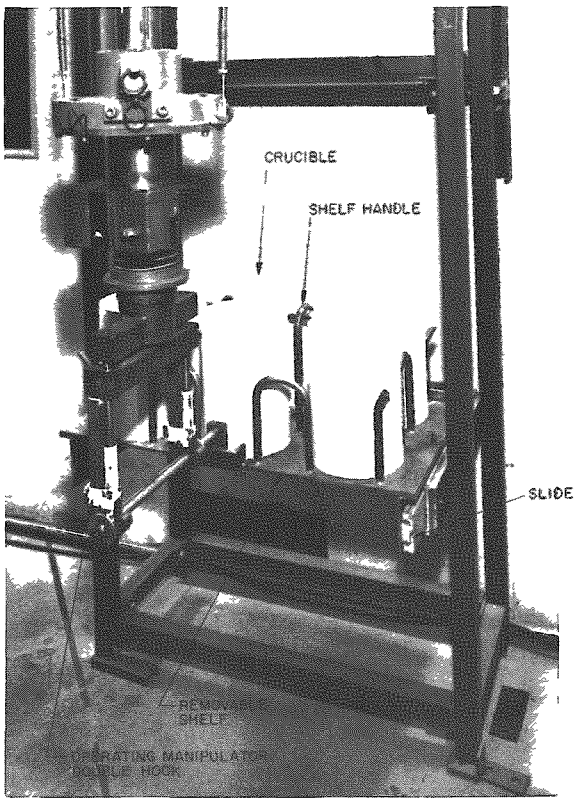

floor of the cell. The feed throughs have previously been described in ANL-6231, pages 35 to 37. Fifty-seven of the required 65 feed throughs have been completed and shipped to Idaho by the vendor. Included in the 57 are 20 blind feed throughs or plugs for sleeves located where services will not be needed initially. The assembly of the remaining eight feed throughs, which are to be used for electrical and thermocouple services, was delayed because of problems encountered in conductor insulation resistance. The insulation resistance between conductors of a twisted-pair signal cable in one type of feed through was found to be as low as 250,000 ohms, as compared with the specified resistance of infinity. The asbestos sleeving used in the cable as insulation is suspected of being the source of trouble. Samples of the asbestos sleeving showed very low resistance, even after heating for 2 hr at 100 C. Resistances of the samples ranged from 100,000 ohms before heating to about 2 megohms after heating. The twisted pair will be used for circuits where the low insulation resistance is acceptable. The vendor has been notified that the assemblies would be acceptable if the insulation resistance of the twisted asbestos wires were 250,000 ohms, conductor to conductor, and 1.0 megohm, conductor to ground.

Installation of the feed throughs in the Argon Cell of the Fuel Cycle Facility has started. Figure 17 is a view in the Argon Cell showing a bank of five feed throughs. Shown are a pneumatic, an induction heating, an electrical and thermocouple, and two $2\frac{1}{2}$-in. vacuum feed throughs. Jumpers from these and other feed throughs will connect equipment to services brought into the Argon Cell.

Figure 17

ARGON CELL SERVICE FEED THROUGHS. BANK OF FEED THROUGHS - CELL SIDE

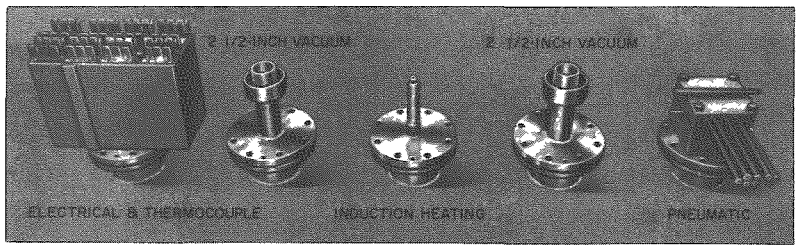

Figure 18 is the same bank of feed throughs shown from beneath the Argon Cell. Figure 19 is a closeup view of the sealing mechanism used on all but the blind feed throughs. Primary sealing is accomplished by tightening the bolts shown in Figure 19 and drawing the feed through down against a copper gasket located between the top flange of the feed through and the top flange of the sleeve (see Figure 17). A secondary seal on the bottom is made with the use of two rubber O-rings located on the middle flange shown in Figure 19. One O-ring bears against the bottom flange of the sleeve, while the other is against the outer diameter of the feed through. Expansion and contraction of the feed through, while in use, is provided for by the use of Belleville spring washers. Figure 20 shows a feed through being lowered into a sleeve by the operating manipulator. All feed throughs can be removed and replaced remotely with the manipulators or cell cranes.

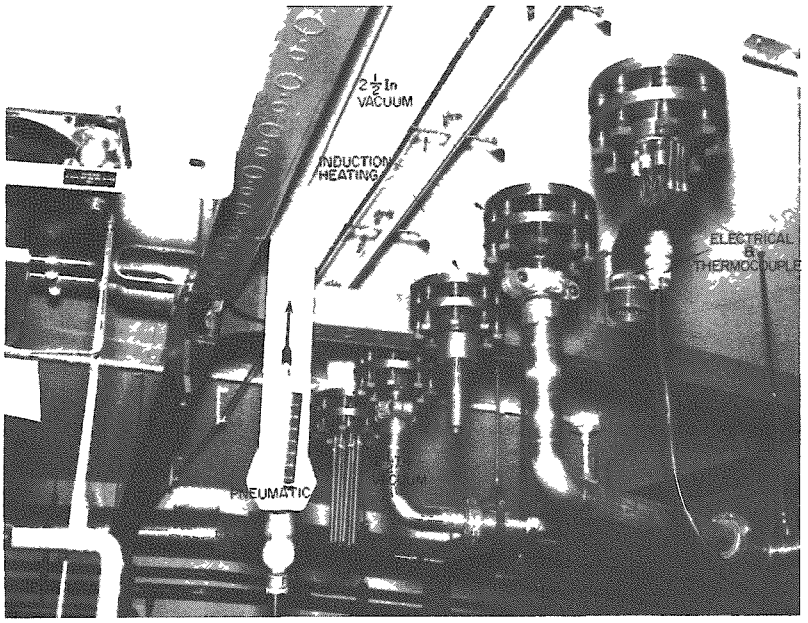

Figure 18

ARGON CELL SERVICE FEED THROUGHS. BANK OF FEED THROUGHS - SUBCELL SIDE

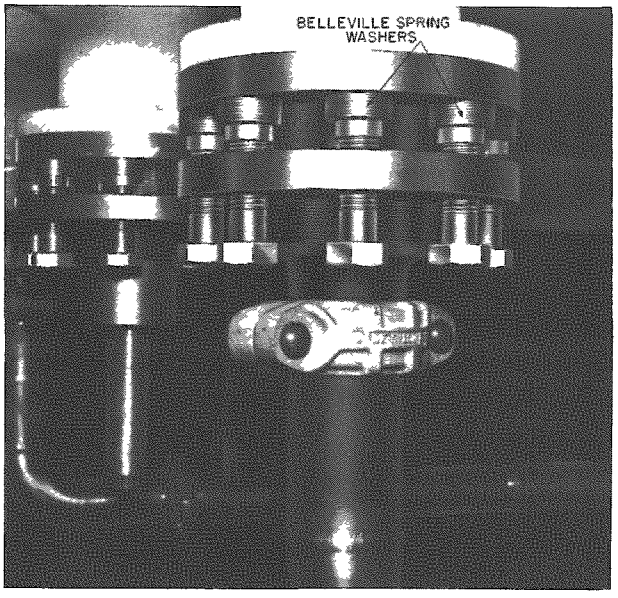

Figure 19

ARGON CELL SERVICE FEED THROUGHS. FEED THROUGH SEALING MECHANISM

The gas-sampling method for the suspect stack-monitoring system has been modified. This system measures the activity of the gas flowing into the stack at the EBR-II site. The original design utilized two horizontal sampling nozzles, one located on each side of the duct between the stack and the "Y" connection to the two stack fans (only one fan operates at a time). The possibility of using a single vertical nozzle instead of two horizontal nozzles was studied and looked promising. Various tap locations along the top of the duct were utilized to make measurements of velocity profile. A tap location was chosen and a single nozzle will be used. This nozzle penetrates 18 in. in from the top of the 5-ft-diameter duct and is located about 2 ft closer to the stack than the planned location of two original nozzles. Use of one nozzle will simplify the sampling system by eliminating two motor-operated valves and extra piping.

Figure 20

ARGON CELL SERVICE FEED THROUGHS. LOWERING A FEED THROUGH INTO A SLEEVE

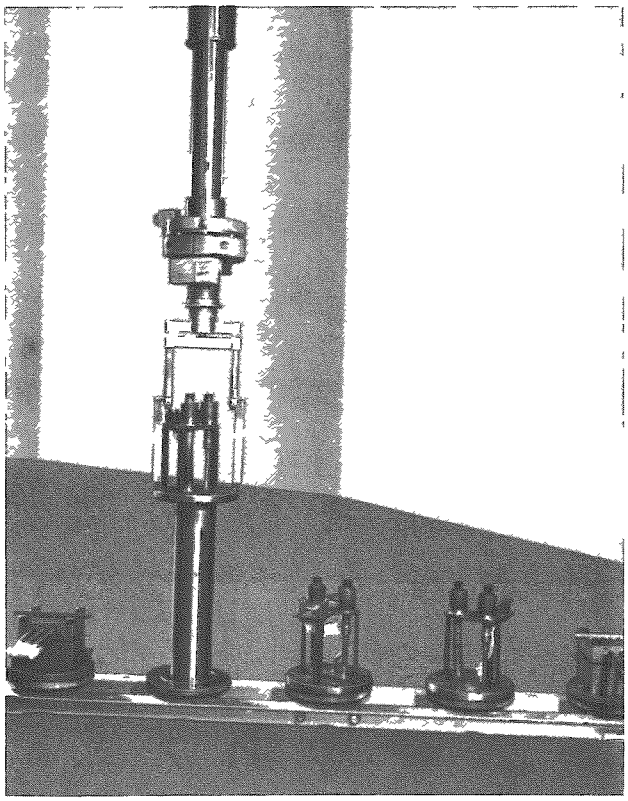

One of the most troublesome problems in the use of remotely controlled manipulators in a large hot cell is the perception of depth. The lack of any sense of "feel" in the manipulator increases the importance of depth perception to avoid serious damage to equipment. Although most operations of the fuel-reprocessing cycle itself are conducted within about 5 ft of a shielding window (10 ft from the operator), some routine cell maintenance operations have to be accomplished at distances up to 24 ft from the operator. To furnish magnification and to enhance depth perception, a prototype instrument was designed and built late in 1957 (see ANL-5858, page 118, and ANL-5959, page 163).

The unit has been redesigned (see Figures 21 and 22) to increase its light efficiency by about 50 percent, to decrease its weight from $16\frac{3}{4}$ to $11\frac{1}{2}$ lb, and to incorporate draw tube focusing for the eyepieces. The last feature makes it possible to focus on objects at distances from infinity to 5 ft away. Commercially available binoculars, such as were used in the prototype, can only cover this range by changing three adapter spacers. Specifications and drawings are being prepared for the fabrication of four stereo-optical depth perceptors of improved design.

Figure 21

STEREO-OPTICAL DEPTH PERCEPTOR
SCHEMATIC PLAN VIEW
(AXIAL RAY TRACE)

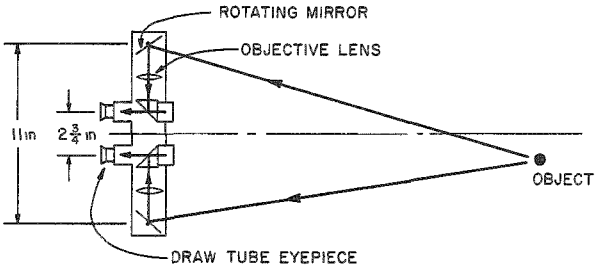

Figure 22

STEREO-OPTICAL DEPTH PERCEPTOR. PERSPECTIVE VIEW OF RIGHT HALF ONLY

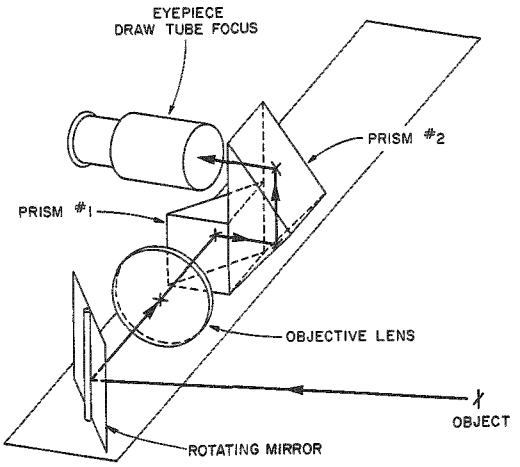

Four wide-angle viewers have been ordered for use in existing sleeves in the roof and through the wall of the Argon Cell. One viewer will have a half angle of view* of $22\frac{1}{2}$ degrees and will be installed in a sleeve located in Face No. 1 of the Argon Cell at a height of 20 ft above the cell floor. This location will be the only vantage point from which all of the top of the center control room and the lower end of the central pivot tower can be seen. In addition, this location will afford a close view of the lifting beam of the removal hoist when it is being used for removing crane or manipulator carriages from their bridges. Three viewers having a half angle of view of 45 degrees will be used through roof sleeves for general viewing and should be particularly useful for observing cranes and manipulators from above. Each objective is a simple double concave lens of cerium-protected shielding glass. The optical path is 2 in. in diameter and is offset $3\frac{3}{16}$ in. at mid-thickness of the shielding wall or roof. A variable-power spotting telescope (up to 30X) will be used for inspecting the panoramic image in greater detail.

c. Manipulators and Cranes
(J. Graae, R. Vree, W. Voss)

The manipulator tool rack and changer with a capacity for one dual hook, one single hook, and one parallel jaw hand has been provided with a means for disengaging and a space for storing the detachable forearm of the manipulator. The design enables the manipulator to engage or disengage any of the tools or the detachable forearm remotely and

*Half angle of view of an optical system is described as that angle, measured from a perpendicular to the plane of the objective lens, which defines a right circular cone within which all points are visible.

unassisted. The rack can be moved about and placed on the floor of the cell without being bolted down before using. This has the advantage of providing a visible indication of contact between the manipulator arm and the rack. An operator can see the rack move or tilt and will thereby get a sensitive indication of the position of the arm. Testing of this prototype rack has suggested a few improvements. A new rack is being built and will be shipped to Idaho for testing in the Fuel Cycle Facility.

The ease with which the forearm can be detached from the manipulator suggests that special attachments with rotary motion be considered. The basic grip drive provides rotary motion which is converted to linear motion in the forearm. Examples of special attachments that might be used in place of the forearm are wrenches, a grease gun, or a direct drive for experimental apparatus.

Magnetic-powder clutches (see ANL-6413, page 83) will be used in the grip drives for the manipulators now at Idaho, rather than electromagnetic clutches. Experience with the prototype manipulator in the mockup has shown that the present electromagnetic friction clutches are not satisfactory as torque-limiting devices because they respond in an unpredictable manner. As a result, the grip would sometimes jam and have to be released manually. The new magnetic-powder clutch has been tested over a period of several months and has performed very successfully. This type of clutch was therefore ordered for the manipulators at Idaho.

The clutches, which have been received and are being inspected, are not identical with the clutch tested in the mockup, but have some modifications. One of the new clutches has been installed temporarily on the prototype manipulator for additional testing.

d. Materials Testing
(G. Bernstein, L. Coleman, A. Chilenskas, J. Graae)

Evaluation of elastomers as possible substitutes for the lead gaskets now specified for use in the large transfer lock is continuing. The elastomers are being irradiated while under compression in the test assembly described in ANL-6477, page 76. An examination of Adiprene C* after it had been exposed to a radiation level of 1×10^9 rad showed that it was still soft and resilient, and it was judged serviceable at this level. Irradiation of this sample is continuing. Neoprene and gum rubber, the two materials previously examined for this use, were judged serviceable up to levels of 2×10^8 rad and 4×10^8 rad, respectively.

*A product of Minnesota Rubber Company.

2. Skull Reclamation Process

a. Skull Oxidation Equipment
(W. E. Miller, M. A. Slawecki, H. Stethers)

After the melt refining step is performed, a skull remains in the zirconia crucible. The skull will be oxidized in order to convert it into a powder which may be easily removed from the crucible. A preliminary mockup of the proposed system was built and used to oxidize ordinary skulls, nitrided skulls, and alloy scrap (ANL-6543, page 84). The major feature of the system is its ability to keep the rate of the oxidation reaction nearly constant throughout the oxidation period.

A preliminary wiring diagram for the panel board of the gas-control system to be used with the skull oxidation equipment has been completed. The panel board provides control for a series of operations necessary to accomplish a complete burning cycle.

Significant concentrations of oxygen will be present in the off-gas from the skull oxidation furnace. Since one of the components of the off-gas system of the fuel cycle facility is a charcoal bed which provides additional hold-up time for the decay of radioactive iodine and the rare gases krypton and xenon, the presence of substantial amounts of oxygen in the off-gas will create a fire hazard and the concomitant hazard of releasing radioactivity. To overcome this difficulty, a unit for the removal of oxygen will be installed between the oxidation furnace and the plant off-gas system.

b. Collection of Metal Vapors
(W. E. Miller)

The product from the precipitation step of the skull reclamation process is uranium coated with magnesium-zinc. Distillation of the magnesium-zinc from the uranium in a standard melt refining crucible in the melt refining furnace would be advantageous, because no other furnace, crucible, or transfer would be required to reintroduce this uranium into a fuel ingot.

In a previous run (see ANL-6543, page 86) in which a 500-g charge of magnesium-zinc was distilled under ordinary melt refining conditions (one atmosphere inert gas pressure and 1400 C maximum melt temperature), only about 95 percent of the charge was collected on a molded Fiberfrax absorber trap. It is believed that vapors amounting to five percent of the charge permeated the zirconia crucible and the graphite susceptor of the furnace. To eliminate vapor escape by this route, a liner of 304 stainless steel was substituted for an inner graphite susceptor and placed between the outer furnace susceptor and the zirconia

crucible. The modified melt refining furnace was used in two runs which were made under reduced pressures (100 and 150 mm) of argon at a maximum temperature of 1020 C in order to protect the liner against excessive heat. In these runs, a considerable amount of the magnesium-zinc charge was found lodged between the liner and crucible, and made the removal of the crucible difficult. The use of a steel liner in the melt refining furnace assembly has been abandoned.

c. Remote Operations Equipment Development
(G. Bernstein, A. Chilenskas, L. Coleman, T. Eckels, W. Miller, H. Stethers)

Fabrication of the first model of a skull oxide-processing furnace has been completed. This furnace will be installed in the EBR-II mockup area for test purposes. The initial assembly will contain a graphite crucible, 15 in. in diameter and 28 in. high, made to plant scale, that is, to process 5 kg of skull oxide. Induction heating at 10,000 cps will be used, together with mechanical stirrring. Subsequent tests will be made with low-frequency induction heating and mixing.

Designs for oxide-charging and product-removal mechanisms have been completed.

d. Inductive Heating and Mixing
(A. A. Chilenskas)

Inductive heating and mixing with low-frequency power is being examined for use in the noble metal-extraction and reduction steps of the skull reclamation process. Appreciable equipment simplification will be possible if inductive heating and mixing should prove feasible.

In one experiment in which a 60-cps power supply was used, the charge consisted of 2 kg skull oxide, 5.6 kg Dow 230 Flux,* 2.95 kg magnesium, and 34 kg zinc. The charge was contained in an insulated graphite crucible, 21 in. high having an ID of $7\frac{1}{2}$ in. and a wall thickness of $\frac{3}{4}$ in. The induction coil was $14\frac{1}{2}$ in. high and consisted of 24 turns of rectangular copper bar, 1 in. by $\frac{1}{2}$ in. in cross section. Each turn was spaced $\frac{1}{8}$ in. and the coil was water cooled. The power supply to the coil was limited to 860 amp at 21 v. A reduction of 17 percent of the skull oxide charged was obtained. No firm conclusion can be drawn from this result regarding the adequacy of inductive mixing for this application since the power-supply system (36-kva transformer, voltage controlled by a 30-kw saturable reactor) was inadequate, because of the low power factor obtained with the inductor coil. Input to the metal-salt charge was

*55 percent KCl, 34 percent $MgCl_2$, 9 percent $BaCl_2$, and 2.0 percent CaF_2. Produced by Dow Chemical Co.

limited to about 3 kw, with a resulting charge temperature of about 700 C. A temperature of 800 C is desirable. Nevertheless, results to date are considered sufficiently encouraging to warrant continued effort along these lines.

Specifications are being written for a variable-frequency power-supply system with power-factor correction, which will permit power inputs up to 15 kw for a frequency range of 20 to 120 cps. Calculations show that charge temperatures of 800 C (the process temperature) will be readily obtained and that the agitation at 20 cps will be about 10 times that obtainable with the present system.

C. Chemistry of Liquid Metals
(I. Johnson, H. M. Feder)

Investigations of the chemistry of liquid metal systems are being conducted to provide basic concepts and data for the design of methods for the reprocessing of reactor fuels. In addition, the results of these studies provide ideas and data for the formulation and testing of theories of liquid metal solutions.

1. Solubilities in Liquid Metals

The solubilities of the metals whose separations are being attempted are of prime importance in the design of fuel-reprocessing methods. The dependence of the solubility on temperature and solvent composition needs to be known. The solubility and temperature coefficients of solubility of a metallic phase in a liquid metal solvent are strongly dependent on the interatomic forces operative in the solution and, consequently, may be used to gain greater insight into the way in which these forces vary with the basic properties of the solute and solvent atoms. For such fundamental studies, it is necessary to know the constitution of the solid phase in equilibrium with the saturated liquid phase.

Solubility of Uranium in Liquid Gallium
(M. G. Chasanov and P. D. Hunt)

The solubility of uranium in liquid gallium was determined with the apparatus described previously (see ANL-6413, page 88). High-purity gallium (99.99 percent) and reactor-grade uranium were used. Back-drainage of liquid metal samples through the filter plug made it necessary to abandon the usual technique of filtered samples in the experiments. A "grab" sample technique, in which the saturated melt entered a sealed quartz tube through a hole in the side of the tube, proved satisfactory. The intermetallic compound present in the solution was allowed to settle for one-half to one hour prior to the insertion of the "grab" tube. Uranium was determined by fluorometric methods.

The experimental data are given in Table 16 and are shown graphically in Figure 23. The data of Table 16 were used to compute the following solubility equation:

(343 to 649 C) Uranium: $\log(\text{atom percent}) = 6.70 - 8840\,T^{-1} + 1.99 \times 10^{6}\,T^{-2}$.

The relative standard deviation for this equation is 17 percent.

Table 16

SOLUBILITY OF URANIUM IN LIQUID GALLIUM

Temp (C)	Uranium (atom percent)	Temp (C)	Uranium (atom percent)
343	0.0041_2	522	0.071_9
420	0.014_0	554	0.086_0
448	0.016_3	580	0.11_8
474	0.024_8	600	0.17_7
499	0.034_5	649	0.25_7

Metallographic examination of the furnace-cooled solubility ingot revealed the presence of an intermetallic phase which was identified as UGa_3 by means of X-ray diffraction.[7] Thermal analysis of a gallium-eight weight percent alloy gave no reproducible arrests in the range from 350 to 750 C. This alloy was quenched after being held at 600 C for about 18 hr; the intermetallic compound present was also identified as UGa_3. It appears that UGa_3 is the solid phase in equilibrium with the liquidus over the range investigated. This is in agreement with Hansen's[8] phase diagram.

Figure 23

SOLUBILITY OF URANIUM IN LIQUID GALLIUM

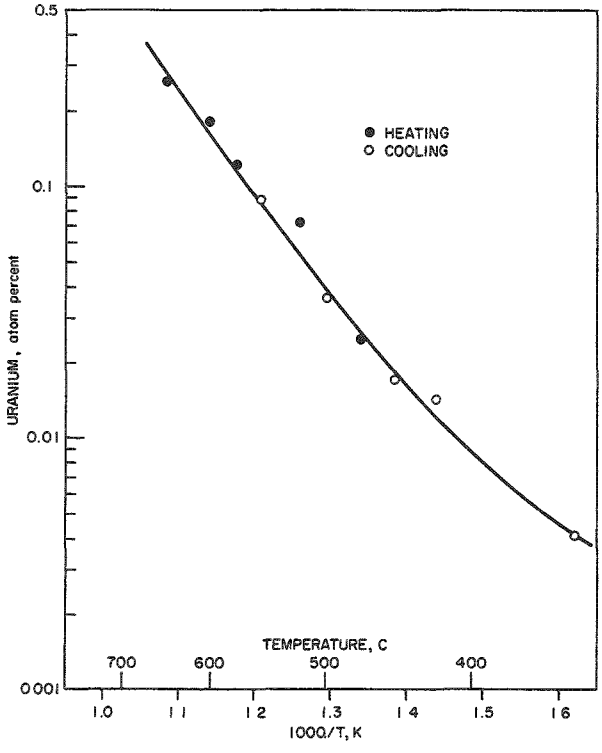

Zinc-Uranium System
(A. E. Martin and C. Wach)

The existence of a second intermetallic phase (designated the epsilon phase) in the zinc-uranium system was confirmed by X-ray and metallographic examinations

[7] Schablaske, R., and Tani, B., private communication.

[8] Hansen, M., and Anderko, K., Constitution of Binary Alloys, 2nd ed., McGraw-Hill Book Co., New York (1958).

of the products of a 53-day anneal of seven zinc-uranium alloys at 650 C. The alloys ranged in composition from 24.8 to 29.7 percent uranium. The alloys were formed initially in sealed tantalum capsules by melting in a rocking furnace at 1050 C, from which temperature they were quenched in ice water to yield alloys with very fine structures. Portions of the alloys were then sealed in Vycor tubes prior to the long annealing period at 650 C.

After the long anneal, the alloys with compositions 24.8, 26.7, 27.2, and 27.7 percent uranium were found to consist essentially of the epsilon phase. The X-ray data obtained with these alloys showed progressive changes characteristic of the changes in composition of a solid-solution alloy. On the other hand, alloys with the composition 28.6_5, 28.9_4, and 29.7_2 percent uranium were observed to consist of the epsilon and delta phases. The percentages of the epsilon phase in the structures were determined from areal metallographic measurements as $71._2$, $53._3$, and $14._4$ percent, respectively.

On the assumptions that the delta phase is the previously established[9] phase of composition U_2Zn_{17} and that the densities of the epsilon and delta phases are substantially the same, the compositions of the epsilon phase in these two-phase alloys were calculated from these areal measurements to be 28.1_0, 28.0, and 28.0_3 percent uranium, respectively. The good agreement of these figures indicates that equilibrium was reached in the alloys during the long anneals and that 28.0 percent uranium is the composition of the uranium-rich boundary of the epsilon phase.

The zinc-rich boundary of the epsilon phase at this temperature was established by another experiment. A 1.5 percent uranium melt was cooled slowly to room temperature from 725 C. A portion of the bed of epsilon crystals in a zinc matrix thus obtained was remelted and held at 650 C for one day to allow equilibration of the crystals with the melt at that temperature and then quenched to room temperature. The crystals were extracted from the resulting ingot by electrolytic etching. The chemical analysis of the crystals was 24.0 percent uranium and 75.7 percent zinc. Corrected to 100 percent, this amounts to 24.1 percent uranium and 75.9 percent zinc.

Thus, at 650 C the epsilon phase field extends from 24.1 to 28.0 percent uranium and the epsilon plus delta field extends from 28.0 to 30.0 percent uranium. (It had previously been established[10] that the delta-plus-uranium field extends from 30.0 to about 100 percent uranium.)

---

[9]E. S. Makarov and S. I. Vinogradov, Kristallografia, 1, 634-643 (1956).

[10]P. Chiotti, H. H. Klepfer, and K. F. Gill, Trans. AIME, 209, 51-57 (1957).

Solubility of Zirconium in Liquid Magnesium-Zinc Solutions

(I. Johnson and K. E. Anderson)

The solubility of zirconium in an approximately 1:1 (by weight) zinc-magnesium solution has been measured as a function of temperature. This study was undertaken to provide auxiliary information for the interpretation of the results of coprecipitation experiments previously reported (see ANL-6477, page 96). The results of this study are also useful in the development of the skull reclamation process.

A melt was prepared from 2.54 g of neutron-irradiated zirconium, 175.0 g of magnesium (99.99 percent), and 175.1 g of zinc (99.99 percent) by heating to 811 C in a high-purity alumina crucible for about 16 hr. Samples were taken by means of tantalum tubes fitted with porous tantalum filters. The zirconium analyses were done radiochemically. Chemical analysis of the initial melt agreed to within 10 percent of that obtained by a radiochemical method. The chemical method was chosen to establish the absolute values. The data are given in Table 17.

Table 17

SOLUBILITY OF ZIRCONIUM IN MAGNESIUM-ZINC SOLUTION

	Solution Composition (weight percent)		
Temp (C)	Zirconium	Zinc	Magnesium[a]
811	0.66[b]	48.1	51.2
759	0.48_7[b]	47.6	51.9
709	0.54	47.5	52.0
652	0.36_1	47.9	51.7
611	0.27_5	47.1	52.6
564	0.16_3	46.8	53.0
507	0.073_6	47.2	52.7
451	0.035_1	46.9	53.1
422	0.021_8	47.4	52.6

[a]Magnesium obtained by difference from 100 percent.

[b]Solutions probably not saturated.

The initial sample was found to contain 48.1 percent zinc and 0.66 percent zirconium. Since the initial charge contained 49.7 percent zinc, it is apparent that some zinc was lost by vaporization to the cooler parts of the furnace tube. If it is assumed that neither zirconium nor

magnesium was lost by vaporization, then 10.6 g of zinc (six percent) was vaporized. The amount of zirconium found in the initial sample is about 11 percent less than the amount charged. This discrepancy is probably within the limits of the uncertainties of analysis and sampling.

The data are shown in Figure 24. The break in the solubility curve at about 610 C suggests that two different intermetallic phases are found as equilibrium solid phases - one phase below 610 C and one phase above 610 C. The two equilibrium phases in the present experiment were not isolated and identified.

Figure 24
SOLUBILITY OF ZIRCONIUM IN LIQUID ZINC-MAGNESIUM SOLUTION, 47-48 WEIGHT PERCENT ZINC

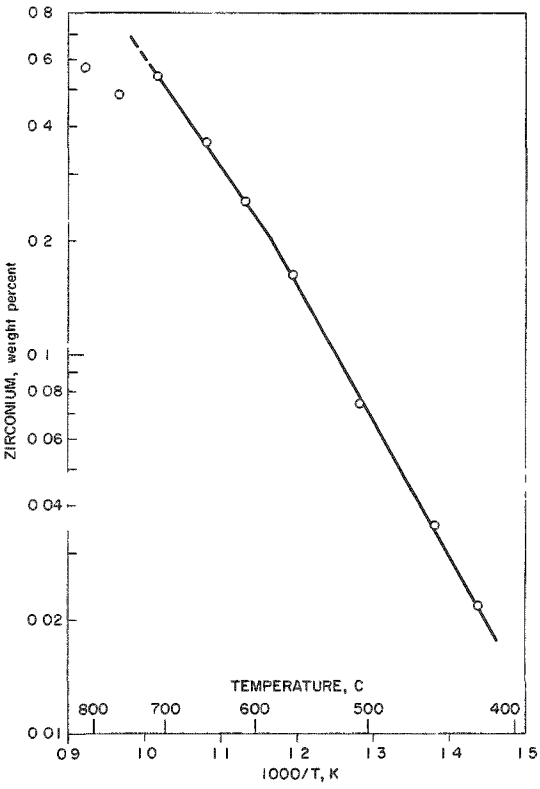

Solubility of Uranium in Magnesium-Zinc Solutions

(I. Johnson, K. E. Anderson, J. Bartos*)

The solubility of uranium in magnesium-zinc solutions has been measured at 750, 700, and 650 C as a function of magnesium concentration.

A solution of zinc, magnesium, and uranium was prepared by stirring the components together at temperature overnight. The initial charge contained 18 to 25 weight percent magnesium and sufficient uranium to obtain a saturated solution at the temperature of the experiment, i.e., a small excess of uranium was used. After the initial charge had been sampled with a tantalum sample tube fitted with a tantalum filter, additional magnesium was added. After equilibrium was attained, the liquid phase was again sampled. Further magnesium additions were made and samples taken until the liquid solution contained about 65 percent magnesium. The samples were analyzed for uranium and zinc. The data obtained are given in Table 18.

The solubility (atom fraction) is shown as a function of magnesium content of the solution in Figure 25. It may be observed that the logarithm of this solubility is not quite a linear function of the atom fraction of magnesium.

*Co-op student.

Table 18

SOLUBILITY OF URANIUM IN MAGNESIUM-ZINC SOLUTIONS

Temp (C)	Composition (weight percent) Zn	Mg[a]	U	Temp (C)	Composition (weight percent) Zn	Mg[a]	U	Temp (C)	Composition (weight percent) Zn	Mg[a]	U
750	72.6	17.7	9.7	698	74.0	18.9	7.1	648	71.7	25.0_6	3.24
748	70.4	25.1_8	4.42	702	67.4	30.07	2.5_3	650	65.3	33.3_6	1.34
751	61.2	37.6_9	1.11	699	60.3	38.8_6	0.84	650	54.5	45.1_6	0.33_8
750	49.9	49.7_5	0.34_9	704	49.8	49.9_0	0.304	651	46.9_6	52.8_7	0.17_4
752	39.8_5	59.9_9	0.16_2	703	40.9_0	58.9_8	0.12_4	651	41.1_9	58.7_2	0.090
751	33.2_5	66.6_6	0.091	707	36.3_2	63.5_8	0.10_1	652	34.8_0	65.1_5	0.054

[a]Mg obtained by difference.

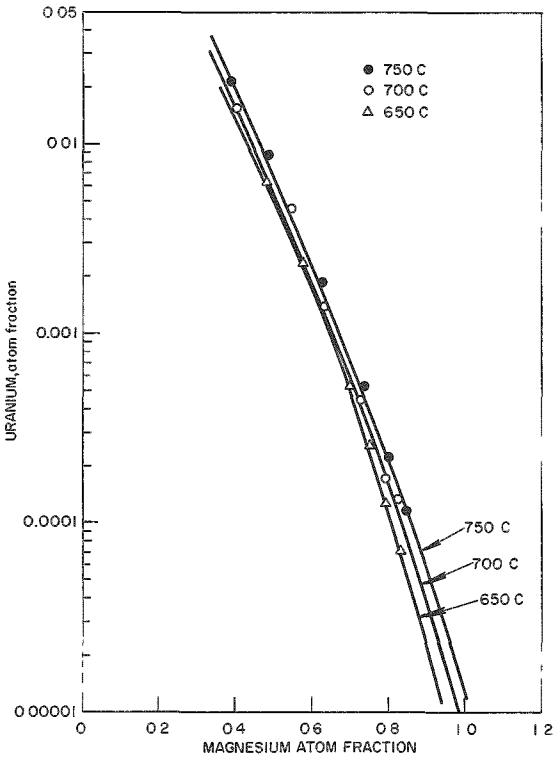

Figure 25

SOLUBILITY OF URANIUM IN ZINC-MAGNESIUM SOLUTIONS

The data for each temperature were used to determine the constants of equations of the form

$$-\log x_U = a + b\, x_{Mg} + c\, x_{Mg}^2$$

The equations were used to estimate the solubility in pure magnesium. The following results, expressed in weight percent uranium, were obtained:

1.27×10^{-2} at 750 C; 9.7×10^{-3} at 700 C; and 4.2×10^{-3} at 650 C.

These estimates are in good agreement with the solubilities reported by P. Chiotti and H. E. Shoemaker;[11] they reported 1.4×10^{-2} weight percent at 750 C.

2. Liquid-Liquid Distribution Studies

Distribution coefficients for a number of elements which occur in nuclear fuels have been measured in the lead-zinc system.* With the zirconium results reported below, the data for the lead-zinc system are essentially complete. The application of these data to process schemes, however, requires further study.

The Distribution of Zirconium-95 between Lead and Zinc in the Presence of Uranium, Cerium, and Ruthenium
(F. Cafasso, and J. Vincenzi)

The distribution coefficients of zirconium between lead and zinc in the presence of uranium, cerium, and ruthenium were measured at three temperatures: 701, 732, and 755 C. The distribution coefficients of uranium, cerium, and ruthenium and also the details of the experimental procedure have been given previously (ANL-6477, page 100). To recapitulate briefly, a sample of irradiated uranium** was placed in an Alumina crucible together with some lead and zinc. The charge was heated to the desired temperature, stirred, and sampled.

The average value of the distribution coefficient of zirconium (cpm per mg zirconium in upper layer/cpm per mg zirconium in lower layer) found at each temperature is given in Table 19. These values are 530 at 701 C, 350 at 732 C, and 110 at 757 C. To allow comparison, the distribution coefficients of uranium, cerium, and ruthenium are included in Table 19.

The low level of zirconium-95 activity in the samples presented a formidable analytical problem which, although solved, introduced a large uncertainty in the zirconium results. Consequently, the recorded zirconium coefficients should be considered only in terms of the order of magnitude. For this reason, it does not seem appropriate to make a serious

[11] P. Chiotti and H. E. Shoemaker, Ind. and Eng. Chem., 50, 137-140 (1958).

*Measurements may be found for uranium, cerium, strontium, and palladium in ANL-6231, page 74; for cerium and palladium in ANL-6333, page 113; for cerium and strontium in ANL-6413, page 92; for uranium and plutonium in ANL-6477, page 98; for uranium, cerium, and ruthenium in ANL-6477, page 100; and for uranium, plutonium, cesium, and strontium in ANL-6543, page 97.

**The sample of normal uranium was irradiated in a neutron flux of 6×10^{13} neutrons/(sq cm)(sec) for 30 hr and cooled for one week before use.

comparison of the absolute values of the zirconium coefficients with those of uranium, cerium, and ruthenium. However, some general comments are possible. The results do indicate that separation of zirconium from uranium and cerium appears to be possible in the lead-zinc system. The large uncertainties in the results make the measured differences in the coefficients of zirconium and ruthenium subject to question. However, it seems quite likely that at the lower temperatures these differences do exist.

Table 19

DISTRIBUTION COEFFICIENTS OF ZIRCONIUM, URANIUM, CERIUM, AND RUTHENIUM BETWEEN LEAD AND ZINC AS A FUNCTION OF TEMPERATURE

$$K = \frac{\text{Distribution Coefficient, concentration of solute in upper layer}}{\text{concentration of solute in lower layer}}$$

Temp (C)	Zirconium[a]	Uranium	Cerium	Ruthenium
701	5.3×10^2	52	8.9	2.1×10^3
732	3.5×10^2	26	5.4	6.3×10^2
755	1.1×10^2	12	3.8	1.6×10^2

[a] The average deviation of the distribution coefficient from its mean value is 0.8×10^2 at 701 C, 1.1×10^2 at 732 C and 0.4×10^2 at 755 C.

The Mutual Solubility of Lead and Zinc
(F. Cafasso and C. Wach)

Previous data on the mutual solubility of lead and zinc reported in ANL-6543, page 99, showed that the consolute temperature of the lead-zinc system must lie between 802 and 784 C. No measurements were made between these temperatures. It was also shown that liquid-sampling methods could be used to obtain information about the width of the immiscibility field near the consolute temperature. In the light of these facts, the mutual solubility of lead and zinc was remeasured as a function of temperature in order to check and extend the earlier data and to locate more precisely the temperature of complete immiscibility.

Lead and zinc were charged to an alumina crucible and heated to the desired temperature. The melt which resulted was stirred with a tantalum paddle for 2 hr and allowed to settle for 3 hr at each temperature before the first samples of the upper and lower phases were withdrawn. Samples were taken at 648 ± 2C, 750 ± 2C, 769 ± 2C, 789 ± 2C, 795 ± 2C, and 770 ± 2C, in the sequence indicated. A second sample of each phase

Figure 26

THE MISCIBILITY GAP IN THE LEAD-ZINC SYSTEM ABOVE 650 C

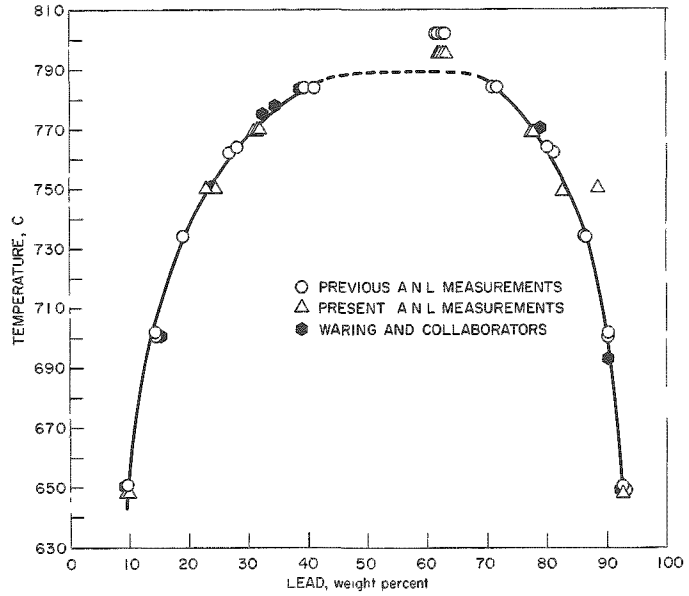

was taken after an additional 2-hr stirring period and an overnight settling period at each temperature. No significant differences were found between samples taken at the two different settling times.

The data are shown in Figure 26 along with the data of Waring and his collaborators.[12] The points at 648, 750, and 770 C agree well with the line drawn through data obtained previously. (The essential agreement of the earlier measurements with those of Waring and his collaborators was noted in ANL-6543, page 100.) The measurements made at 789 and 795 C indicated that at these temperatures the melt was a single phase. Apparently, at 789 C the lead-zinc system is at or above its consolute temperature. Since earlier measurements (see ANL-6543, page 101) showed that a lead-zinc melt consists of two phases at 784 C, the consolute temperature must lie between 784 and 789 C.

Two other measurements of the consolute temperature have been made. Waring and his collaborators,[12] using an X-ray absorption method, found the consolute temperature to lie between 770 C and 800 C. Their liquid-sampling measurements showed, however, that complete miscibility occurred by 790 C. Seith and Johnen[13] determined the consolute temperature to be 798 C from an extrapolation of their cooling curve data. In view of the experimental difficulties associated with the determination of a critical solution temperature, the agreement between the three studies is reasonably good.

3. Thermodynamic Studies

Thermodynamic functions for key elements in liquid metal solvents and for the more important solid intermetallic phases are being measured. Two methods are being used. Galvanic cells have proved to

---

[12] Waring, R. K., Anderson, E. A., Springer, R. D., and Wilcox, R. L., Trans. AIME, 111, 255 (1934).

[13] Seith, W., and Johnen, H., Z. Elektrochem., 56, 140 (1952).

be especially useful for the measurement of activities in liquid metal solutions as well as for the determination of the free energy of formation of the equilibrium solid phase in solid-liquid two-phase regions. On the other hand, for systems containing several well-defined intermetallic phases, measurement of the decomposition pressure by the effusion method is proving to be useful. The two methods supplement each other.

Cerium-Cadmium System (Effusion Studies)
(E. Veleckis and E. Van DeVenter)

The phase relations in the system cerium-cadmium have been studied by Iandelli and coworkers[14,15] who employed metallographic and X-ray techniques. They have reported the existence of the following intermediate phases: CeCd, $CeCd_2$, $CeCd_3$, and $CeCd_{11}$. In addition, the metallographic evidence indicated the existence of the compounds Ce_2Cd_9 and $CeCd_6$. However, the structural confirmation of these two compounds was not attempted because of the complexity of their diffraction patterns.

Elliott and Lemons[16,17] have measured the thermodynamic activity of cadmium in cerium-cadmium alloys by measuring the cadmium vapor pressure. They found single phases of narrow composition range extending from $CeCd_{5.967}$ to $CeCd_{6.093}$ and from $CeCd_{4.5}$ to $CeCd_{4.6}$.

At Argonne National Laboratory, the system cerium-cadmium has been studied by means of the recording effusion balance as a part of a systematic investigation of the phase diagrams of the rare earth elements with cadmium and zinc. Two typical effusion isotherms for the cerium-cadmium system at 370 and 442 C were obtained and are shown in Figure 27. The existence of two line compounds, $CeCd_{11}$ and Ce_2Cd_9, is obvious from the inspection of the isotherms. In addition, the low-temperature isotherm (A) shows a pressure variation which is indicative of the formation of a phase with the probable composition range of $CeCd_{5.8-6.4}$.

Between the compositions Cd/Ce = 4.1 and Cd/Ce = 3.1 (see Isotherm B), there is a linear decrease in pressure, which suggests the formation of a phase which is homogeneous between these boundaries. The absence of a plateau immediately following this phase may be due to an excessive depletion of cadmium from the surface of the sample, accompanied by the formation of a layer through which diffusion of cadmium

---

[14]Iandelli, A., and Botti, E., Gazz. chim. ital., 67, 638 (1937).

[15]Iandelli, A., and Botti, E., Gazz. chim. ital., 84, 463 (1954).

[16]G. R. B. Elliott and J. F. Lemons, J. Phys. Chem., 64, 137 (1960).

[17]J. F. Lemons and G. R. B. Elliott, paper presented at the XVIIIth International Congress of Pure and Applied Chemistry, Montreal, August, 1961.

Figure 27

CERIUM-CADMIUM SYSTEM. ISOTHERMS AT (A) 370 C (LOWER SCALE) AND (B) 442 C (TOP SCALE)

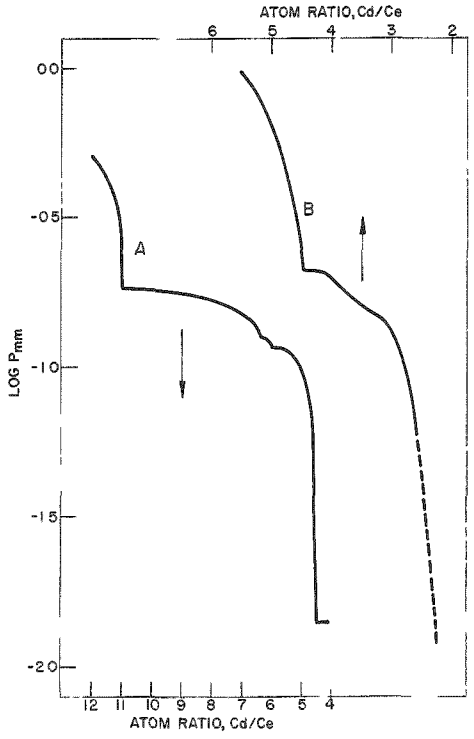

does not take place rapidly enough to maintain the saturation pressure. This interpretation is supported by a very gradual pressure decrease (indicated in Figure 27 by a dashed line) as the composition $CeCd_2$ is approached. Liquefaction of the powdered alloy would tend to enhance the surface-depletion effects. One may therefore suppose that, unlike the systems lanthanum-cadmium (ANL-6543, page 106) and praseodymium-cadmium (ANL-6477, page 103) wherein no such extensive depletion was observed, the solid-liquid transition in the cerium-cadmium system may occur at temperatures below 442 C for this composition range.

To verify the phase relationships established from the effusion data, X-ray powder diffraction analyses were performed with a series of alloys having different cadmium contents. These alloys were prepared in the effusion apparatus by stopping the cadmium vaporization when a preselected composition of the alloy was reached. The results of the X-ray analyses are shown in Table 20. The symbol "E" refers to arc patterns that could not be identified with the known patterns in this or similar systems. Comparison of the X-ray data with the effusion isotherm indicates the correspondence between "E" and Ce_2Cd_9. The agreement between the X-ray and effusion results is generally good except for the samples with compositions Cd/Ce = 3.7, 4.0, and 6.2, for which X-ray analyses show the presence of two phases even though these compositions fall within the homogeneity ranges of phases $CeCd_3$ and $CeCd_6$.

Table 20

X-RAY DIFFRACTION ANALYSES* OF SOME Ce-Cd ALLOYS

Composition (atom ratio, Cd/Ce)	Diffraction Results	Composition (atom ratio, Cd/Ce)	Diffraction Results
~20	Cd + $CeCd_{11}$	4.0	"E" + $CeCd_3$
11.0	$CeCd_{11}$	3.7	"E" + $CeCd_3$
9.6	$CeCd_{11}$ + $CeCd_6$	3.3	$CeCd_3$ + $CeCd_2$
7.9	$CeCd_{11}$ + $CeCd_6$	3.0	$CeCd_2$ + $CeCd_3$
6.2	$CeCd_6$ + $CeCd_{11}$	2.4	$CeCd_2$
5.9	$CeCd_6$	2.0	$CeCd_2$
5.0	"E" + $CeCd_6$	1.8	$CeCd_2$ + CeCd
4.5	"E"		

*Analyses performed by R. Schablaske and B. Tani.

Figure 28

SCHEMATIC REPRESENTATION OF THE INTERMEDIATE PHASES IN THE SYSTEMS La-Cd, Ce-Cd and Pr-Cd

Single vertical lines denote stoichiometric compounds. Shaded areas denote solid solutions.

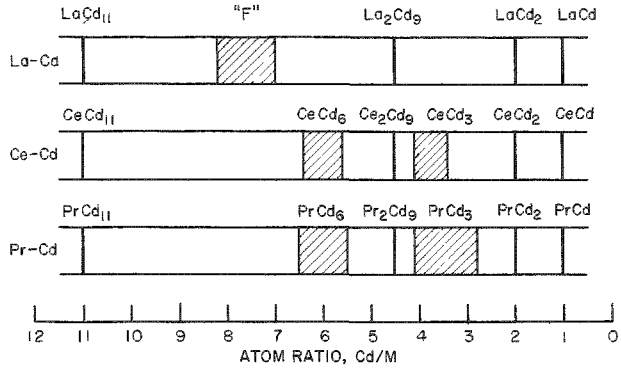

A comparison of the intermediate phases found at ~400 C in the systems lanthanum-cadmium, cerium-cadmium, and praseodymium-cadmium is represented schematically in Figure 28. In spite of the close structural and electronic similarity of these three elements, some differences in their ability to form compounds with cadmium are apparent. The phases $MeCd_6$ and $MeCd_3$ do not appear in the lanthanum-cadmium system but are present in the cerium-cadmium and praseodymium-cadmium systems, with the homogeneity ranges being somewhat wider for praseodymium than they are for cerium. The phase "F" is peculiar to the lanthanum-cadmium system.

4. Structure of Intermetallic Compounds

(R. Schablaske,* B. Tani,* M. Homa*)

a. Scandium-Cadmium System

Measurements of the solubility of scandium in liquid cadmium led to the isolation and characterization of the new intermetallic phase $ScCd_3$. X-ray diffraction powder photographs of $ScCd_3$ can be indexed on the basis of a hexagonal unit cell with $a_0 = 6.325$ Å and $c_0 = 4.852$ Å. With eight atoms in the unit cell, the calculated density is 7.55 g/cc; the pycnometric density is 7.7 g/cc.

The $ScCd_3$ structure can be referred to space group D_{6h}^4 - $P6_3/mmc$; structure type is $CdMg_3$ (DO_{19}). Atomic coordinates are

2 Sc at 0, 0, 0; 2/3, 1/3, 1/2

6 Cd at 1/2, 0, 0; 0, 1/2, 0
1/2, 1/2, 0; 1/6, 1/3, 1/2
1/6, 5/6, 1/2; 2/3, 5/6, 1/2

The structure of $ScCd_3$ is hexagonal close-packed as in the A_3-type structure but with the a-axes doubled. One atom in four of each of the layers at z = 0 and z = 1/2 differs from the other three; the layers are arranged with respect to each other in such a manner that each

*Members of the X-ray Diffraction and Spectroscopy Group.

scandium atom is in contact with three cadmium atoms in the adjacent layers. Other examples of the DO_{19} structure type are $ThAl_3$, $LiHg_3$, $SnNi_3$, WCo_3, $CdMg_3$, and $MgCd_3$.

b. Vanadium-Zinc System

Two intermediate phases are observed in the vanadium-zinc system. The high-zinc compound is VZn_3, and its structure has been characterized previously (see ANL-6477, page 91). The more vanadium-rich compound has been tentatively labeled V_4Zn_5 and is described herein.

Heats of mixtures of vanadium and zinc indicated early in the investigation that the more vanadium-rich intermediate phase has a nominal composition corresponding to an atomic ratio of 1 V:1 Zn. Preparations of 25-35 weight percent vanadium quenched in the 616 to 670 C temperature region yield the more vanadium-rich intermediate phase plus free zinc. In order to define the composition of the intermediate phase more precisely, the free zinc was leached away from it with saturated ammonium nitrate solution and the resultant intermetallic was chemically analyzed.

The results of these chemical analyses are recorded in Table 21 and indicate that the intermetallic composition corresponds more precisely to an atomic ratio of 4 V:5 Zn. Three such intermetallic preparations and subsequent chemical analyses were made in order to substantiate the stoichiometry. The measured density of each of the leached preparations is also recorded in Table 21.

Table 21

CHEMICAL ANALYSES AND DENSITY MEASUREMENTS

Preparation	Chemical Analysis w/o V	Chemical Analysis w/o Zn	Zn/V Atom Ratio	Density, g/cc
H20	38.1	60.1	1.23	6.9_1
A5250	37.4	60.6	1.26	6.9_0
H32U	37.7	62.8	1.30	6.8_0
(V_4Zn_5)	(38.4)	(61.6)	(1.25)	-

X-ray diffraction powder photographs of V_4Zn_5 can be indexed on the basis of a body-centered tetragonal cell whose lattice dimensions are $a_0 = 8.910 \pm 0.003$ Å and $c_0 = 3.227 \pm 0.002$ Å. No variation of lattice parameters, indicative of a range of composition for this phase,

is evident. With eight vanadium and ten zinc atoms in this unit cell, the calculated intermetallic density is 6.88 g/cc, a value which is in agreement with the measured densities.

The details of the V_4Zn_5 structure are not as yet complete. Data are being readied for the determination of the atomic coordinates by means of a crystallographic least-squares refinement program for the IBM 704. The V_4Zn_5 structure is thought to resemble that of Te_4Ti_5.[18] This compound is also tetragonal with eight tellurium and ten titanium atoms arranged in a body-centered lattice whose dimensions are $a_0 = 10.164$ Å and $c_0 = 3.7720$ Å. The space group is $I\,4/m\text{-}C_{4h}^5$.

---

[18] F. Gronvold, A. Kjekshus, and F. Raaum, Acta. Cryst., 14, 930 (1961).

II. FUEL CYCLE APPLICATIONS OF VOLATILITY AND FLUIDIZATION TECHNIQUES*

A Direct Fluorination Volatility Process has been proposed for the recovery of uranium and plutonium from irradiated nuclear reactor fuels. This process is based on the volatilities of uranium and plutonium hexafluorides. In this process fluidization techniques are also used to advantage. Progress continues to be made in application of this process to uranium dioxide and zirconium matrix fuels.

Decladding spent uranium dioxide fuel may be accomplished by the appropriate reaction in a fluidized bed. Plutonium and uranium hexafluorides, which result from the reaction of the declad oxide fuel with fluorine, may be separated from volatile fission products by distillation and separated from one another by thermal decomposition of the plutonium hexafluoride.

Recovery of uranium from enriched uranium-Zircaloy alloy fuels involves reaction of the alloy with hydrogen chloride (or other chlorinating agents) while the alloy is submerged in an inert fluidized bed. During the reaction of the alloy with hydrogen chloride, the zirconium is sublimed as the tetrachloride, and particulate uranium chloride is left in the reactor assembly. Uranium is recovered as volatile uranium hexafluoride in a subsequent fluorination step.

Fluidization techniques have been applied to a process for the conversion of uranium hexafluoride to high-density uranium dioxide by simultaneous reaction with steam and hydrogen.

Fluid-bed calcination studies are being extended to small-diameter columns for application to solutions containing enriched uranium or plutonium where nuclear criticality must be considered.

A. Laboratory Investigations of Fluoride Volatility Processes
(J. Fischer)

Fluorination of Uranium-Plutonium Dioxides
(R. L. Jarry, T. D. Baker, J. J. Stockbar)

In the Direct Fluorination Volatility Process spent uranium dioxide fuel elements will be fluorinated in a fluidized Alundum bed to convert the uranium and plutonium to their respective hexafluorides. A typical charge for a fluid-bed fluorinator will contain 100 kg uranium, 0.4 kg plutonium, and about 30 kg Alundum. The fuel elements will also contain about one kilogram of fission product elements for 100 kg of uranium.

*A summary of this section is given on pages 6 to 9 .

The development of fluorination techniques for the effective removal of plutonium from mixed oxides of uranium and plutonium mixed with granulated Alundum is continuing. Previously reported experimental results (ANL-6379, page 137, ANL-6413, page 112, and ANL-6477, page 111) demonstrated that upon fluorination, when fission product element oxides had been added to the mixture, 95 percent of the plutonium was removed. Removals of 98 and 95 percent after fluorination would result in plutonium concentrations in the Alundum residues of 0.03 and 0.06 weight percent, respectively. The following variants in the procedure have been found, individually, to minimize the retention of plutonium in the Alundum residues: (1) the use of a mild initial fluorination using 10 volume percent fluorine (plus 65 percent nitrogen and 25 percent oxygen) at 450 C, (2) the use of a hydrofluorination step prior to direct fluorination, and (3) the use of higher temperatures of fluorination using 75 volume percent fluorine (plus 25 percent oxygen) at 550 C following the initial fluorination at 450 C. The second fluorination at the higher temperature of 550 C carried out for 10 hr resulted in a residual plutonium content in the residues of 0.03 weight percent corresponding to a removal of 98 percent of the plutonium.

Results are reported for experiments using step (1) above, followed by step (3). Results are also reported for (a) experiments in which the quantity of Alundum used was varied for a constant amount of uranium-plutonium oxide and (b) several experiments in which the same charge of Alundum was used for the fluorination of several additional samples of uranium-plutonium oxides.

A mixture of uranium dioxide, uranium dioxide-plutonium dioxide solid solution, fission product oxides, and pure crystalline alumina was used in the fluorination experiments. The ratio of components was representative of the proportion of components which may be found in the charge to the fluorinator in the Direct Fluorination Process. The compositions of the mixtures used are given in Tables 22 and 23. A detailed description of the apparatus used for these experiments was given in a previous report (ANL-6379, page 139).

A series of experiments were performed in which a fluorination period at 450 C, using 10 volume percent fluorine, was immediately followed by a second period at 550 C or at 650 C using 75 volume percent fluorine. In the series of experiments in which the fluorination during the second period was performed at 650 C, the usual nickel reaction boat was replaced with one made of refractory Alundum. The Alundum boat was placed in an Alundum tube, which served as a liner for the horizontal, tubular nickel reactor. This modification to the reaction system was necessary to prevent the mixture of nickel fluoride with the residue which is formed in serious quantities at this elevated temperature. The Alundum liner also served to reduce the severity of the reaction of fluorine with the nickel system.

Table 22

SUMMARY OF RESULTS OF FLUORINATION OF URANIUM OXIDE PLUTONIUM OXIDE MIXTURES WITH ALUNDUM INERT SOLIDS

Solid Mixture: (1) 3 42 g uranium oxide-plutonium oxide; (2) 0 9 g Al_2O_3; (3) 0 03 g fission products
Fluorination Gas Mixture: 1st Period 10 v o F_2 65 v o N_2 25 v/o O_2; 2nd Period 75 v/o F_2 25 v/o O_2
Fluorinating Gas Flow Rate: 800 ml/min

	Fluorination Reaction Conditions								
	1st Period		2nd Period[a]		Initial Sample		Residue		
Item No	Time (hr)	Temp (C)	Time (hr)	Temp (C)	Pu (w/o)	Wt Pu (mg)	Pu (w/o)	Wt Pu (mg)	Percent of Original Pu Removed
1[b]	4	450	6	550	0 36	12 8	0 079	0 80	93 7 ± 1 9
2[c]	3	450	10	550	0 33	11 1	0 068	0 72	93 5
3[d]	10	450	10	550	0 36	12 2	0 031	0 31	97 4 ± 0 3
4[e]	10[f]	450	10	550	0 42	14 4	0 028	0 30	97 9
5[g]	10	450	5	650	0 33	11 1	0 016	0 14	98 7 ± 0 2
6[h]	5	450	5	650	0 33	11 1	0 027	0 26	97 6

[a]The two fluorination periods were run consecutively
[b]Average of Experiments 136 139 144 153 154 and 155 (see Table 23)
[c]Experiment 148 Table 23
[d]Average of Experiments 142 149 150 Table 23
[e]Experiment 143 Table 23
[f]The fluorinating gas mixture for the 1st period was 75 v/o F_2 25 v o O_2
[g]Average of Experiments 157 158 Table 23
[h]Experiment 159 Table 23

Table 23

FLUORINATION OF URANIUM OXIDE-PLUTONIUM OXIDE MIXTURES WITH ALUNDUM INERT SOLIDS

Uranium-Plutonium Oxide: Batch III[a] 3 42 g which contained 2990 mg U 14 4 mg Pu and 0 03 g Fission Product Oxides
Batch IV[a] 3 42 g which contained 3040 mg U 11 1 mg Pu and 0 03 g Fission Product Oxides
Inert Solid: Al_2O_3 0 9 g 60 mesh
Fluorinating Gas Flow Rate: 800 ml/min

				Fluorinating Gas Mixture			Residue		
Exp No	$(U\text{-}Pu)O_2$ Batch[a] No	Temp (C)	Time (hr)	v/o F_2	v/o N_2	v/o O_2	Pu (w/o)	Wt Pu (mg)	Percent of Original Pu Removed
136	III	450	4	10	65	25	0 050	0 46	96 8
		550	6	75		25			
139	III	450	4	10	65	25	0 072	0 74	94 9
		550	6	75	-	25			
144	III	450	4	10	65	25	0 078	0 78	94 6
		550	6	75		25			
153	IV	450	4	10	65	25	0 114	1 11	90 0
		550	6	75	-	25			
154	IV	450	4	10	65	25	0 092	0 92	91 8
		550	6	75		25			
155	IV	450	4	10	65	25	0 072	0 77	93 1
		550	6	75		25			
							Average value		93 7 ± 1 9
148	IV	450	3	10	65	25	0 068	0 72	93 5
		550	10	75		25			
142	III	450	10	10	65	25	0 032	0 30	97 9
		550	10	75	-	25			
149	IV	450	10	10	65	25	0 034	0 34	97 0
		550	10	75		25			
150	IV	450	10	10	65	25	0 028	0 30	97 3
		550	10	75	-	25			
							Average value (142 149 & 150)		97 4 ± 0 3
143	III	450	10	10	65	25	0 028	0 30	97 9
		550	10	75	-	25			
157	IV	450	10	10	65	25	0 018	0 16	98 6
		650	5	75		25			
158	IV	450	10	10	65	25	0 014	0 13	98 9
		650	5	75	-	25			
							Average value (157 and 158)		98 7 ± 0 2
159	IV	450	5	10	65	25	0 027	0 26	97 6
		650	5	75	-	25			

[a]Prepared by the addition of UO_2 and FP III mixture (which contains the following oxides BaO ZrO_2 La_2O_3 CeO_2 Y_2O_3, Nd_2O_3, Sm_2O_3, Pr_6O_{11}, Eu_2O_3 and Gd_2O_3) to the UO_2 and PuO_2 mixture containing about four weight percent Pu

		U(w o)	Pu(w/o)
Analyses	Batch III	87 2	0 42
	Batch IV	89 0	0 33

The results obtained from these experiments, some of which are average values of several experiments, are summarized in Table 22. The detailed data for the individual experiments are listed in Table 23. When the fluorinations were carried out for 4 hr at 450 C, followed by 6 hr at 550 C, the average concentration of plutonium in the residues was 0.079 weight percent (Item 1, Table 22; average of Experiments 136, 139, 144, 153, 154, and 155, Table 23). This residual concentration corresponds to a percentage removal of plutonium from the inert solids of 93.7 ± 1.9 percent. In a single experiment, Item 2, Table 22 (Experiment 148, Table 23), the fluorination period at 550 C was extended to 10 hr with no significant decrease in the plutonium concentration in the Alundum residue. By increasing both fluorination periods to 10 hr, the plutonium concentration in the Alundum residue was reduced to an average value of 0.031 weight percent (Item 3, Table 23; average of Experiments 142, 149, and 150, Table 23). The corresponding plutonium removal from the solid mixture was 97.4 ± 0.3 percent. Increasing the fluorine concentration to 75 volume percent for the 10-hr period at 450 C did not result in a greater removal of plutonium from the inert solids (Item 4, Table 22, Experiment 143, Table 23). The lowest plutonium concentration in the Alundum residue was obtained for experiments in which the second fluorination was performed at a temperature of 650 C for 5 hr. This procedure resulted in an average plutonium concentration in the residue of 0.016 weight percent, corresponding to a removal of 98.7 percent of the plutonium (Item 5, Table 22; average of Experiments 157, and 158, Table 23). In one experiment (Item 6, Table 22; Experiment 159, Table 23), the period at 450 C was reduced to 5 hr; there resulted a somewhat lower plutonium removal from the inert solids, 97.6 percent.

From the results listed in Table 22 it appears, therefore, that a fluorination scheme employing an initial 10-hr period at 450 C and using 10 volume percent fluorine followed by a second 5-hr period at 650 C using 75 volume percent fluorine is satisfactory. However, the effect of time of fluorination may be applicable only to these small-scale, static, shallow-bed experiments. Variation of time of fluorination will be studied more fully in fluid-bed experiments which will be performed in the near future.

An important variable in the reaction scheme is the quantity of Alundum used as the inert solid. The plutonium retained in the Alundum residue of the fluorination is dispersed upon the surface of the inert solid. To indicate the effect of the quantity of Alundum used upon the recovery of plutonium, several experiments were performed in which the amount of Alundum was varied for a constant amount of uranium-plutonium oxides, 3.42 g. The amounts of Alundum used were 0.9, 1.5, and 3.0 g. The data and reaction conditions for these experiments are given in Table 24.

When the Alundum was increased in amount from 0.9 to 1.5 g (Experiments 139 and 138), there was a corresponding increase in the retention of plutonium in the Alundum residues from 0.072 to 0.118 weight percent. Upon a further increase in the amount of Alundum to 3 g (Experiment 141), the plutonium content of the residue remained relatively constant at 0.107 weight percent. The plutonium removals from the mixtures containing 0.9, 1.5, and 3.0 g Alundum were 94.9, 87.1, and 77.4 percent, respectively.

Table 24

EFFECT OF THE QUANTITY OF ALUNDUM INERT SOLIDS ON THE REMOVAL OF PLUTONIUM FROM URANIUM-PLUTONIUM MIXED OXIDES BY FLUORINATION

Uranium-Plutonium Oxide:	Batch III,[a] 3.42 g which contained 2290 mg U, 14.4 mg Pu, and 0.03 g Fission Product Oxides
	Batch IV,[a] 3.42 g which contained 3040 mg U, 11.1 mg Pu, and 0.03 g Fission Product Oxides
Inert Solid:	Al_2O_3, 0.9 g, 60 mesh
Fluorinating Gas Flow Rate:	800 ml/min
Temperature, Time, Gas Mixture:	450 C, 4 hr, 10 v/o F_2, 65 v/o N_2, 25 v/o O_2, followed by 550 C, 6 hr, 75 v/o F_2, 25 v/o O_2

Exp No.	Wt Al_2O_3 (g)	Residue Pu (w/o)	Residue Pu (mg)	Percent of Original Pu Removed
139	0.9	0.072	0.74	94.9
138	1.5	0.118	1.86	87.1
141	3.0	0.107	3.26	77.4
151	3.0[b]	0.128	4.29	69.4

[a]Prepared by the addition of UO_2 and FP III mixture (which contains the following oxides: BaO, ZrO_2, La_2O_3, CeO_2, Y_2O_3, Nd_2O_3, Sm_2O_3, Pr_6O_{11}, Eu_2O_3, and Gd_2O_3) to the UO_2 and PuO_2 mixture containing about four weight percent Pu.

		w/o U	w/o Pu
Analyses:	Batch III	87.2	0.42
	Batch IV	89.0	0.33

[b]120 mesh.

An experiment (No. 151) was performed to show the effect of the surface area of Alundum on the retention of plutonium. This experiment, a replicate of Experiment 141 except that 120 mesh Alundum was used, resulted in a greater retention of plutonium on the Alundum residue (0.128 weight percent vs 0.107 weight percent).

Two experiments, the results of which are summarized in Table 25, were performed to determine the feasibility of using a single batch of Alundum as the inert solid for consecutive fluorinations with addition of uranium-plutonium oxide prior to each experiment. Four separate fluorinations were performed consecutively in each experiment.

Table 25

RECYCLE USE OF ALUNDUM INERT SOLIDS FOR THE FLUORINATION OF URANIUM-PLUTONIUM OXIDE MIXTURES

Uranium-Plutonium Oxide:	Three additions of uranium-plutonium dioxide at the start of each of the first three fluorination periods.
	Batch III,[a] 3.42 g which contained 2990 mg U, 14.4 mg Pu, and 0.03 g Fission Product Oxides
	Batch IV,[a] 3.42 g which contained 3040 mg U, 11.1 mg Pu, and 0.03 g Fission Product Oxides
Temperature, Time, Gas Mixture:	
Three fluorination cycles:	450 C, 4 hr, 10 v/o F_2-65 v/o N_2-25 v/o O_2
	550 C, 6 hr, 75 v/o F_2-25 v/o O_2
One fluorination cycle:	550 C, 10 hr, 75 v/o F_2-25 v/o O_2
Fluorinating Gas Flow Rate:	800 ml/min

	Initial Sample				Residue		
Exp No.	$(U-Pu)O_2$ Batch No.	Wt Al_2O_3 (g)	Total Uranium Added (g)	Total Plutonium Added (mg)	Pu[b] (w/o)	Wt Pu (mg)	Percent of Original Pu Removed
140	III	1.50	8.97	43.2	0.024	0.53	98.8
145	IV	0.90	9.12	33.3	0.067	0.87	97.4

[a]Prepared by the addition of UO_2 and FP III mixture (which contains the following oxides: BaO, ZrO_2, La_2O_3, CeO_2, Y_2O_3, Nd_2O_3, Sm_2O_3, Pr_6O_{11}, Eu_2O_3, and Gd_2O_3) to the UO_2 and PuO_2 mixture containing about four weight percent Pu.

		U(w/o)	Pu(w/o)
Analyses:	Batch III	87.2	0.42
	Batch IV	89.0	0.33

[b]The residues contained NiF_2 produced during the reactions. Converting the w/o Pu to the Alundum base gives 0.035 and 0.088 w/o for Experiment 140 and Experiment 145, respectively.

In the first three fluorinations, uranium-plutonium oxide was present in the solid mixture, and in the fourth the residue resulting from the previous three fluorinations was further fluorinated. The first three fluorinations were each carried out in two parts, one at 450 C for 4 hr with 10 volume percent fluorine and a second part at 550 C for 6 hr with 75 volume percent fluorine.

The initial solid mixture for the first fluorination of recycle Experiment 140 consisted of 3.42 g of a mixture of uranium-plutonium oxide and fission product oxides, and 1.5 g of high-purity Alundum. The solid mixtures for the second and third fluorinations were the residues of the preceding fluorination to which had been added 3.42 g of the uranium-plutonium oxide and fission product oxides mixture. The residue resulting from these three fluorinations was then fluorinated, without further addition of the uranium-plutonium oxide mixture, for 10 hr at 550 C with 75 volume percent fluorine. The second recycle experiment, Experiment 145, differed only in the quantity of Alundum used, 0.9 g, and in the plutonium content of the uranium-plutonium oxide mixture, 0.33 weight percent.

In each of these two experiments about 98 percent of the original plutonium content was removed by conversion to the hexafluoride. The recycle of Alundum did not result in a greater removal of plutonium than would have been obtained if three separate batches of Alundum had been employed, as in Experiment 142, Table 23. It is interesting to note that the use of a greater amount of Alundum in Experiment 140 did not result in a greater retention of plutonium in the residue. The longer fluorinating time at 550 C in Experiment 140 (16 hr vs 10 hr in Experiment 138) might be responsible for this effect. Advantages of the recycle use of the Alundum rather than performing three separate fluorinations are, (1) the fluorination time is 40 hr compared with 60 hr for three separate fluorinations, and (2) less fission product-containing Alundum needs disposal.

B. Engineering-scale Investigations of Fluoride Volatility Processes (A. A. Jonke)

1. Direct Fluorination of Uranium Dioxide Fuel (W. J. Mecham, J. D. Gabor, L. Anastasia, J. Wehrle, R. Kinzler, A. Rashinskas)

The engineering-scale experimental studies of the direct fluorination of uranium dioxide reactor fuel have been directed toward optimization of process conditions for the complete fluorination of batches of fuel pellets in a single step to form uranium hexafluoride product. The maximum production rates attainable in practice are limited by rates of heat transfer rather than by chemical kinetics. Fluidization of an inert bed of

refractory alumina grain in and above the voids of the pellet bed has been used as an aid in heat removal. Positive control of the reaction at all times is provided by regulation of the inlet fluorine flow. The major process variables under study have been bed heights and reagent gas rates and compositions. The major process objective has been to demonstrate short batch-fluorination time (<20 hr) and satisfactory fluorine utilization efficiency (>75 percent) under practical operating conditions.

Preliminary studies (ANL-6379, pages 159 to 171, and ANL-6477, pages 138 to 141) were made with 6-in.-deep uranium dioxide pellet beds and approximately 36-in.-deep beds of inert fluidized material. Recycle of process gas to the fluorinator resulted in fluorination rates of about 50 lb uranium hexafluoride/(hr)(sq ft of reactor cross section), together with satisfactory temperature control and fluorine utilization efficiency. The recycle of oxygen product gas produced a moderate amount of uranium oxide fines which was beneficial to the fluorination without impairing the fluidization.

In subsequent experiments different batch quantities were charged to the fluorinator, i.e., a larger uranium dioxide pellet bed and a smaller fluid bed of granular alumina. Investigation of deeper pellet beds was in accord with a practical interest in handling maximum pellet batch size in a reactor of given diameter. The lower batch ratio of alumina to uranium was investigated because of the anticipated advantages in processing a plutonium-bearing fuel, since laboratory fluorinations have shown that a portion of the plutonium is retained in the alumina bed.

A series of batch fluorinations with 18-in.-deep pellet beds has now been completed. Earlier runs in this series were reported in ANL-6543, pages 128 to 144, and ANL-6477, pages 133 to 144. In the present series of runs, an attempt has been made to optimize the following three factors for pellet bed depths of 18 in. and alumina/uranium charge ratios of 0.30 or less.

1) Fluidization Quality. This refers to a fluidization of the inert solids which is adequate for the equalization of temperatures in the reaction zone and for the conduction of reaction heat to the cooling wall without large temperature differentials. Efficient contacting of the reagent gas with the solid, freedom from caking of solids, and freedom from gas channelling in the bed are also involved in fluidization quality. A final criterion is that the bed consists of free-flowing inert solids at the end of the fluorination.

2) Fluorine Utilization Efficiency. This refers chiefly to overall fluorine economy and for this study is defined as 3x molar rate of UF_6 collection/molar rate of F_2 input. The overall economy depends on

fluorine utilization efficiency in the fluorinator and on the amount of gas recycle relative to gas throughput. The fluorine utilization efficiency in the reactor depends largely on the amount of fines and the efficiency of contacting these fines with fluorine gas. Overall fluorine efficiencies of about 90 percent have been achieved, and efficiencies less than about 75 percent are regarded as unsatisfactory.

3) Rate of Uranium Hexafluoride Production. While all present experiments have been carried out in a 3-in.-diameter fluorinator, it is considered that the equipment could be scaled up to larger diameters for higher production rates. Good fluidization has been obtained in some runs for uranium hexafluoride production rates up to 50 lb uranium hexafluoride/(hr)(sq ft reactor cross-sectional area). For practical reasons, rates below 20 lb uranium hexafluoride/(hr)(sq ft) have been regarded as unsatisfactory.

In the preceding report (ANL-6543, pages 133 to 144), two runs, UOF-52 and UOF-53, were described. In UOF-52, gas recycle was not used, but oxygen in moderate concentration was added to the fluorine and nitrogen inlet gas streams during a major part of the run to simulate the oxygen content of a partial-recycle gas system. This run was favorable with respect to fluidization quality and uranium hexafluoride production rate, but fluorine utilization efficiency was low. In Run UOF-53, a partial-recycle gas system was initiated with the aim of improving fluorine utilization efficiency while limiting the amount of product oxygen recycled. Previous experiments have shown that high rates of oxygen introduction to the reactor can result in the accumulation of fines, which leads to poor fluidization and caking. Run UOF-53 was considered successful with respect to uranium hexafluoride production rate and fluorine utilization efficiency, but fluidization quality was low and the bed caked. The caking tendencies were attributed to excessive amounts of oxygen in the recycled gas. Consequently, a more complete analysis is being made of oxygen control via the partial-recycle method previously described (ANL-6543, page 130).

In an attempt to define optimum process conditions, two additional deep-bed runs were made with partial gas recycle. These runs (UOF-54 and 55) are reported below. All the runs in this series are compared and evaluated at the end of this section.

Run UOF-54

In Run UOF-54, a batch charge consisting of an 18-in.-deep bed of uranium dioxide pellets was completely fluorinated in a 3-in.-diameter, air-cooled fluorinator using a partial-recycle gas system. The charge of $\frac{1}{2}$-in. x $\frac{1}{2}$-in. pellets was of fuel grade and weighed 13.2 kg.

Also charged was 3.3 kg of refractory grain alumina (-60 +200 mesh) as an inert fluid bed. The temperature control point was 500 C. These conditions were similar to those used in other runs in the present series. The major objective was to investigate the relative amount of gas recycle that would provide improved fluorine efficiency but would not result in caking of the bed.

A few minor modifications were made for this run. Nickel balls were used as a pellet bed support rather than the perforated plate employed in previous runs (see ANL-6287, page 149). The balls were $\frac{1}{4}$ in. in diameter, and their bed height extended one inch above the top of the conical gas distributor. This type of pellet-bed support has the advantage of not restricting the removal of solids at the end of the run. The balls can be recovered for re-use by screening or by magnetic trapping.

A sodium fluoride absorber was installed in the recycle gas stream for this run in order to remove any traces of uranium hexafluoride in the recycle gas. Molecular Sieve dryers were provided in the nitrogen inlet to ensure the introduction of dry gas.

The alumina charge in Run UOF-54 was sufficient to cover the pellets by 3 in. in the static condition and by about 6 in. when fluidized. The control temperature was measured by a thermocouple in a vertical thermowell from the bottom of the fluorinator; the thermocouple junction was 2 in. above the bottom of the pellet bed.

The gas and product rates in Run UOF-54 are shown in Figure 29 together with bed pressure drop data.

Figure 29

AVERAGE NITROGEN AND FLUORINE INPUT RATES AND URANIUM HEXAFLUORIDE COLLECTION RATES IN THE RUN UOF-54

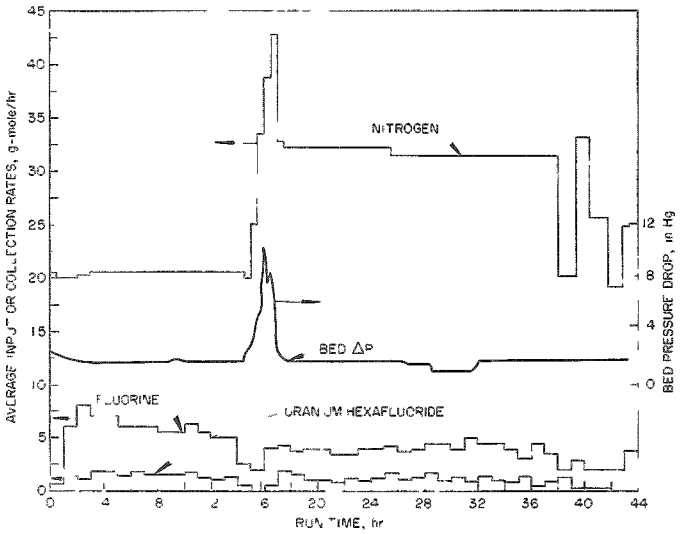

3-in. diameter fluorinator with gas recycle
Temperature: 500 C
UO_2 pellet bed: 18 in.
Weight ratio Al_2O_3/UO_2, 0.25
Recycle gas rate: 0.78 and 0.86 cfm (25 C, 1 atm)
Fluidizing velocity: $\geq$0.9 ft/sec (500 C, 1 atm)

The column was brought to 500 C with nitrogen as the fluidizing gas. The rate of nitrogen introduction to the column was 0.27 cfm (25 C and 1 atm), and the gas recycle rate was 0.78 cfm, for an initial superficial fluidizing velocity of 1.05 ft/sec at 500 C. Fluorine was introduced at a rate of 0.055 cfm for the first hour and was held at about 0.081 cfm for the next 11.5 hr. Uranium hexafluoride production began soon after fluorine introduction at a rate of 200 g/hr and reached a maximum of 750 g/hr during the ninth hour of operation. Operation was smooth and under control until the fourteenth hour, when a partial cake of the fluid bed developed. This was evident from an increase in pressure drop across the bed, and a sudden divergence of temperatures in the bed. The bed pressure drop increased from the normal value of 1.8 in. Hg to 10.5 in. Hg, and the control temperature dropped from 450 to 200 C. The fluorine input was somewhat lower during this period than during the second to fourteenth hour of the run. The duration of the disruption was 3 hr (from 14.5 to 17.5 hr). The cake apparently disintegrated shortly after the nitrogen input rate was increased from 0.27 to 0.54 cfm and the recycle rate was increased from 0.78 to 0.86 cfm. During this period, fluorine introduction was also raised or lowered in a manner dictated by an increase or decrease in the bed pressure drop, i.e., if the pressure drop increased, the rate of fluorine introduction was decreased. The maximum superficial fluidizing velocity attained was 1.35 ft/sec during the period of disruption. Once normal operation was resumed, a superficial fluidizing velocity of about 1.2 ft/sec was maintained for the remainder of the run. For the latter portion of the run, heat transfer and temperature control were satisfactory, and uranium hexafluoride production was moderate. A plot of the uranium hexafluoride cumulative gain is shown in Figure 30.

Figure 30

CUMULATIVE MOLES FLUORINE INPUT AND CUMULATIVE MOLES URANIUM HEXAFLUORIDE COLLECTED IN RUN UOF-54

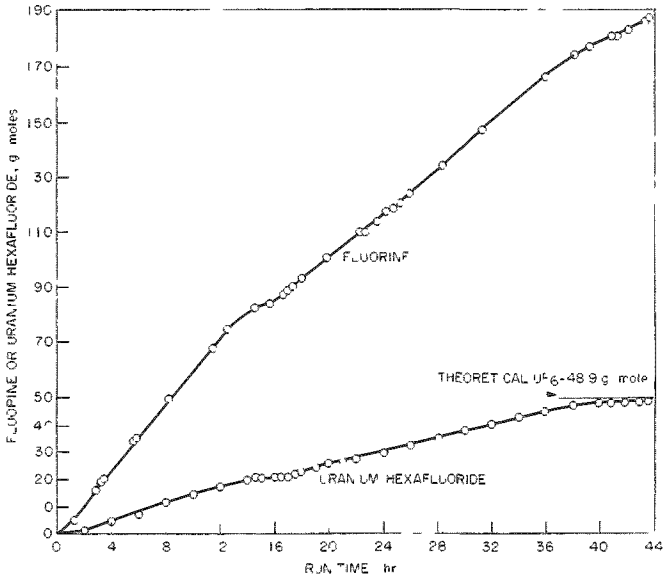

3-in. diameter fluormator with recycle
Temperature: 500 C
UO_2 pellet bed: 18 in.
Weight ratio Al_2O_3/UO_2, 0.25
Recycle gas rate: 0.78 and 0.86 cfm (25 C, 1 atm)
Fluidizing velocity: $\geq$0.9 ft/sec (500 C, 1 atm)

For a period of 11 hr (run time 3 to 14 hr, Figure 30), the average rate of fluorine introduction was 5.7 g-mole/hr and the uranium hexafluoride production rate was 1.33 g-mole/hr for an overall fluorine utilization efficiency of 70 percent. From the 16th through the 36th hours, fluorine introduction and hexafluoride collection averaged 4.05 and 1.25 g-mole/hr, respectively, for an overall fluorine efficiency of 92 percent.

The overall performance in this run was as follows: 98.8 percent of the uranium charge was collected as uranium hexafluoride in a total of 43.5 hr. This corresponded to an overall production rate of about 17 lb uranium hexafluoride/(hr)(sq ft of reactor cross-sectional area). The overall batch fluorine efficiency was 78 percent. Although a partial cake appeared during a 3-hr portion of the run, fluidization and temperature control were excellent during the remainder of the run, and the bed was entirely free-flowing at the conclusion of the run.

Run UOF-55

In Run UOF-55, an 18-in.-deep batch charge (13.2 kg) of pellets was used, the same amount as in the previous run, UOF-54, and in other runs of this series. However, a smaller amount of refractory alumina, 2.0 kg, was used as the inert fluid bed. The pellet bed support and control thermocouple position were also similar to those for the previous run. An additional set of thermocouples was provided in a vertical thermowell at the bottom of the reactor to measure temperatures at pellet bed heights of 6, 10, 14, and 18 in. Other operating conditions were similar to those in Run UOF-54.

The major aim of this run was to maintain the favorable results of the previous run with respect to fluorine utilization efficiency and fluidization quality, which was good for the greater part of the run, while obtaining greater rates of production of uranium hexafluoride. It was planned to achieve this by using greater rates of introduction of fluorine while adjusting the inlet nitrogen and the gas-recycle rate to maintain the same oxygen concentration in the reactor as prevailed in the last two-thirds of the previous run. The calculated values were based on the analysis of the partial-recycle system given in ANL-6543, pages 130 to 133.

The gas and product rates in UOF-55 are shown in Figure 31 together with bed pressure drop data. The initial gas rates for Run UOF-55 were inlet fluorine, 0.10 cfm; inlet nitrogen, 0.90 cfm; gas recycle, 0.50 cfm. The initial operating conditions were continued for a period of 5 hr, and only moderate rates of production were achieved. The recycle rate was then increased to 0.65 cfm. Pressure drop across the bed began to decrease from the normal fluid-bed value shortly thereafter. No improvement in production rate was observed at this time. At the 7th hour

Figure 31

AVERAGE NITROGEN AND FLUORINE INPUT RATES AND URANIUM HEXAFLUORIDE COLLECTION RATES IN RUN UOF-55

3-in. diameter reactor with gas recycle
Temperature: 500 C
UO_2 Pellet Bed Depth: 18 in.
Weight Ratio Al_2O_3/UO_2: 0.15
Recycle Gas Rate: 0.5 and 0.65 cfm (25 C, 1 atm)
Fluidizing Velocity: ≥1.0 ft/sec (500 C, 1 atm)

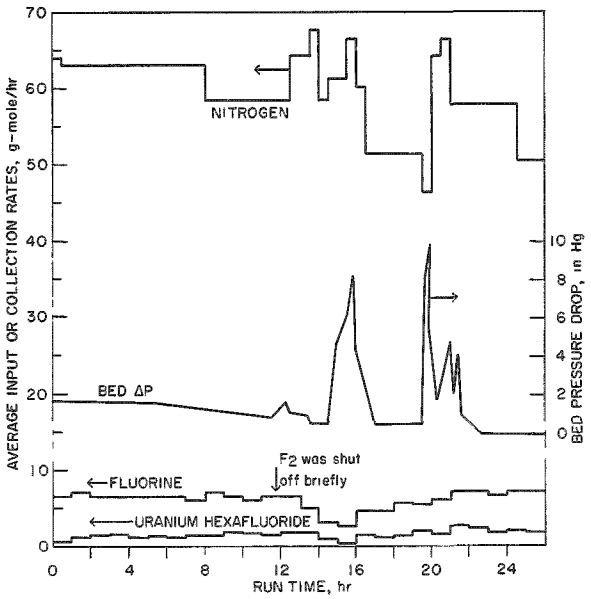

of operation, temperature gradients in the column increased somewhat. At the 8th hour, nitrogen input was decreased from 0.88 to 0.82 cfm, and slightly higher production rates were obtained. Shortly thereafter, the need for improved heat transfer to maintain the 500 C bed temperature required the lowering of reactor wall temperatures by forced air cooling. At the 12th hour of operation, the bed pressure drop increased from 0.8 to 1.6 in. Hg and the temperature at the control point fell to about 400 C. Recycle was decreased to 0.50 and nitrogen increased to 0.90 cmf. Fluorine was shut off briefly to purge reactive components from the gas and to allow the upper part of the column to cool. This procedure had good results. Fluorination was resumed, and a production rate of 745 g uranium hexafluoride/hr was established during the 13th hour.

At this point, the reactor was shut down. The top of the reactor was removed to determine if the bed had caked or if a large quantity of fines was present. A probing operation indicated the absence of cake in the portion of the inert bed above the pellets. An Alundum bed sample was taken for screen analysis. This analysis indicated that less than three percent of the bed was present as fines.

Operations were resumed, but a partially caked condition developed during the 14 hr of operation, and the pressure drop across the bed increased to 8.2 in. Hg while the control temperature dropped to 420 C. The bed obstruction was successfully reduced in approximately 2.5 hr. However, the very low pressure drop across the bed (0.3 in. Hg) indicated that a channelling condition was present. Rapping of the column with an automatic hammer was used at this point with no definite results. During the 19th hour of operation, the production rate increased sharply to 920 g/hr, and once again a partial caking condition was encountered. The cake was subsequently disintegrated, but the pressure drop across the bed sharply

decreased, which indicated that channelling was occurring. Because of these unstable conditions, the run was terminated after 25.8 hr of operation, at which point 73 percent of the uranium charge had been collected as uranium hexafluoride product. Fluorination could have been continued, but it was thought that no further information could be gained by doing so.

The bed was observed to be caked and a well-defined channel surrounded the vertical thermowell. Of a total of 3926 g of solids in the fluorinator bed, one-half was in the cake and one-half in free-flowing material (which contained 228 g of pieces larger than 40 mesh). Almost without exception the uranium dioxide pellets in the cake appeared to have a thick inner layer of oxide fines, a thin middle layer of uranium tetrafluoride, and a thick outer layer of uranyl fluoride. Uranyl fluoride appeared to bridge the gap between pellets and thus cause caking. Channelling in the bed, which may have become progressively more serious from the 5th hour of operation, when the recycle rate was increased from 0.5 cfm to 0.65 cfm, may have prevented sufficient fluorine from contacting these intermediates to fluorinate them completely.

Figure 32

CUMULATIVE MOLES FLUORINE INPUT AND CUMULATIVE MOLES URANIUM HEXAFLUORIDE COLLECTED IN RUN UOF-55

3-in. diameter reactor with gas recycle
Temperature: 500 C
UO_2 Pellet Bed Depth: 18 in.
Weight Ratio Al_2O_3/UO_2: 0.15
Recycle Gas Rate: 0.5 and 0.65 cfm (25 C, 1 atm)
Fluidizing Velocity: $\geq$1.0 ft/sec (500 C, 1 atm)

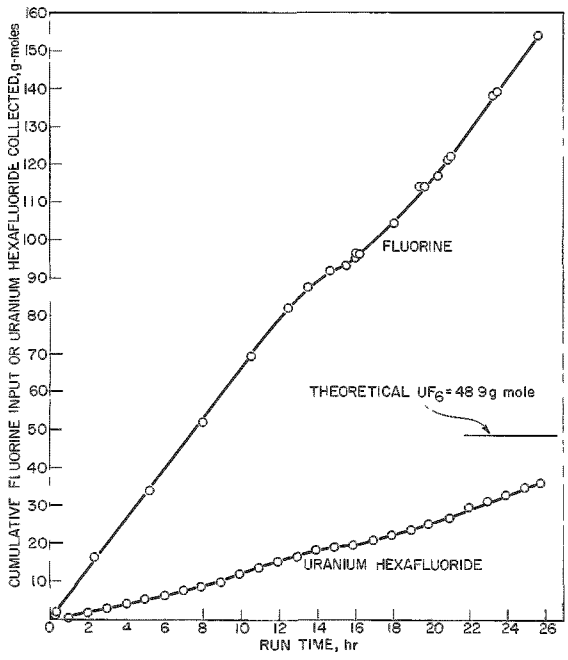

The cumulative moles of fluorine fed to the reactor and the moles of uranium hexafluoride collected are shown in Figure 32. Fluorine utilization efficiencies as determined from these curves indicate that during the first 7 hr of operation only 53 percent of the fluorine was recovered as the hexafluoride. In subsequent periods, the fluorine utilization efficiencies were greater (8 to 13 hr, 76 percent; 16 to 21 hr, 85 percent; 21 to 25 hr, 78 percent). The overall fluorine utilization efficiency for the run was 70 percent.

The maximum spread of longitudinal temperature in the bed was 20 C during the first 7 hr of operation (at centerline points 2, 6, 10, 14, and 18 in. above the bottom of the pellet bed). During the 12th hour of operation, bed temperatures ranged from 500 C at 6 in. to 740 C at 14 in.; this was the widest variation

in temperature during the run. When the run was resumed after the initial shutdown, the normal temperature difference was approximately 45 C and the maximum was of the order of 150 C. It is apparent that under conditions of good heat transfer (and, consequently, good fluidization), longitudinal temperature variation in the bed was small and of the order of about 20 C.

Results of analysis of gas-flow conditions in Run UOF-54 and UOF-55, made according to the method described in ANL-6543, page 130, are given in Tables 26 and 27. For this analysis, Run UOF-55 was divided into five periods, and average gas flows and compositions are shown for each period. Data from Run UOF-54 and other runs in this series are included in the tables and are discussed in the concluding part of this section.

Table 26

CONDITIONS FOR "DEEP-BED" PELLET RUNS

Note: Volumetric gas rates at 1 atm and 25 C. Linear gas rates are at 1 atm and 500 C, based on total cross-sectional area of reactor.

Run No. (UOF-)	Run Time (hr)	U Reacted (%)	Gas Input (cfm)			Gas Recycle (cfm)	UF_6 Rate (cfm)	UF_6 Production Rate (lb/(hr)(sq ft))	Total Gas Velocity (ft/sec)
			F_2	N_2	O_2				
50	20-26	54-87	0.233	0.66	0	0	0.038	42	0.78
52	2.5-6.5	4-14	0.253	0.735	0	0	0.018	20	0.84
	8.1-13.2	26-46	0.359	0.735	0.025	0	0.028	31	0.99
	16.3-18.7	62-75	0.302	0.735	0.072	0	0.041	45	0.90
	22-25.6	83-90	0.133	0.735	0	0.5	0.14	15	1.2
	26.4-29.2	90-95	0.088	0.735	0	0	0.12	13	0.66
53	1-9	3-29	0.096	0.195	0	0.7	0.022	24	0.86
	9-17.3	29-91	0.150	0.150	0	0.7	0.052	57	0.93
	17.3-22.3	91-96	0.043	0	-	0.7	0.007	7.8	-
54	1-12.5	2-37	0.083	0.27	0	0.78	0.019	21	1.0
	17-37	42-92	0.053	0.43	0	0.87	0.018	20	1.2
55	1-5	0.8-10	0.094	0.85	0	0.5	0.0164	18	1.3
	5-7	10-15	0.10	0.85	0	0.65	0.0164	18	1.4
	8-13	17-34	0.094	0.82	0	0.65	0.0237	26	1.4
	16-21	40-55	0.076	0.78	0	0.5	0.0213	23	1.2
	21-25	55-71	0.095	0.78	0	0.5	0.0255	28	1.2

Table 27

RESULTS OF "DEEP-BED" PELLET RUNS

Run No. (UOF-)	Run Time (hr)	UF_6 Rate [lb/(hr)(sq ft)]	Total Gas Velocity (ft/sec)	Overall F_2 Utilization Efficiency (%)	Nitrogen Dilution Factor[a]	Recycle Gas Ratio[b]	Gas Composition			
							Fluorinator Inlet		Fluorinator Outlet	
							(% F_2)	(% O_2)	(% UF_6)	(% O_2)
50	20-26	42	0.78	49	2.9	0	25.5	0	3.8	4.0
52	2.5-6.5	20	0.84	21	2.9	0	25.6	0	1.9	1.9
	8.1-13.2	31	0.99	23	2.0	0	32.0	2.5	2.6	2.7
	16.3-18.7	45	0.90	41	2.4	0	27.3	6.5	4.1	4.3
	22-25.6	15	1.2	31	5.5	3.8	13.3	0.6	1.6	1.7
	26.4-29.2	13	0.66	42	8.3	0	10.7	0	1.5	1.5
53	1-9	24	0.86	77	2.3	8.1	14.2	6.0	2.2	8.4
	9-17.3	57	0.93	87	1.0	3.9	22.5	12.3	5.0	18.5
	17.3-22.3	7.8	-	48	-	16.3	-	-	-	-
54	1-12.5	21	1.0	70	3.3	9.5	12.2	3.9	1.7	5.6
	17-37	20	1.2	92	7.0	15.0	4.8	2.4	1.3	3.8
55	1-5	18	1.3	53	9.3	5.3	9.0	0.6	1.6	1.7
	5-7	18	1.4	53	8.8	6.5	8.2	0.6	1.6	1.7
	8-13	26	1.4	76	8.7	6.9	8.0	1.1	2.6	2.7
	16-21	23	1.2	85	10.3	6.6	6.1	1.0	2.4	2.5
	21-25	28	1.2	78	10.0	6.4	8.3	1.1	3.0	3.1

[a]Nitrogen dilution factor - N_2 entering system, moles per hour/F_2 entering system, moles per hour.

[b]Recycle gas ratio - Recycle gas stream, moles per hour/F_2 entering system, moles per hour.

These data and calculations show that average oxygen concentrations in Run UOF-55 were held to the desired levels, which were about the same as those considered satisfactory in previous runs (especially in UOF-54). But despite good oxygen control, partial caking and channelling occurred in UOF-55. It also appeared that fines accumulated, possibly because of poor gas-pellet contact in local portions of the bed. Since the total gas velocities and oxygen concentrations were about the same in Runs 54 and 55, these factors probably do not account for the difference in operational behavior between these two runs, the behavior of Run UOF-54 being considerably more satisfactory than that of Run UOF-55.

The uranium hexafluoride concentration in the gas leaving the reactor was 1.6 to 3 mole percent in Run UOF-55. In the first part of Run UOF-54, the uranium hexafluoride concentration was about 1.7 percent, and in the last half of the run, which was operationally better than the first half, the concentration was about 1.3 percent. Since partial caking did occur in the first part of Run UOF-54 but not in the second part, it is possible that small differences in uranium hexafluoride concentration may be significant. The differences in uranium hexafluoride concentration within a run were due solely to the difference in rate of uranium hexafluoride production. No uranium hexafluoride was returned to the reactor in the recycle gas in either run.

One other difference between Runs UOF-54 and -55 was the amount of inert bed. The former used 3.3 kg and the latter 2.0 kg. This difference may have influenced the operational behavior of the runs. In earlier runs, in which 6-in. pellet beds were successfully fluorinated at a rapid rate, deeper inert beds than those above (by about a factor of six) were used.

Summary of Results of "Deep-bed" Runs

The series of "deep-bed" pellet fluorinations consisted of six batch runs, UOF-49, -50, -52, -53, -54, and -55, each with a charge of 13.2 kg of $\frac{1}{2}$-in.-diameter and $\frac{1}{2}$-in.-high uranium dioxide pellets forming a fixed bed, 18 in. deep in the 3-in. reactor. The major objectives and standards of evaluation for these runs have been described in the beginning of this section. A comparison of these six runs in terms of these standards is given in summary form in Table 28.

The rating of fluidization quality is an expression of the experimenter's opinion concerning the operational behavior of the system during a run. Of these runs, only in UOF-49 was caking so severe that continued fluorination was impossible. In Run UOF-55, for example, control was difficult at the desired fluorination rate because of partial caking, but fluorination probably could have been continued at a lower rate.

Table 28

SUMMARY EVALUATION OF SIX "DEEP-BED" PELLET RUNS

3-in.-diameter fluorinator
13.2-kg UO_2 charge: 18-in.-deep pellet bed
Refractory Al_2O_3 inert fluid bed (60-200 mesh)

Run (UOF-)	Control Temp (C)	Charge Ratio $\frac{Al_2O_3}{UO_2}$	Gas Recycle	Overall Estimate of Fluidization Quality (Rating)	Overall Fluorine Utilization Efficiency (%)	Overall Fluorine Utilization Efficiency (Rating)	Overall Average UF_6 Rate lb/(hr)(sq ft)	Overall Average UF_6 Rate (Rating)	Time for Complete Fluorination (hr)
49	450	0.12	Max Recycle; High O_2	Poor	-	-	-	-	-
50	450	0.29	No	Good[a]	37	Poor	24	Fair	30
52	500	0.29	No; but some O_2 added	Good	29	Poor	25	Fair	29
53	500	0.25	Partial Recycle	Poor	77	Good	32	Fair	22
54	500	0.25	Partial Recycle	Good[a]	78	Good	17	Undesirably Low	44
55	500	0.15	Partial Recycle	Poor	70	Fair	21[b]	Undesirably Low	35[c]

[a]Better period was last part of run (see text and Table 27).

[b]Run was terminated at 73 percent of complete fluorination.

[c]Calculated for 100 percent fluorination; 73 percent fluorination in 26 hr.

Study of the table shows that every run had a "poor" rating in at least one of the three categories of evaluation. Fluorine economy and fluidization quality appear promising only for bed conditions for which uranium hexafluoride production rates were below 20 lb/(hr)(sq ft) (in Run UOF-54 only).

Pertinent data for the "deep-bed" run series are presented in Tables 26, 27 and 28. Runs UOF-50 and UOF-52 were "no recycle" runs, and Runs UOF-53, -54, and -55 were partial-recycle runs. As expected, higher fluorine input rates were accompanied by higher rates of production of uranium hexafluoride. From these and other data it also appears that a higher average oxygen concentration in the reactor is associated with higher fluorine utilization efficiency. Although the partial-recycle scheme employed in Runs UOF-53, -54, and -55 was successful in limiting oxygen concentrations in the fluorinator while retaining some of the benefits of gas recycle, it did not eliminate caking tendencies, nor did it provide consistently good fluidization. In Run UOF-55 in particular, the control of oxygen concentration was expected to avoid caking, but did not. When Runs UOF-54 and -55 are compared, it does not appear that oxygen concentration was decisive with respect to caking, since the latter run had a lower oxygen concentration and more caking. On the other hand, the data suggest the possibility of a correlation between caking (decrease of fluidization quality) and higher uranium hexafluoride rates (and concentrations).

Moreover, as shown by production rates given in Table 26, it is possible that lower aluminum oxide/uranium dioxide ratios favor caking. This observation would also be consistent with the good results obtained

earlier with 6-in.-deep beds which had much higher inert bed to uranium dioxide ratios. (For example, in Run UOF-34 the ratio aluminum oxide/uranium dioxide was 1.9.)

Although it is still considered possible to refine operations with 18-in.-deep beds, it now appears more profitable to investigate various pellet bed depths and to study the effect of different aluminum oxide/uranium dioxide ratios, since these variables seem critical. A new series of runs is planned with the equipment modified for continuous pellet feed, which will allow a steady-state operation to be maintained with virtually constant bed height. A constant bed height during a run should make experimental effects easier to analyze. A more important advantage of constant bed height may be semicontinuous process operation at steady bed conditions favorable to the most desirable combination of production rate, fluorine efficiency, and fluidization quality.

In summary, the work thus far indicates that 6-in.-deep beds can be fluorinated satisfactorily at rates up to about 50 lb uranium hexafluoride/(hr)(sq ft), while 18-in.-deep pellet beds are subject to caking tendencies at rates above 20 lb uranium hexafluoride/(hr)(sq ft). Further studies of process optimization will be made for various intermediate pellet-bed heights and various aluminum oxide/uranium dioxide bed ratios.

2. Design and Construction of Engineering-scale Plutonium Handling Facility
(G. J. Vogel, E. Carls, W. J. Mecham, L. Marek, and W. Murphy)

Construction activities in the building of the engineering-scale high-alpha handling facility are proceeding on a schedule which should allow plutonium operation to begin about May 1963. The Critical Path Method,[14] in conjunction with an IBM 704 computer program, is being used to expedite construction and installation. Initially, the process variables in the fluorination of uranium-plutonium oxide pellets are to be studied in a fluidized-bed reactor. Later, equipment will be added to the facility to study methods for the separation of the uranium from the plutonium. The behavior of the fission products can also be investigated in this system at gamma levels that allow direct personnel access.

The engineering facility includes two alpha boxes as shown in Figure 33. The larger alpha box will hold all of the plutonium-processing equipment and will be located inside an enclosed cell. The smaller alpha

[14]Glaser, L. B., and Young, R. M., Chem. Eng. Prog., 57, 59 (Nov 1961).

box will contain the aqueous scrubber and process-gas-metering manifold; this box will be located in the main operating area, along with the panel board from which the process is controlled.

Figure 33

ENGINEERING-SCALE PLUTONIUM HANDLING FACILITY

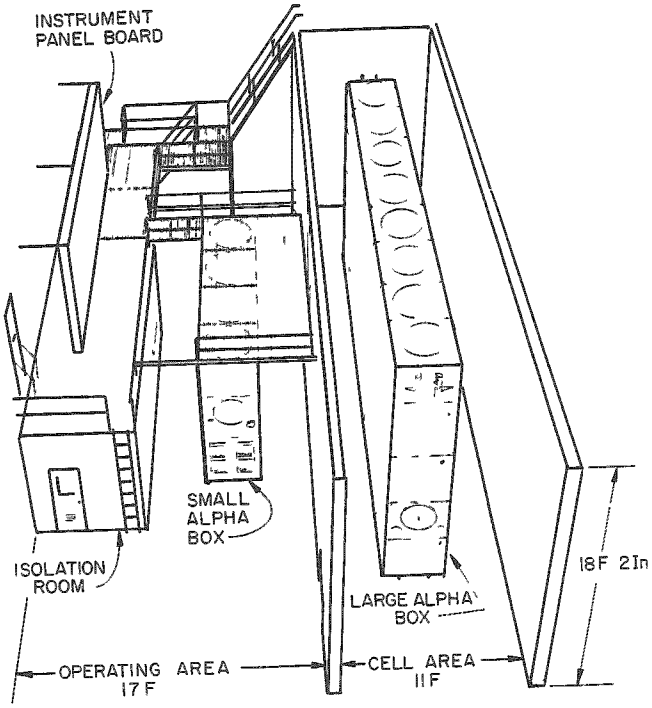

The layout of equipment in the larger alpha box is shown in Figure 34, a photograph of a scale model constructed to facilitate the layout of equipment and lines. Near the middle of the box is the fluidized-bed reactor unit complete with process gas filters and fuel charger. To the right of this unit are three condensers, each mounted on a weighing scale, in which the uranium and plutonium hexafluoride products will be collected. Gas will be recirculated to the fluorinator by the diaphragm pump at the lower right. Process purge gas will pass through alumina traps at the upper right, before being exhausted from the box along with the box ventilation air. Also in the box are the gas preheater and the product containers, one of which is shown at the upper middle on a weigh scale. A plutonium hexafluoride decomposer and distillation column for uranium-plutonium separation studies are shown in the left half of the box, but have not yet been installed.

The handling of large quantities of plutonium in the gaseous state rather than in the liquid or solid state would present a safety problem if the gaseous plutonium hexafluoride were inadvertently released from the equipment. Laboratory test data have shown that, whereas plutonium hexafluoride vapor is not efficiently removed from air by absolute filters, the hydrolyzed solid product is efficiently removed by filtration. Consequently, all air and process-gas streams are humidified to hydrolyze the fluoride off-gas before being exhausted through absolute filters to the outside air. Also, to minimize the spread of any alpha contamination during any accidental release, a series-connected ventilation system is used with increasing negative pressures in the personnel operating area, cell area, and alpha boxes. The box-ventilation air is drawn into the box from the cell area through a filter and is exhausted along with the process-gas waste successively through a filter, aqueous scrubber, and two absolute filters before being mixed with the ventilation air from the operating and cell areas. As a final safety precaution, before final release all ventilation air exhaust is put through another (larger) aqueous scrubber and a set of absolute filters (six in parallel).

Figure 34

DIRECT FLUORINATION PROCESS SCALE MODEL OF PILOT-PLANT EQUIPMENT IN PLUTONIUM ENCLOSURE

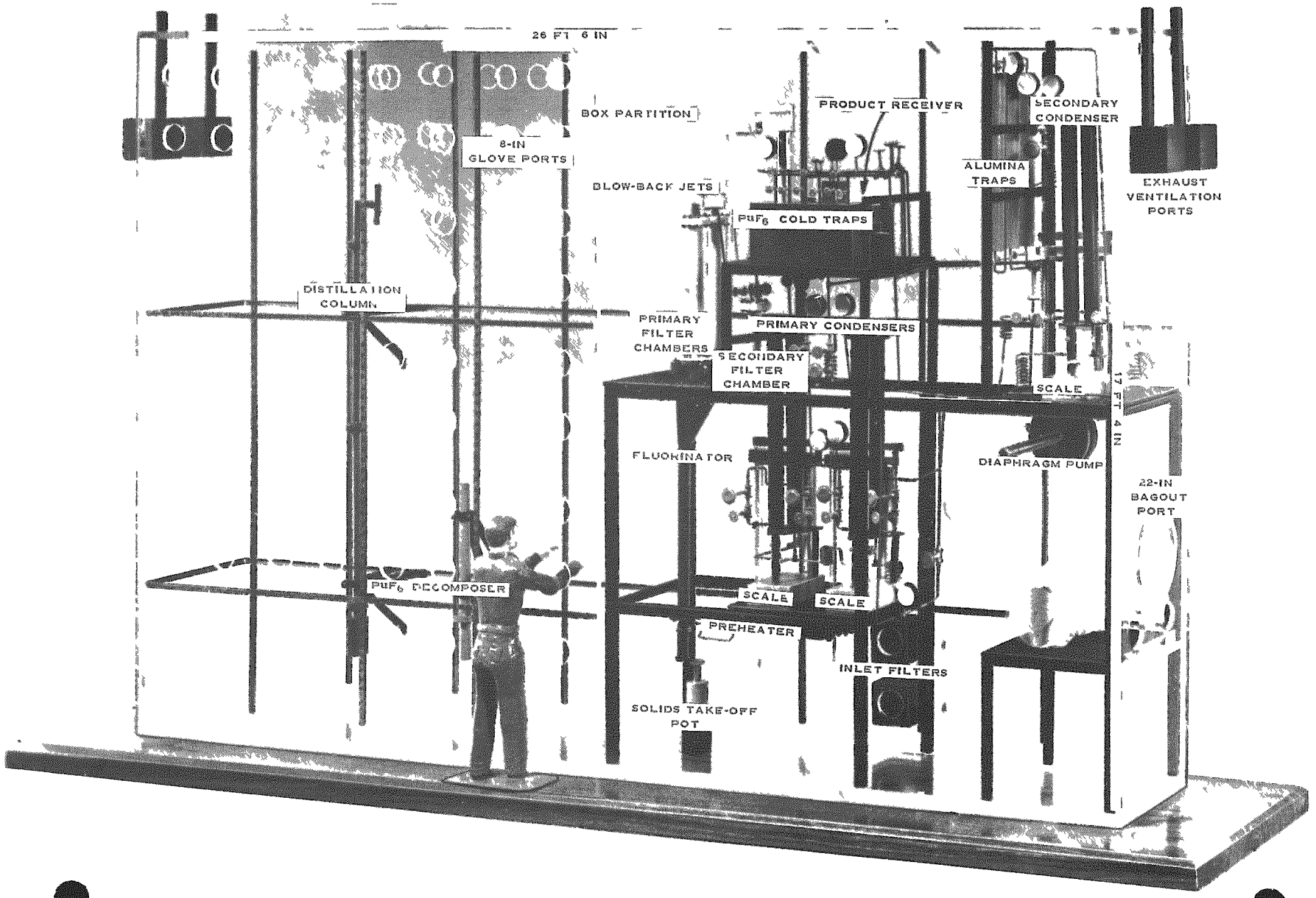

3. Separation of Uranium from Zirconium-alloy Fuels
(N. Levitz)

a. Process Studies on Recovery of Uranium from Enriched Uranium-Zirconium-alloy Fuels
(D. Ramaswami, J. T. Holmes, and C. Schoffstoll)

A fluidization-volatility process scheme for the recovery of uranium from enriched uranium-zirconium-alloy nuclear fuels is being investigated. The process involves reaction of the alloy with hydrogen chloride while the uranium-zirconium fuel is submerged in an inert fluidized bed. During the reaction of the alloy with hydrogen chloride, the zirconium is sublimed as the tetrachloride, leaving particulate uranium chloride in the reactor assembly. Uranium is recovered as volatile uranium hexafluoride during a subsequent fluorination step.

In order to demonstrate the feasibility of this process, the reactions with hydrogen chloride and with fluorine are being investigated in a bench-scale fluid-bed unit. The reactions are being carried out in a prefluorinated nickel reactor (1.61-in. inside diameter) containing a fluidized bed of prefluorinated Alundum (Norton, Type RR). Temperatures in the range from 400 to 550 C are being used. Particulate matter (including uranium) entrained from the fluidized-bed reactor is collected by flow of the gas stream downwards through an Alundum bed-filter (1.61-in. inside diameter) maintained at 350 to 550 C. The off-gases from the filter are cooled to condense volatile reaction products. The waste gases are treated, and remaining inert diluent gases are discharged to the stack.

Previous studies (ANL-6413, page 136 and ANL-6543, pages 149 to 150) indicated that:

1. Less than 0.2 percent of the uranium reacted in the fluid bed was lost during the reaction with hydrogen chloride when the downflow Alundum bed filters were used.

2. Uranium retained by the Alundum in the fluid-bed reactor was about five percent of the uranium reacted during a single chlorination-fluorination cycle. The cumulative uranium loss to the Alundum residue decreased to one percent when the same bed material was used in five consecutive runs.

3. Satisfactory collection of uranium hexafluoride from dilute gas streams can be expected during fluorination.

The object of the present work is to determine process conditions which will result in loss of less than one percent uranium to the Alundum in each cycle in the fluidized-bed reactor

Apparatus. The apparatus (see Figure 35) consists of 1) a fluid-bed reactor, 2) a downflow static-bed filter, 3) a zirconium tetrachloride condenser, 4) a hydrogen chloride-absorption tower, 5) cold traps, and 6) a fluorine-disposal tower. In practice, the zirconium tetrachloride condenser is completely removed after the hydrogen chloride reaction is completed, and the cold traps are installed prior to fluorination. The apparatus for off-gas analysis which was recently installed and is undergoing testing and calibration is also shown in Figure 35.

Figure 35

APPARATUS FOR CHLORINATION AND FLUORINATION OF URANIUM-ZIRCONIUM ALLOY FUELS

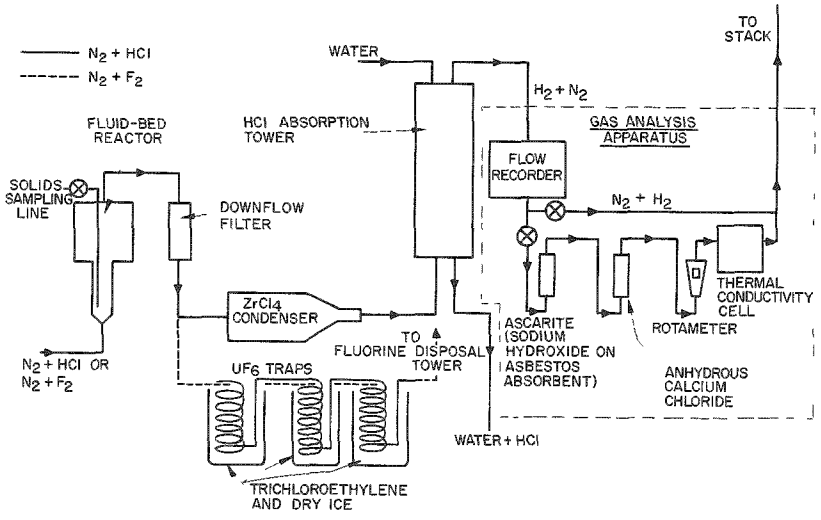

The fluid-bed reactor has a 1.6-in. inside diameter and a 14-in.-high section topped by a 3-in.-diameter disengaging section of similar height. A sampling line (for solids) of $\frac{1}{8}$-in. inside diameter dips into the fluidized bed with its open end 2 in. above the bottom of bed. The downflow filter (1.6-in. inside diameter and 14 in. high) is connected to the top of the disengaging section of the reactor by a 1-in. inside diameter by 14-in.-long tube. The entire reactor and downflow filter assembly is made of nickel and is provided with external heaters.

The zirconium tetrachloride condenser is an air-cooled Pyrex glass section of 4-in. inside diameter by 19 in. long. The hydrogen chloride-scrub tower is a 4-in. Pyrex glass pipe packed with $\frac{1}{2}$-in. ceramic Raschig rings to a height of 28 in.

The cold-trap system consists of three copper coils, each wound from a 5-ft length of $\frac{1}{2}$-in.-inside-diameter tubing. The coils are immersed individually in a bath of trichloroethylene and dry ice. The fluorine disposal tower is made of nickel (3-in. inside diameter and 36 in. tall) and contains activated alumina spheres ($\frac{1}{4}$-in. diameter) to a height of 32 in. from the bottom.

Experimental Procedure. A predetermined quantity of Alundum (Norton Type RR) is charged to the reactor and filter sections. Alundum in the reactor is fluidized by a flow of nitrogen. After the reactor and filter sections are brought to the desired temperature, the entire assembly is prefluorinated for approximately 2 hr with an equimolar mixture of nitrogen and fluorine. After prefluorination, the reactor assembly is purged with nitrogen for 0.5 hr. Uranium-zirconium alloy fuel is then charged from the top of the reactor. A preheated mixture of nitrogen and hydrogen chloride is admitted to the reactor at a manually regulated rate. When the desired amount of chlorinating agent has been fed, the system is purged with pure nitrogen. Then fluorination is carried out for the desired time interval. Because of the high reactivity of the system, the temperature of the reaction zone is manually controlled by regulating the concentration of the reactant gas at the inlet and the heat input to the system during the initial stages of the reactions.

During the first of the current studies, unusually large pressure buildups across the downflow Alundum-bed filter were encountered. These were attributed to the formation of fine particulate material in the fluid bed during the chlorination with hydrogen chloride and the entrainment of this material in the gas stream to the filter bed. In order to avoid this pressure effect, the use of the filter bed was suspended temporarily by removing the contained Alundum.

Results. Results show that higher fluorination temperatures give improved uranium removal, as indicated by analysis for residual uranium in the inert bed material. Typical values (see Table 29) are 0.05 weight percent uranium for a fluid bed at 400 C (Run 26) and 0.03 weight percent uranium for a fluid bed at 500 C (see Run 25).

Table 29

CHLORINATION AND FLUORINATION OF URANIUM-ZIRCALOY ALLOY

Equipment: 1 1/2-in.-diameter column
Zircaloy Sample: No. GR 126 (Irregularly shaped chips ~1/8 to 1/4 in. on a side)
w/o U in Zircaloy = 5.1
w/o oxygen in Zircaloy = 0.126
Bed Material: Alundum Type RR, -40 +60 mesh
(No downflow filter except in Runs 23 and 24)

Run No.	Inert Bed Charge (g)	Alloy Charge (g)	Chlorination			Fluorination			Final Bed Analysis (w/o)		% Initial Zr Retained in Fluid Bed	% Initial U Retained in Fluid Bed
			Fluid Bed Temp (C)	Time (hr)	Quantity of HCl[a] (X Stoich)	Fluid Bed Temp (C)	Time (hr)	Quantity of F_2[b] (X Stoich)	Zr	U		
27	320	240	400	28	25	400	7	140	0.04	0.04	0.06	1.1
						500[c]	2	40	0.04	0.03	0.06	0.8
						500[c]	4	80	0.04	0.03	0.06	0.8
26	320	240	400	17	13	400	6.5	130	0.13	0.05	0.18	1.3
						500[c]	2	40	0.13	0.03	0.18	0.8
25	320	240	500	12.5	11	500	5	100	0.04	0.03	0.06	0.8
						500[c]	2	40	0.04	0.03	0.06	0.8
						500[c]	4	80	0.04	0.03	0.06	0.8
24	550	350	550	6.5	4	550	6	120	0.44	0.05	0.73	1.5
23	550	350	450	5	4	450	6	120	0.23	0.06	0.38	1.9

[a]Stoichiometric amount based on total alloy.
[b]Based on uranium content of alloy only ($UCl_3 + 3\,F_2 \rightarrow UF_6 + 3/2\,Cl_2$).
[c]Refluorination of bed.

Further improvement was noted when a bed, initially fluorinated at 400 C, was refluorinated at 500 C (as in Runs 26 and 27). The value of 0.03 weight percent uranium in the residue corresponds to 0.8 percent of the initial uranium charge.

Utilization of greater excesses of hydrogen chloride resulted in a slightly lower overall uranium residue after subsequent fluorination of the inert bed material (compare Runs 26 and 27 and also Runs 24 and 25). The reduction in zirconium content with greater excesses of hydrogen chloride was somewhat more pronounced.

In two experiments phosgene was used at the end of the chlorination step to promote removal of the residual amounts of zirconium (possibly present as oxide). This was expected to make more uranium available for recovery, since it has been suspected from previous work that residual uranium is associated with residual zirconium. In the initial scouting experiment (see Table 30), 4 g of chlorinated Alundum bed from Run No. 24 were treated with phosgene at 400 C in an Alundum boat and then subjected to fluorination at 400 C. In the second experiment (Run 28), Zircaloy was chlorinated at 400 C in a fluidized bed of Alundum. The resultant bed was treated with phosgene at 400 C and subsequently fluorinated at 400 and again at 500 C. In both of these experiments, less than 0.2 percent of the uranium and 0.05 percent of the zirconium charged to the reactor bed was retained by the Alundum.

Table 30

EFFECT OF PHOSGENE TREATMENT ON RETENTION OF URANIUM BY ALUNDUM

Equipment: 1 1/2-in.-diameter column
Zircaloy Sample: No. GR126 (Irregularly shaped chips ~1/8 to 1/4 in. on a side)
w/o U in Zircaloy: 5.1
w/o oxygen in Zircaloy: 0.126
Alloy Charge: Run No. 24, 26 refer to Table 29; Run No. 28: 240 g
Bed Material: Alundum Type RR; -40 +60 mesh, No down-flow filter
Inert Bed Charge: Run No. 24, 26 refer to Table 29; Run No. 28: 320 g

	Chlorination With													
	Hydrogen Chloride				Phosgene				Fluorination[a]					
			Final Reactor Bed Analysis				Final Reactor Bed Analysis				Final Reactor Bed Analysis			
Type of Run	Reactor Bed Temp (C)	Time (hr)	w/o Zr	w/o U	Reactor Bed Temp (C)	Time (hr)	w/o Zr	w/o U	Reactor Bed Temp (C)	Time (hr)	w/o Zr	w/o U	% Initial Zr Charge Retained in Reactor Bed	% Initial U Charge Retained in Reactor Bed
Fluid Bed (Run 26)	400[b]	17	-	0.74	-	-	-	-	400	6.5	0.13	0.05	0.18	1.3
									500	2.0	0.13	0.03	0.18	0.8
Boat[c]	550	6.5	0.8	1.29	400	3	0.8	1.22	400	3	< 0.02	0.005	< 0.03	< 0.2
Fluid Bed (Run 28)	400[b]	7	-	0.79	400[d]	5.2	-	1.03	400	9	< 0.03	0.03	< 0.04	0.8
									500	2	< 0.03	< 0.01	< 0.04	< 0.2

[a]Fluorine excess was ~100 times the stoichiometric requirement (based on uranium content of the alloy) in all runs.
[b]Excess HCl was 13 times stoichiometric in Run 26 and 3.3 times stoichiometric in Run 28. The stoichiometric amount was based on the total alloy.
[c]Material was taken from Run 24 and was hydrochlorinated in the fluid-bed unit.
[d]Total phosgene fed was 29.3 cu ft, approximately 7 times stoichiometric.

In a subsequent fluid-bed experiment (which will be discussed more fully in the next quarterly) in which the reaction procedure involved a hydrogen chloride-phosgene mixture, then a phosgene treatment followed by fluorination, unexpected ignitions occurred upon venting (to air) of the cold traps used for collecting the uranium hexafluoride. The traps are normally kept at about -80 C with a dry ice-trichloroethylene bath and are purged with nitrogen. In order to hydrolyze the material in the traps (for subsequent chemical analysis), the traps are disconnected from the reactor system and the coolant is removed. The ignitions occurred during the initial stages of warm-up, at which time the traps were vented to the atmosphere. An investigation into the possible causes of these ignitions is being made.

Improvement of the Laboratory Unit. It has been observed that only about one percent of the uranium which reacted in the fluid bed passed into the zirconium tetrachloride condenser in Runs 25, 26, and 27. Most of the entrained uranium chloride particulate matter appeared to be deposited on the inner walls of the empty downflow filter section. If this behavior continues, the use of a separate "settling" chamber prior to the use of the Alundum-bed filter may have the following benefits: 1) the rate of pressure buildup across the Alundum-bed filter may be reduced and 2) the filter efficiency of the whole system may improve. Since the downflow filter section will contain a filter bed in future work, an intermedate chamber will be installed to test further this unexpected behavior.

Preliminary experiments with a thermal conductivity cell indicate that the exit gas stream consists of 0 to 30 percent hydrogen during chlorination with hydrogen chloride. Based on this experience, necessary equipment (see Figure 35) is being assembled to measure the concentrations of gaseous products in the exit gas stream The gas analysis assembly consists of 1) a sample-purification section, 2) a sample-metering unit, 3) an "on stream" ambient temperature-controlled thermal conductivity cell, and 4) a recorder for product concentration in the gaseous stream during chlorination. A thermal flowmeter is being installed to record the flow of exit gases. With the above equipment, the progress of the reactions can be observed and recorded, and quantitative data, including reaction rates, may be obtained for the entire run. A similar scheme may be usable during the fluorination step.

Future work. The future work will be directed toward establishing process conditions for obtaining maximum recovery of uranium and smooth operation of the bench-scale unit. The effect of the following independent variables will be investigated:

1) Zircaloy containing a lower percentage of uranium;

2) shape of Zircaloy (long strips in comparison with the chips being used at present);

3) weight ratio of Zircaloy to Alundum;

4) consecutive chlorinations of fresh charges of alloy prior to fluorination;

5) use of phosgene-hydrogen chloride mixtures;

6) in situ mixing of hydrogen and chlorine instead of using hydrogen chloride gas;

7) use of hydrogen fluoride prior to fluorination.

b. Fluid-bed Hydrolysis of Zirconium Tetrachloride
(K. Sutherland, and D. J. Raue)

A study is continuing of the pyrohydrolysis of zirconium tetrachloride by steam in a fluidized bed. This work is directed toward developing a method for disposal of the waste tetrachloride produced by chlorination of the zirconium in fuel elements. In the reaction, the tetrachloride is converted into the more easily stored oxide. It has previously been demonstrated that the process is feasible on a small batch scale with low feed rates, but attempts to increase the tetrachloride flow rate to that required for a proposed pilot plant have been troubled by the occurrence of large pressure drops across the exit-gas filters due to excessive buildup of fines on the filters. The currently reported work was aimed at finding operating conditions which would eliminate these excessive pressure drops by increasing the percentage of solid product deposited on the bed material. It was hoped that deposition of oxide would be promoted by increasing the gas-residence time in the bed and decreasing the reaction temperature, thus reducing the proportion of hydrolysis occurring in the gas phase.

A major change in the experimental setup from that previously reported (ANL-6543, page 151) is the use of the same stream of nitrogen to transport the tetrachloride and to fluidize the bed, thereby eliminating the need for a separate diluting nitrogen stream for fluidization. A diagram of the apparatus now used is shown in Figure 36, and the run conditions are given in Table 31. The starting bed material for each series of runs was refractory-grade alumina with a size range of -60 +200 mesh. The bed depth in the 6-in.-diameter column was maintained at about 20 in. During the longest runs, enough material was produced so that solids had to be removed semicontinuously in order to maintain a constant bed height. Runs were carried out with bed temperatures of 300, 350, and 450 C. A low feed rate (1.2 kg/hr) was used in the first two runs in order to avoid overloading the rebuilt apparatus, the later higher figure (2.2 kg/hr) being slightly greater than that for the proposed pilot plant (see Figure 50, ANL-6543, page 153). The nitrogen flow rate was increased for the last run in order to simulate more closely the conditions of a pilot-plant gas stream.

Figure 36

DIAGRAMMATIC FLOWSHEET OF EXPERIMENTAL APPARATUS FOR THE FLUID-BED HYDROLYSIS OF ZIRCONIUM TETRACHLORIDE

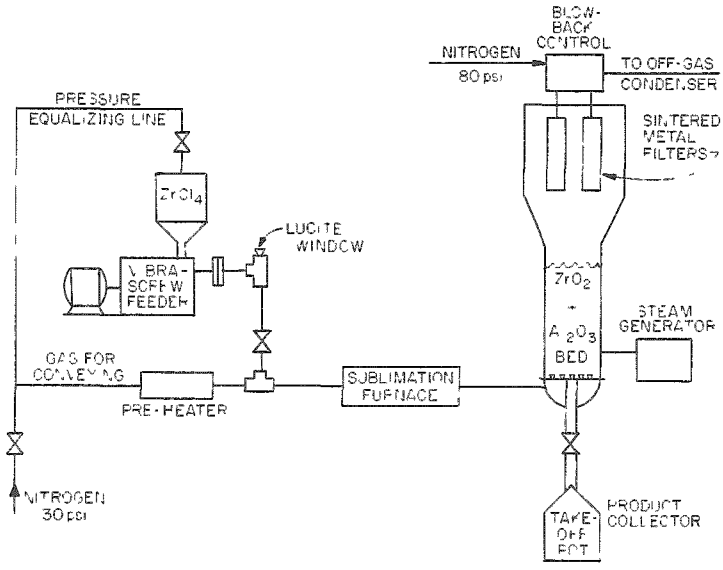

Table 31

OPERATING CONDITIONS FOR THE FLUID-BED HYDROLYSIS OF ZIRCONIUM TETRACHLORIDE

Equipment: 6-in.-diameter column
Nitrogen Flow Rate: 2 scfm[a]
Steam Rate: 0.9 scfm
Starting Bed Weight: 15.2 kg

Run No.	Bed Material	Run Duration[b] (hr)	$ZrCl_4$ Feed Rate (hr/hr)	Steam Quantity (X Stoich)	Bed Temp (C)	Blowback Pressure (psig)
CO-20	Fresh Al_2O_3	3.0	1.2	6.5	450	30
CO-21	Coated Al_2O_3 from CO-20	3.2	1.2	6.5	350	30
CO-22	Coated Al_2O_3 from CO-21	1.8	2.2	3.5	350	30
CO-23	Fresh Al_2O_3	0.8	2.2	3.5	350	30
CO-24	Coated Al_2O_3 from CO-23	6.0	2.2	3.5	350[c]	30
CO-25	Coated Al_2O_3 from CO-24	3.5	2.2	3.5	300	80
CO-26	Coated Al_2O_3 from CO-25	1.8	2.2	3.5	300	80

[a]Increased to 2.5 scfm for Run CO-26.

[b]Time of feeding $ZrCl_4$.

[c]Reduced to 300 C for last hour.

The major results are presented in Tables 32 and 33. Included are the observed increases in pressure drop, the material balances for each run, and the changes in particle size for each of the two fresh batches of alumina. The most important effects are the increases in pressure drop, which were very high (10 to 16 in. Hg) for two of the runs and low (< 1 in. Hg) in the other five. When the bed temperature was decreased from 450 C in Run CO-20 to 350 C in Run CO-21, the pressure drop problem was relieved for the short durations of Runs CO-21 to CO-23 (0.8 to 3.2 hr), but the pressure buildup occurred again in the longer Run CO-24 (6 hr). However, the increase in pressure drop in this particular run did not start until the elapsed time had exceeded $2\frac{1}{2}$ hr, i.e., a longer period than the total run time for the previous two runs at the higher tetrachloride feed rate.

Table 32

EXPERIMENTAL RESULTS FOR THE FLUID-BED HYDROLYSIS OF ZIRCONIUM TETRACHLORIDE

(See Table 31 for other run conditions)

Run No.	Increase in Pressure Drop[a] (in. Hg)	Material Input (kg)			Material Output (kg)			
		Starting Bed	Equivalent ZrO_2 Fed	Total	Final Bed	Product Takeoff	Filter Fines	Total
CO-20	10.3	15.23	1.85	17.08	16.52	0	0.52	17.04
CO-21	0.9	16.47	2.09	18.56	18.34	0	0.22	18.56
CO-22	0.3	18.31	2.09	20.40	20.11	0	0.25	20.36
CO-23	0.3	15.99	0.96	16.95	16.83	0	0.07	16.90
CO-24	16.2	16.78	6.40	23.18	19.23	1.23	1.56	23.54
CO-25	0.4	16.00	3.66	19.66	18.54	0.88	0.42	19.84
CO-26	0.4	16.00	2.08	18.08	17.78	0	0.32	18.10

[a]Initial value, 1.6 in. Hg.

Table 33

DISTRIBUTIONS OF ALUMINA PARTICLE SIZE DURING THE FLUID-BED HYDROLYSIS OF ZIRCONIUM TETRACHLORIDE

(See Table 32 for run conditions and source of bed material)

Run No.	USS Sieve Fractions (w/o)				Run No.	USS Sieve Fractions (w/o)			
	+60	-60 +100	-100 +200	-200		+60	-60 +100	-100 +200	-200
CO-20 Start	0	47.0	53.0	0	CO-23 Start	0	49.2	50.7	0.1
CO-20 Finish	0	47.0	53.0	0	CO-23 Finish	0.3	46.9	52.7	0.1
CO-21 Finish	0.6	52.8	46.6	0	CO-24 Finish	1.7	58.4	39.6	0.3
CO-22 Finish	2.6	56.6	40.5	0.3	CO-25 Finish	2.9	61.2	31.9	4.0
					CO-26 Finish	2.6	58.6	29.8	9.0

It seemed reasonable to assume from this last fact that an inefficient blowback system (each of the four filters is blown back once each minute) might be the cause of the large pressure drops. Accordingly, the last two runs were performed with a greater blowback pressure (80 psi as opposed to 30 psi), and the increase in pressure drop across the filters was once again reduced to an insignificant value. The use of a higher blowback pressure was accompanied by a further reduction of bed temperature from 350 to 300 C. However, the overall effect of reducing the temperature is still somewhat obscure. Operations have improved in general, although the percentage of material deposited on the bed particles

seemingly did not increase. This is indicated by the increased proportion of -200 mesh particles present at the end of Runs CO-25 and 26 (see size analyses in Table 33). Despite the increasing quantity of fines, a general trend towards particle growth can also be observed.

The material balances given in Table 32 are all good, the differences between total input and total output being well within the error in the bed weights. The current series of runs are the first for which good balances have been obtained.

Although it is now probable that a long run can be made without large pressure buildup, the operating conditions do not yet seem to be favoring maximum deposition of product oxide on the bed material. Future work will therefore be directed towards finding conditions such that a minimum amount of -200 mesh material is generated. The main variables to be studied will be bed temperature and the amount of excess of steam in relation to the stoichiometric value. In addition, the reaction must be carried out successfully in the presence of a high proportion of hydrogen chloride, which constitutes 62 volume percent of the proposed pilot-plant stream.

c. Process Design Work for the Fluoride Volatility Pilot Plant for Recovery of Uranium from Zirconium Alloy Fuels

(N. Levitz, J. Barghusen, and J. Holmes)

Shop prints have been submitted to Argonne National Laboratory's Central Shops for fabrication of essentially all of the major process vessels. The Lapp Insulator Company, LeRoy, New York, submitted the low bid on the remote-head diaphragm compressor for fluorine recycle, and the order has been placed. An order has been placed for construction of the panel board. This will include off-site mounting of the instruments, complete with piping and electrical wiring, and delivery of the packaged unit for installation. Preliminary discussions with Argonne Plant Engineering personnel have been held to coordinate other phases of the work.

C. Conversion of Uranium Hexafluoride to Uranium Dioxide Preparation of High-density Particles

(I. Knudsen, N. Levitz, M. Jones)

Process development studies were continued on a simple fluid-bed scheme for preparing high-density uranium dioxide particles by the simultaneous reaction of uranium hexafluoride with steam and hydrogen. The dense spheroidal product would be used as shot in dispersion or packed fuel elements. Material made in earlier studies of conversion rate (see ANL-6145, pages 124 to 128) was of relatively low density (about 4 g/cc,

bulk density) and required sintering for densification (93 percent of theoretical density was achieved; see ANL-6183, page 123). Recent efforts have been directed towards establishing operating conditions which will give dense particles directly.

In the previous quarter (see ANL-6543, page 157), particle density, as measured by mercury displacement, was found to increase from 6.4 g/cc to 8.9 g/cc as the ratio of steam to hydrogen in the reactant stream was decreased. Current studies explored further the effect of steam concentration on particle density.

The studies are being conducted in a 3-in.-diameter cone-bottom Monel column described previously (see ANL-6379, page 183). The run procedure involved alternate periods of hexafluoride feed time followed by a period when residual fluoride was removed and only steam and hydrogen were fed. In some cases, a greater steam feed rate was used during the cleanup period than during the hexafluoride feed period. Uranium hexafluoride feed periods have ranged from 20 min to one hour. Product was removed semicontinuously (after each cleanup period) so that the bed weight remained approximately constant. A recycle stream of -60 +200 mesh particles was fed to the column to offset the effect on particle size distribution of particle growth. The recycle rate has been about 10 percent by weight of the hexafluoride feed rate. The average bed particle size has remained near 350 μ.

In the current experiments (Runs 66H through 66K), the steam rate was varied from 0.1 to 1.4 times the stoichiometric requirement,* while the hydrogen rate was kept relatively high, at 10 to 20 times the requirement. Relatively little nitrogen was fed in with the reactants so that steam and hydrogen comprised both the fluidizing medium and the reactant stream.

Particle densities of 9.5 g/cc, 86 percent of theoretical density (10.96 g/cc), were achieved in Run 66H with 40 percent excess steam (see Table 34). Lesser amounts of steam, for example, down to 10 percent of the stoichiometric requirements for complete reaction to the dioxide, gave lower results, such as 8.4 g/cc in Run 66J. Density measurements by xylene displacement on material of 75 to 85 percent theoretical density gave values of 10.5 to 10.7 g/cc, indicating that relatively few closed pores exist in the particles. Pores smaller than 17 μ are not penetrated in the mercury displacement method and are therefore included in the solids volume, giving the overall, not skeletal, particle density. The effect of steam concentration in the reactant stream is shown in Figure 37. A possible explanation for these density changes may be that uranium tetrafluoride (rather than uranyl fluoride and/or U_3O_8) is formed as an intermediate reaction product at lower steam concentrations. Some sintering

*Based on the reaction $UF_6 + 2H_2O + H_2 \rightarrow UO_2 + 6HF$.

densification of the particles may then occur at normal operating temperatures because of the reduced melting point of the outer layer of tetrafluoride-oxide mixture.

Table 34

PREPARATION OF HIGH-DENSITY URANIUM DIOXIDE PARTICLES FROM URANIUM HEXAFLUORIDE IN FLUIDIZED BEDS

Equipment: 3-in.-diameter Monel column
Temperature: 650 C
Bed Weight and Height: 6 kg; 8 to 12 in. static
Superficial Velocity: 0.75 to 1.0 ft/sec

Run No.	Quantity of Reactants (X Stoich)[a] Steam	Hydrogen	UF_6 Rate (g/min)	UF_6 Feed On-time (min/hr)	Run Duration (hr)	Residual Fluoride (w/o)	Bulk Density (g/cc)	Particle Density[b] (g/cc)
66B	12.6	12.6	10	50[c]	29.0	0.015-0.033	4.2	6.6
66C	5.4	5.6	22	45	11.75	0.025	4.6	7.6
66D	3.5	12.8	19	45	10.3	0.022	5.9	8.1
66F	3.2	12.6	26	40	6.0	0.032	6.0	8.5
66G	2.8	14.8	24	40	6.0	0.024	6.1	8.5
66E	1.9	9.4	27	45	6.0	0.30	6.2	8.9
66H	1.4	16.8	26	30	11.0	0.049	6.7	9.5
66K	1.30	16.5	25	20	24.0	0.024	6.3	9.0
66I	1.1	17.8	25	30	6.0	0.043	6.6	9.3
	0.75	15.9	28	30	4.0	0.125	6.5	9.3 10.5[d]
66J	0.10	18.8	26	30	10.0	0.104	5.7	8.4 10.7[d]

[a]Based on the reaction $UF_6 + H_2 + 2H_2O \rightarrow UO_2 + 6\ HF$.

[b]Mercury displacement method.

[c]Intermittent feed during last 8 hr.

[d]Xylene displacement results.

Figure 37

DENSITY OF URANIUM DIOXIDE PRODUCED BY SIMULTANEOUS REACTION OF STEAM AND HYDROGEN WITH URANIUM HEXAFLUORIDE IN A FLUID-BED
(Density determined by mercury displacement)

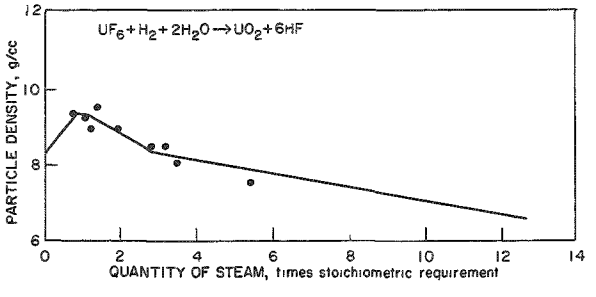

Residual fluoride contents have been held to 200 to 300 ppm in most runs. To maintain low fluoride levels during operation at low steam concentrations (less than stoichiometric), reduction of the hexafluoride feed time period and increased steam concentration during cleanup were required. Nickel content of the products ranged from 17 to 30 ppm, indicating low corrosion rates in the reactor. Fines carry-over to the filter vessel has averaged about nine percent by weight of the hexafluoride feed input, although it has been as low as two percent in some runs. Bed weight has been held constant in these experiments

resulting in a decrease in height from about 12 to 8 in. (static) as the density increased. This decrease in bed height has not adversely affected the rate of fines formation despite the significant reduction in gas residence time.

Additional work is planned to determine the maximum density attainable directly by control of process conditions.

D. Fluid-bed Calcination Studies in Small-diameter Columns
(J. W. Loeding, J. Kincinas, D. Benzing*)

Development studies involving a scheme which extends the technique of fluid-bed calcination to small-diameter columns were continued. The principal aim of this scheme is to facilitate the processing of solutions containing enriched uranium or plutonium for which nuclear criticality (size) safeguards must be considered. Operations involve the upward atomization of a feed stream into a heated bed (currently $2\frac{1}{4}$-in. inside diameter) of appropriate granular particles fluidized entirely by means of the atomizing gas plus the feed decomposition gases. An advantage results from the concomitant reduction in total off-gas volume. In earlier work operation at low-air-to-liquid volume ratios was attempted. A significant reduction in this ratio from 2000 to 600 was achieved during a series of short-duration (2-hr) runs (see ANL-6543, page 158). Recent attempts to operate for longer periods have been thwarted by the problem of large quantities of particle fines returned to the bed at unpredicted times from the sintered metal filters above the bed. Particle growth, although not an operational deterrent as yet, has also been evident in these studies. Recent work has been directed toward minimizing both fines production and particle growth, as well as toward producing reliable operations of extended length. The system is currently being tested with beds of granular aluminum oxide and a feed solution of 1M aluminum nitrate. Bed temperatures of 425 and 450 C and a feed rate of about 18 ml/min have been selected as operating conditions. A submerged-tip nozzle (ANL-6543, Figure 51, page 158) is being used in these studies.

The calciner is so constructed that product may be removed from either of two overhead locations. The lower take-off line is used with a 325-g granular shallow bed (expanded height, about 10 in.) and the upper with a 490-g deep bed (expanded height, about 18 in.). In shallow-bed runs reported here, the starting bed consisted of relatively coarse aluminum oxide: 200 g of -20 +40 mesh particles, and 125 g of -40 +80 mesh particles. Under these conditions the residence time in the bed was 5.2 hr. In the deep-bed runs residence time was 7.8 hr.

---

*Cooperative student from the University of Detroit.

Experimental Results

Shallow-bed Runs. Experimental operating conditions and results of recent shallow-bed runs may be seen in Table 35 and Figures 38 and 39.

Table 35

OPERATING CONDITIONS AND RESULTS OF RECENT CALCINATION RUNS

Column: 2-1/4-in. ID
Bed Weight: Shallow Bed 325 g Al_2O_3 (200 g -20 +40 mesh; 125 g -40 +80 mesh)
Deep Bed 490 g Al_2O_3 (45 g +20; 357 g -20 +40; 56 g -40 +50; 11 g -50 +60; 9 g -60 +70; 9 g -70 +100; 2 g -100 +200; 1 g -200)
Feed: 1M Al $(NO_3)_3$
Average Feed Rate: 18.4 ml/min
Nozzle: Submerged tip

Run No.	Bed Type	Run Duration (hr)	Average Bed Temperature (C)	Average Air-Liquid Volume Ratio	Comments
60-61	Shallow (~10 in. expanded height)	14.0	448	817	Actually two 7-hr runs, voluntarily terminated. Automatic control used on heat input to upper section of bed. Particle growth and fines production both evident (see Figure 38).
63	Shallow (~10 in. expanded height)	11.8	425	822	Actually one 7-hr run and one 5-hr run. Excellent operation for 11.6 hr. Run failure at this point was due to the return of a relatively massive amount of filter fines to bed. Again, particle growth and fines production occurred (see Figure 39).
67-68	Deep (~18 in. expanded height)	11.5	445	812	Actually two runs of 5-1/2-hr and 6-hr duration, respectively; run failure after 11-1/2 hr due to excessive fines return (see Figure 40).

Figure 38

PARTICLE SIZE DISTRIBUTION IN SMALL-DIAMETER CALCINER RUNS SD-60 AND SD-61

Bed Depth: 10 in.
Air/Liquid Vol Ratio: 817
Bed Temp: 450 C
Column Diameter: 2-1/4 in.
Atomizing Air: 0.53 cfm

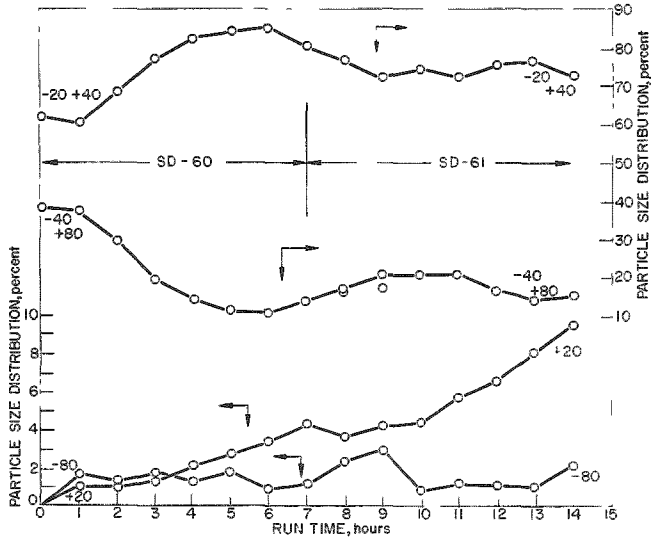

Figure 39

PARTICLE SIZE DISTRIBUTION IN SMALL-DIAMETER CALCINER RUN SD-63

Bed Depth: 10 in.
Air/Liquid Vol Ratio: 822
Bed Temp: 425 C
Column Diameter: 2-1/4 in.
Atomizing Air: 0.53 cfm

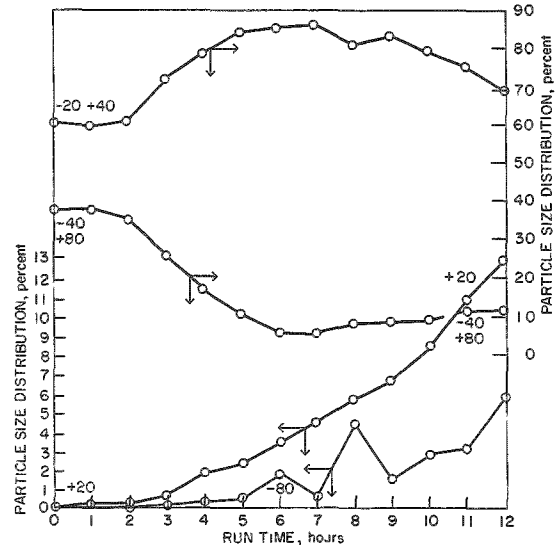

Particle growth occurred in each of these runs at bed temperatures of 425 and 450 C. This may be seen in the figures by comparing the quantity of -20 +40 mesh material in the starting beds with the increase in the total +40 mesh particles (that is, the -20 +40 mesh fraction and the steadily increasing +20 mesh fraction). Somewhat more +20 mesh material and more fines were formed at the lower temperature (425 C) than at 450 C. This particle growth is similar to that experienced previously (ANL-5466, page 82), and per se it is doubtful that operations of extended length can be made successfully.

The amount of fines returned to the bed by blowback and rapping following each run was about 30 g (about 10 percent of the total bed inventory). It seems certain that this material (rather than the small percentage of fines found in the grab samples) leads to run failures when returned to the bed.

Deep-bed Runs. Two runs have thus far been performed in which 490 g of aluminum oxide were used as a starting bed in conjunction with the higher overhead product take-off line. The effect of the deeper bed (with other operating conditions remaining constant) is, of course, to increase the residence time of the particles in the calciner. The starting bed for the first deep-bed run (Run 67) was in essence the final bed of a shallow-bed run (Run 61) and was used to study the effect of a greater depth on a bed known to exhibit growth characteristics. Particle size fractions as a function of time are plotted in Figure 40, and it may be noted that both the trend toward particle growth and the trend toward fines production appear to have been halted. Although $11\frac{1}{2}$ hr (Runs 67 and 68) of operation represents slightly over one bed throughput, previous experience indicated that continued operations would be possible with one exception - the matter of filter fines return to the bed. Run 68 was, in fact, terminated for this reason.

The formation of particulate fines is caused by attrition in the bed, by the atomizing gas, or from droplets formed during initial atomization. Depending upon which mechanism controls and the extent to which it controls, increased residence time could have several results:

1) The fine particles might grow in size.

2) The number of fine particles might increase, with a consequent decrease in the size and number of large particles.

3) Both of these might occur simultaneously.

Figure 40

PARTICLE SIZE DISTRIBUTION IN SMALL-DIAMETER CALCINER

Runs SD-67 and SD-68
Bed Depth: 16 in.
Air/Liquid Vol Ratio: 812
Bed Temp: 445 C
Column Diameter: 2-1/4 in.
Atomizing Air: 0.53 cfm

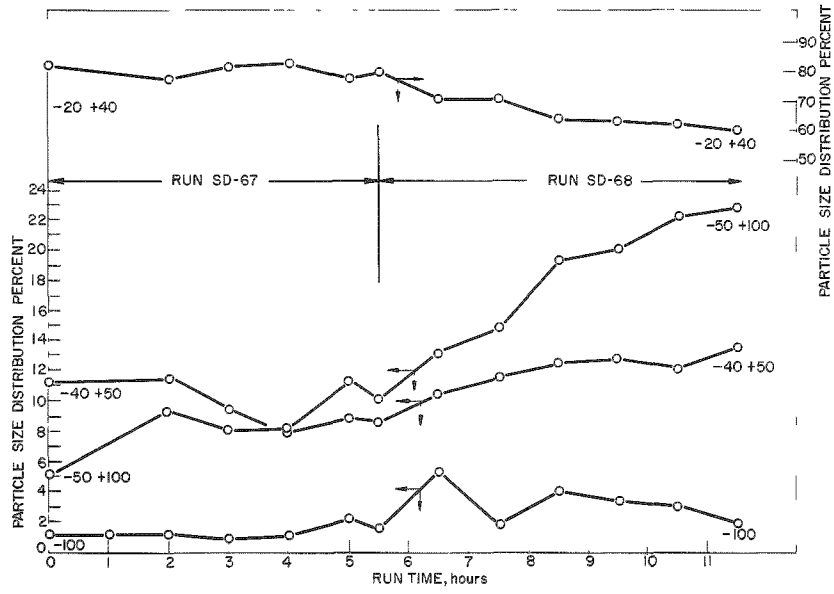

Blowback Operations. Experiments aimed at optimizing blowback frequency and burst duration have been only partially successful because of nonuniform quantities of fines being returned to the bed from the filters.

Changes in bed level and changes in pressure drop across the filters are indicated by pressure-sensing devices. Ideally, these instruments would show no changes during the course of operations and would thereby indicate a constant bed level, because product is removed at the rate at which it is produced. Also, return of fines to the bed from the filters should prevent accumulation on the filters. In some instances, however, the instruments have indicated a buildup of fines on the filters with a corresponding decrease in bed level. However, for reasons as yet unexplained, the fines are returned to the bed at unpredictable times. If the intervals between the return of fines to the bed are short (~1 min), the bed can usually absorb the fines without any serious consequences. However, if the intervals are long (~10 to 15 min), bed failures occur. The problem of large quantities of fines being returned to the bed may be alleviated by using deeper beds. The ratio of the quantity of fines returned from the filters to the total bed

quantity is less when deep beds are used than in runs with shallow beds and, therefore, steady-state conditions are disturbed less by the return of the fines. Moreover, by using filters having a smaller area, the quantity of fines held on the filters can be reduced with a consequent reduction in the quantity of fines returned to the bed. Two 18-in. bayonet, sintered stainless steel filters are currently in use. In a run planned for the immediate future, two 9-in. bayonet filters will be employed.

III. CALORIMETRY*

(W. N. Hubbard, H. M. Feder)

Thermodynamic data are lacking for many compounds of interest in high-temperature chemistry because of the experimental difficulties involved in making the necessary measurements. A program has been undertaken to determine some of these data.

The basic data needed are heats of formation at 25 C. Part of the program at Argonne National Laboratory consists of determinations of heats of formation by the method of oxygen bomb calorimetry. However, many of the compounds of interest are difficult to burn in oxygen and, consequently, cannot be studied by oxygen bomb calorimetry. To study compounds which are not amenable to oxygen bomb calorimetry, the techniques of the bomb calorimetric method, a method which has been developed to a high degree of precision and accuracy, were modified so that fluorine could be used as the oxidant.

The accumulation of basic heat of formation data for fluorides is a necessary preliminary adjunct to the general use of fluorine bomb calorimetry for the study of compounds and is a valuable program on its own merit. To date, values of the heat of formation have been published for zirconium tetrafluoride, molybdenum hexafluoride, boron trifluoride, and silicon tetrafluoride. The heats of combustion in fluorine of two compounds, boron nitride and silicon dioxide, have been determined by bomb calorimetry. To obtain the heats of formation for these compounds, boron nitride required the use of the value obtained previously for the heat of formation of boron trifluoride, and silicon dioxide required the use of the value obtained for silicon tetrafluoride. The heats of formation of boron trifluoride and zirconium tetrafluoride will be used in the study of zirconium diboride, which is now under way.

The heats of formation at 25 C from oxygen or fluorine combustion calorimetry will be combined with values of the change in enthalpy, which will be measured by means of a high-temperature enthalpy calorimeter, to determine thermodynamic properties at high temperatures. A calorimetric system for measurements up to 1500 C has been designed and is now being assembled. Design concepts for an electron beam furnace to operate up to 2500 C are being tested in the laboratory.

During the report period, Calorimetry Group personnel were engaged in moving calorimetry equipment to a newly assigned laboratory.

---

*A summary of this section is given on page 10.

A. Combustions of Zirconium Dihydride and Zirconium Dideuteride in Oxygen

(D. R. Fredrickson and R. L. Nuttall)

In a previous report (ANL-6477, page 156), results were presented for the heats of formation of zirconium dihydride and dideuteride, and the problem of oxygen contamination of the samples was discussed. These experiments are to be repeated with new samples of definite oxygen content.

New samples of zirconium dihydride and zirconium dideuteride were prepared by Howard Flotow of the Chemistry Division. The oxygen contents of these samples are 564 and 562 ppm, or approximately 0.05 percent, for the hydride and deuteride, respectively. The correction for these amounts of oxygen will amount to less than 0.2 percent of the measured heat, and a certain amount of uncertainty in the application of the correction can be tolerated. The calorimetric system was recalibrated and a second series of combustion measurements made with the new samples. The results of the measurements on zirconium dihydride and dideuteride have not yet been calculated.

B. Combustions of Cadmium and Magnesium in Fluorine

(E. Rudzitis and R. Terry)

The calorimetric system, ANL-R1-Ni4, used for the combustions of cadmium and magnesium in fluorine was recalibrated. The mean value of the energy equivalent of the system obtained from six calibration experiments with benzoic acid was $\mathcal{E}$(calor) = 3603.77 ± 0.43 cal/deg. The previous calibration of the system (August 1961) had resulted in a value $\mathcal{E}$(calor) = 3602.86 ± 0.07 cal/deg which was corrected to $\mathcal{E}$(calor) = 3603.25 ± 0.15 for changes made in the system. The difference in the values obtained from the two series is of borderline significance. No explanation for the difference is apparent. Because the results of the recent series do not require corrections for changes in the system, they are considered to be more reliable.

A series of combustions of cadmium in fluorine and a series of combustions of magnesium in fluorine were completed. The results obtained are summarized in Tables 36 and 37. The entries are: (1) the identification number of the run; (2) the mass of sample burned; (3) the corrected temperature rise; (4) the energy equivalent of the system multiplied by the corrected temperature rise of the system; (5) the correction for the heat capacities of the contents of the bomb applied in such a manner that the measured heat refers to the isothermal reaction at 25 C; (6) the correction for the energy input into the firing curcuit necessary to ignite the sample; (7) the correction of the bomb gases to standard state conditions; (8) the correction for the combustion of the impurities in the sample and a significant amount of combustion of impurities in the sample

support disk (see ANL-6543, page 162); (9) the sum of items 4 through 8 divided by the mass of sample burned, which quantity represents the measured energy change at 25 C for the reaction

$$Cd\ (or\ Mg)\ (c) + F_2\ (g) \longrightarrow CdF_2\ (or\ MgF_2)\ (c) \qquad (1)$$

in which each reactant and product is in its respective standard state.

Table 36

RESULTS OF CADMIUM COMBUSTION EXPERIMENTS

Item						
(1) Run No.	Cd-4	Cd-5	Cd-6	Cd-7	Cd-8	Cd-9
(2) m (g)	2.39173	2.01504	1.97869	1.72399	2.01427	1.95572
(3) Δt_c (C)	0.98829	0.82956	0.81358	0.71167	0.82871	0.80496
(4) $\mathcal{E}$ calor x Δt_c(cal)	-3561.57	-2989.54	-2931.96	-2564.69	-2986.48	-2900.89
(5) ΔE contents (cal)	-7.54	-3.56	-3.32	-3.11	-3.58	-3.73
(6) ΔE ignition (cal)	0.10	0.10	0.10	0.10	0.10	0.10
(7) ΔE gas (cal)	-0.42	-0.35	-0.35	-0.31	-0.35	-0.38
(8) ΔE impurities (cal)	18.08	6.65	8.88	9.55	7.47	4.83
(9) $\Delta E_c^\circ/M$ (cal/g)	-1484.85	-1480.20	-1479.08	-1484.03	-1480.85	-1482.87
(10) Average $\Delta E_c^\circ/M$ for cadmium: -1482.31 cal/g Std dev of mean: 0.86 cal/g or 0.06%						

Table 37

RESULTS OF MAGNESIUM COMBUSTION EXPERIMENTS

Item					
(1) Run No.	Mg-1	Mg-2	Mg-3	Mg-6	Mg-8
(2) m (g)	0.29055	0.30017	0.29786	0.28874	0.30424
(3) Δt_c (C)	0.88524	0.91244	0.90543	0.88030	0.91852
(4) $\mathcal{E}$ calor x Δt_c(cal)	-3190.20	-3288.22	-3262.96	-3172.40	-3318.89
(5) ΔE contents (cal)	-10.56	-10.52	-9.52	-7.79	-8.23
(6) ΔE ignition (cal)	0.10	0.10	0.10	0.10	0.10
(7) ΔE gas (cal)	-0.46	-0.46	-0.44	-0.43	-0.65
(8) ΔE impurities (cal)	37.40	27.64	27.14	22.86	23.99
(9) $\Delta E_c^\circ/M$ (cal/g)	-10888.72	-10899.35	-0896.66	-10935.99	-10829.93
(10) Average $\Delta E_c^\circ/M$ for magnesium: -10890.13 cal/g Std dev of mean: 14 cal/g or 0.13%					

Table 38 lists the derived standard thermal data for crystalline cadmium and magnesium difluoride.

Table 38

THERMODYNAMIC DATA AT 25 C DERIVED FROM CALORIMETRIC COMBUSTIONS OF MAGNESIUM AND CADMIUM IN FLUORINE

	$MgF_2(c)$	$CdF_2(c)$
Energy of Formation $\Delta E_f^\circ = \Delta E_c^\circ$ (kcal/mole)	-264.79 ± 0.70	-166.61 ± 0.20
Heat of Formation ΔH_f° (kcal/mole)	-265.38 ± 0.70	-167.20 ± 0.20
Entropy of Formation ΔS_f° [cal/(deg)(mole)]	-42.62 ± 0.30	-40.96 ± 1
(Gibbs) Energy of Formation $\Delta G_f^\circ = \Delta H_f^\circ - T\Delta S_f^\circ$ (kcal/mole)	-252.68 ± 0.80	-156.23 ± 0.32

The standard heats of formation for magnesium difluoride and cadmium difluoride were found to be -265.38 ± 0.70 kcal/mole and -167.20 ± 0.20 kcal/mole, respectively; the uncertainties in the results are uncertainty intervals equal to twice the combined standard deviations arising from known sources and are primarily due to the precision in experimental measurements. Previously reported values for magnesium difluoride are: -268.0 ± 1.8 kcal/mole obtained by measuring the heat of the reaction $Mg + PbF_2 \longrightarrow MgF_2 + Pb$;[15] -260.85 and -266.2 kcal/mole derived by Armstrong and Krieger[16] from the measurements of heats of solution of magnesium[17] and magnesium hydroxide;[18] in hydrofluoric acid; -260.2 kcal/mole calculated from the data on high-temperature hydrolysis equilibrium of magnesium difluoride.[19] Values for cadmium difluoride obtained from

[15]Gross, P., Hyman, C., and Levi, D. L., Trans. Faraday Soc., 50, 477 (1959).

[16]Armstrong, G. T., and Krieger, L. A., National Bureau of Standards, Unpublished Communication, July 1, 1960.

[17]von Wartenburg, H., Z. anorg. chem., 249, 100 (1942).

[18]Torgeson, D. R., and Sahama, T. G., J. Amer. Chem. Soc., 70, 2156 (1948).

[19]Domange, L., Ann. Chim., 7, 225 (1937).

the literature are as follows: -164.9 kcal/mole;[20] -166.5 kcal/mole;[21] -168 kcal/mole;[22] a value of the heat of formation calculated from emf measurements on a system, cadmium amalgam, cadmium difluoride, hydrofluoric acid, lead fluoride, lead amalgam,[23] was corrected using an improved value for the potential of the lead amalgam, lead fluoride electrode[24] and a more reliable value for the vapor pressure[25] to give the corrected value, -165.3 kcal/mole. The reliability of such data, which are based on auxiliary thermodynamic quantities, is difficult to estimate. Considering the directness of the ANL method and the precision achieved, the new values represent an improvement over the previous data.

There are no thermophysical data available for the calculation of thermodynamic functions of cadmium difluoride. For magnesium difluoride, however, low-temperature heat capacity, high-temperature heat content, and heats of fusion and sublimation have been measured. Thermodynamic functions based on these measurements and previous literature values for the heat of formation of magnesium difluoride are tabulated in the JANAF Interim Thermochemical Tables.[26] Revised values of enthalpies and Gibbs free energies of formation ($\Delta G = \Delta H - T\Delta S$) based on the results of this study are given in Table 39. Values for temperatures of 900 K and below are based on the formation of magnesium difluoride from solid magnesium; for temperatures of 1000 to 1300 K, liquid magnesium; and for temperatures 1400 K and above, gaseous magnesium.

---

[20] Selected Values of Chemical Thermodynamics, National Bureau of Standards Circular 500, U.S. Government Printing Office, Washington, D. C. (1952).

[21] Kubaschewski, A., and Evans, E. L. L., Metallurgical Thermochemistry, Third Ed., John Wiley and Sons, Inc., New York (1958).

[22] Brewer, L., Bromley, L. A., Gilles, P. W., and Lofgren, N., Paper 6, The Chemistry and Metallurgy of Miscellaneous Materials: Thermodynamics, L. L. Quill, Editor, McGraw-Hill Book Co., Inc., New York (1950).

[23] Jahn-Held, W., and Jellinek, K., Z. Elektrochem., 42, 401 (1936).

[24] Broene, H. H., and DeVries, T., J. Am. Chem. Soc. 69, 1644 (1947).

[25] Brosheer, J. C., Lenfesty, F. A., and Elemore, K. L., Ind. Eng. Chem., 39, 423 (1947).

[26] Prepared under the auspices of the Joint Army-Navy-Air Force Thermochemical Panel by D. R. Stull et al., Dow Chemical Company (1960).

Table 39

ENTHALPY AND GIBBS ENERGY OF FORMATION OF MgF_2

T(K)	ΔH_f^0 (kcal/mole)	ΔG_f^0 (kcal/mole)	T(K)	ΔH_f^0 (kcal/mole)	ΔG_f^0 (kcal/mole)	T(K)	ΔH_f^0 (kcal/mole)	ΔG_f^0 (kcal/mole)
	Solid			Liquid			Ideal Gas	
0	-264 46	-264 46	0			0	-179 07	-179 07
100	-265 14	-261 08	100			100	179 22	-179 51
200	-265 44	-256 86	200			200	-179 55	-179 66
298	-265 38	-252 68	298	-256 20	-244 01	298	-179 78	-179 67
300	-265 36	-252 60	300	-256 19	-243 43	300	179 78	-179 67
400	-265 17	-248 37	400	-255 31	-239 98	400	-179 94	-179 60
500	-264 92	-244 20	500	-254 50	-236 25	500	-180 08	-179 50
600	-264 65	-240 08	600	-253 73	-232 66	600	-180 21	-179 37
700	-264 39	-236 00	700	-253 02	-229 22	700	-180 36	-179 22
800	-264 14	-231 97	800	-252 35	-225 86	800	180 53	-179 05
900	-263 90	-227 96	900	-251 73	-222 59	900	-180 73	-178 85
1000	-265 79	-223 80	1000	-253 28	-219 21	1000	-183 10	-178 45
1100	-265 55	-219 62	1100	-252 71	-215 83	1100	-183 34	-177 98
1200	-265 31	-215 45	1200	-252 18	-212 50	1200	-183 60	-177 48
1300	-265 07	-211 30	1300	-251 68	-209 21	1300	-183 90	-176 95
1400	-295 26	-206 71	1400	-281 64	-205 20	1400	-214 65	-175 94
1500	-294 62	-200 41	1500	-280 79	-200 09	1500	-214 58	173 18
1600	-293 96	-194 15	1600	-279 94	-194 74	1600	-214 52	-170 42
1700	-293 27	-187 93	1700	-279 10	-189 44	1700	-214 46	-167 67
1800	-292 56	-181 76	1800	-278 26	-184 19	1800	-214 41	-164 92
1900	-291 83	-175 62	1900	-277 43	-178 98	1900	-214 35	-162 17
2000	-291 08	-169 53	2000	-276 59	-173 82	2000	-214 30	-159 42
2100	-290 30	-163 47	2100	-275 76	-168 71	2100	-214 24	-156 68
2200	-289 50	-157 45	2200	-274 94	-163 63	2200	214 19	-153 94
2300	-288 68	-151 46	2300	-274 11	-158 58	2300	-214 14	-151 21
2400	-287 83	-145 52	2400	-273 29	-153 38	2400	-214 09	-148 47
2500	286 97	-139 60	2500	-272 47	-148 61	2500	-214 05	-145 74
2600	-286 07	-133 73	2600	-271 66	143 67	2600	-214 01	-143 01
2700	-285 16	-127 88	2700	-270 84	-138 76	2700	-213 97	-140 27
2800	-284 22	-121 08	2800	-270 03	-133 89	2800	-213 93	137 55
2900	-283 27	-116 30	2900	-269 22	129 03	2900	-213 89	-134 82
3000	-282 28	-110 56	3000	-268 42	-124 22	3000	-213 86	-132 09
			3100	-267 62	-119 42	3100	-213 83	-129 37
			3200	-266 83	-114 66	3200	-213 81	-126 65
			3300	-266 04	-109 91	3300	-213 79	-123 92
			3400	-265 25	-105 19	3400	-213 78	-121 20
			3500	-264 47	-100 50	3500	-213 77	-118 47
			3600	-263 69	- 95 82	3600	-213 76	-115 75
			3700	-262 93	- 91 17	3700	-213 76	-113 03
			3800	-262 17	- 86 54	3800	-213 77	-110 31
			3900	-261 41	- 81 93	3900	-213 79	-107 59
			4000	-260 66	- 77 33	4000	-213 81	-104 86
			4100	-259 93	- 72 76	4100	-213 84	-102 14
			4200	-259 20	- 68 20	4200	-213 88	- 99 41
			4300	-258 48	- 63 66	4300	-213 93	- 96 68
			4400	-257 77	- 59 14	4400	-213 99	- 93 96
			4500	-257 07	- 54 63	4500	-214 06	- 91 23
			4600	-256 38	- 50 14	4600	-214 14	- 88 50
			4700	-255 71	- 45 67	4700	-214 23	- 85 77
			4800	-255 04	- 41 20	4800	-214 34	- 83 03
			4900	-254 39	- 36 75	4900	-214 45	- 80 29
			5000	-253 75	- 32 32	5000	-214 58	- 77 55
						5100	-214 73	74 82
						5200	214 89	- 72 07
						5300	-215 06	- 69 32
						5400	-215 25	- 66 57
						5500	-215 45	- 63 81
						5600		

C. Combustion of Niobium and Tantalum in Fluorine
(E. Greenberg)

Preliminary exploratory experiments for combustions of niobium and tantalum in fluorine have been carried out. The development of satisfactory combustion techniques for niobium and tantalum was reported in ANL-6333, page 127. In ANL-6543, page 164, it was reported that further work awaited procurement of samples of sufficiently high purity.

High-purity samples of niobium wire and foil have been received. Analytical data on the ingots used for fabrication of these samples indicates that the materials should be satisfactory for calorimetric work. Niobium sample rod is expected soon. Similar components, i.e., wire, foil, and rod, for the tantalum sample arrangement are also expected soon. Calorimetric studies will be started as soon as the samples are available and have been analyzed.

D. Further Exploratory Combustion Studies
(E. Greenberg)

1. Sulfur. Techniques have been worked out for the combustion of sulfur in fluorine (see ANL-6543, page 164). Calorimetric studies will be made when they can be conveniently worked into the program of the group.

2. Carbon. Preliminary combustion experiments indicated that one of the most suitable methods for burning carbon in fluorine was the technique which originally was worked out for zirconium and which was also used for titanium and hafnium. This technique involved the use of a fuse wire threaded through holes drilled in a small piece of foil which is, in turn, inserted in a slot cut in the top of a vertically supported sample rod. A series of experiments was conducted with fluorine pressures ranging from 3 to 10 atm. Samples of the product gas were analyzed by means of infrared and mass spectrometry. The product of combustion was found to be tetrafluoromethane (CF_4) which contained a small amount of higher fluorocarbons. The use of higher fluorine pressures appeared to reduce the quantity of higher fluorocarbons (primarily C_2F_6) that were produced. At the higher pressures, however, the sample rod invariably burned through near its base and fell to the nickel support plate.

For expediency, zirconium fuse wire and foil had been used to ignite the carbon sample in the preliminary experiments. Attempts are also being made to procure for use as calorimetric sample material carbon in its standard state, i.e., graphite similar to that used by the National Bureau of Standards for determination of the heat of formation of carbon dioxide.

IV. REACTOR SAFETY*

The oxidation, ignition, and combustion processes of uranium and zirconium are being studied to provide information to aid in minimizing the hazards associated with handling these materials.

An experimental program to determine the rates of reaction of molten reactor fuel and cladding metals with water is continuing. Methods currently being used to examine these reactions are the volumetric method in the laboratory and in-pile reactor transients in the TREAT reactor.

A. Metal-oxidation and -ignition Kinetics
(L. Baker)

1. Theory of Uranium Ignition
(L. Baker, J. D. Bingle)

Studies of the isothermal oxidation of uranium at temperatures above 300 C were reported in previous quarterly reports (ANL-6413, page 160 and ANL-6543, page 168).. The purpose of these studies was to provide reaction rate data needed to develop a quantitative understanding of previously reported ignition data. It has been noted that a quantitative relationship between isothermal oxidation rates and ignition temperature should exist if the ignitions are purely thermal in character. A thermal ignition is merely an accumulation of heat, in which the reacting system is generating more heat than can be dissipated by heat loss mechanisms, leading to a rapidly increasing temperature.

a. Summary of Oxidation Results

Isothermal oxidation studies with uranium prepared at Argonne (see ANL-5974 , page 146, for typical analysis) showed that a self-accelerating reaction occurred at 350 and 400 C although nearly linear reaction occurred at 450 C. The oxidation between 500 and 700 C resulted in a somewhat protective oxide and, consequently, a decelerating reaction. The high-temperature results are expressed (ANL-6543, page 172) by an empirical rate law of the following formula:

$$w^{6/5} = kt \qquad (1)$$

where w is the weight of oxygen reacted in $\mu g/sq\ cm$, t is time in min, and k is a constant. Similarly, the data at 350 and 400 C can be expressed by a rate law of the following form:

$$w^{4/5} = kt \quad . \qquad (2)$$

*A summary of this section is given on pages 10 to 12.

Average values of k for the above equations were determined at each temperature studied. Arrhenius plots (log k vs reciprocal temperature) were then used to determine apparent activation energies. The resulting equations are as follows:

Temp Range (C)	Rate Equation	
$300<T<450$	$w^{4/5} = 2.6 \times 10^{7} t \exp[-16{,}800/RT]$	(3a)
$T = 450$	$w = 840\ t$	(3b)
$T > 450$	$w^{6/5} = 7.3 \times 10^{7} t \exp[-14{,}300/RT]$	(3c)

b. Ignition Calculations

The above rate equations were used to simulate mathematically burning-curve ignition experiments with uranium in a manner similar to that used to simulate shielded ignition experiments with zirconium (see ANL-6413, page 152). In a burning-curve experiment, the sample is heated uniformly (usually 10 deg/min) in a flowing, oxidizing atmosphere. The temperature at which the sample begins to self-heat rapidly and finally ignite is then determined by a graphical method. The following heat balance was used to describe the burning-curve experiment with uranium:

$$C_p \frac{dT}{dt} = \underbrace{\frac{QM_U S}{10^6 M_{O_2}} \frac{dw}{dt}}_{\text{self heating}} - \underbrace{hS(T - T_a)}_{\text{convection heat loss}} - \underbrace{\sigma \epsilon S(T^4 - T_a^4)}_{\text{radiation heat loss}} , \qquad (4)$$

where

C_p is the specific heat of uranium, 0.044 cal/(g)(K)

T is the metal temperature, K

t is time, min

Q is heat of reaction, 1089 cal/g U

M_U is atomic weight of uranium, 238 g/g-atom

M_{O_2} is molecular weight of oxygen, 32 g/mole

S is specific area, sq cm/g

w is quantity of oxygen reacted, μg/sq cm

h is heat transfer coefficient, 0.03 cal/(sq cm)(K)(min)

σ is Stefan-Boltzman constant, 81.6×10^{-12} cal/(sq cm)(min)(K^4)

ϵ is total emissivity of oxidized surface, 0.75.

Equation 4 is solved simultaneously with the reaction rate obtained by differentiating Equations 3a and 3c as follows:

Temp Range (C)	Differential Form of Rate Equation	
$300<T<450$	$\frac{dw}{dt} = w^{1/5}\,(5/4)\,2.6 \times 10^{7} \exp[-16{,}800/RT]$	(5a)
$T>450$	$\frac{dw}{dt} = \frac{(5/6)}{w^{1/5}}\,7.3 \times 10^{7} \exp[-14{,}300/RT]$.	(5b)

The initial temperature was taken as 300 C. It was necessary to estimate the extent of reaction the sample would have achieved while heating from room temperature to 300 C at 10 deg/min. This was taken to be 200 μg O_2/ sq cm. Burning-curve experiments have shown that initial preoxidation had no significant effect on the character of the burning curve. The assumption was made that the low-temperature rate law, Equations 2 and 5a, changed abruptly to the high-temperature rate law, Equations 1 and 5b, when the sample temperature T reached 450 C. It was also assumed that no protective oxide had been formed on the metal until the temperature reached 450 C. This seemed justified in view of the striking differences in appearance and effect on the reaction between oxide formed below 450 C and oxide formed above 450 C.

The simulated temperature-time curves were calculated from the equations by a step-wise method. The amount of reaction and the heat exchange occurring during short time intervals were calculated and accumulated. Burning curves were computed for uranium specimens having specific areas of 0.5, 5, and 50 sq cm/g. Computed and experimental burning curves are compared in Figure 41 for specific area values of about 0.5 and 5 sq cm/g. The agreement in both the shape of the curves and the indicated ignition temperatures seems excellent. The ignition temperature comparison is shown in the following table and in Figure 42.

Specific Area (sq cm/g)	Burning-curve Ignition Temperature (C)	
	Calculated	Experimental*
0.5	608	575
5.	390	410
50.	380	335

*ANL-5974, page 27

Figure 41

COMPARISON OF CALCULATED AND EXPERIMENTAL BURNING CURVES FOR ANL BASE URANIUM IN FLOWING OXYGEN

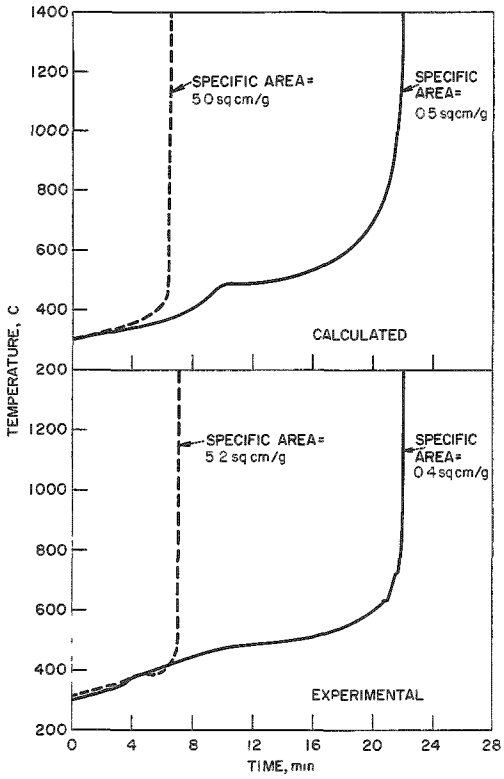

The calculated burning-curve and ignition temperatures for a specific area of 50 sq cm/g differed only slightly from the results for a specific area of 5 sq cm/g. It seems clear from the calculations that no significant decrease in ignition temperature would result from further increases in specific area. The experimental values, however, show a decreasing trend with increasing specific area. This deviation at higher values of specific area is not presently understood. It seems likely, however, that the thermal insulating qualities of the powdery oxide produced between 300 and 450 C serve to insulate effectively smaller specimens preventing attainment of the computed heat loss rates.

The sharp break in both the experimental and computed ignition temperatures in samples having specific areas between 0.5 and 5 sq cm/g results from the manner in which the sample undergoes transition to the protective oxide. This transition to a protective oxide is clearly responsible for the humps noted in the burning

Figure 42

SPECIFIC AREA DEPENDENCE OF URANIUM IGNITION

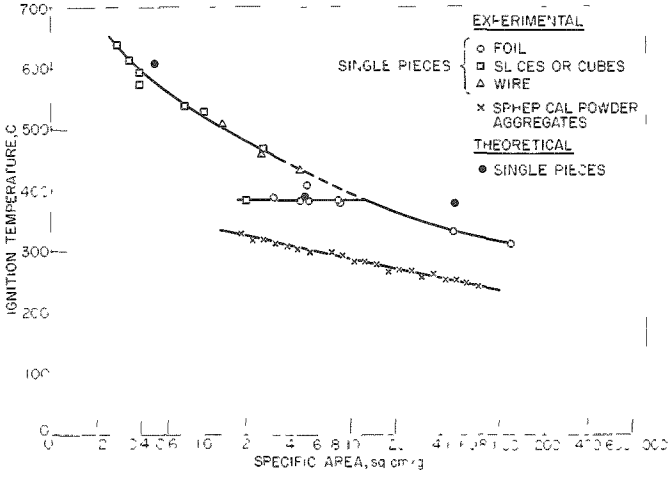

curves (see Figure 42). Further calculations are required to define the character of burning curves in the specific area region between 0.5 and 5 sq cm/g.

2. Theory of Burning Propagation Velocity
(L. Leibowitz, L. W. Mishler)

Considerable attention has been given to measurement of the velocity of burning propagation along strips of uranium and zirconium foils and wires (see e.g., ANL-6068, page 128; ANL-6287, page 177). It has proven possible to apply to this case a theory similar to that used in gaseous flame propagation. A treatment outlined by Semenov[27] and by Frank-Kamenetskii[28] has been used. It is assumed that burning is controlled by the rate of gas-phase diffusion of oxygen through a nitrogen boundary layer and that the rate of propagation of combustion along the foil is determined by the rate of conduction of heat through the foil. The extent to which calculated and experimental values agree is a measure of the validity of this model.

In addition to the fundamental interest existing in this area as an attempt to clarify a little-studied combustion problem, there is the related practical matter of combustion of metal chips and turnings. Although the combustion of a large mass of metal scrap is a more difficult problem, the results presented here are directly related to the combustion in air of single pieces of scrap metal as will be discussed later.

Consider a foil strip of width L, thickness t, and infinite length burning in air. Burning proceeds along the foil at a velocity v. For simplicity, consider the foil to be moving in the opposite direction with velocity v, so that the burning front is stationary. The temperature distribution in the region of the burning front is shown schematically in Figure 43, where T_a denotes the ambient temperature, T_b the maximum burning temperature, and T' will be defined below.

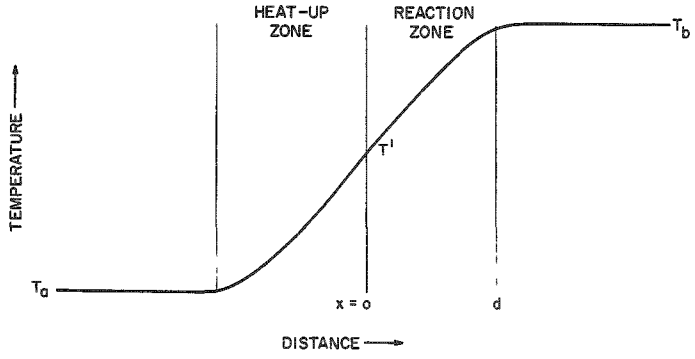

Figure 43

TEMPERATURE DISTRIBUTION AT FRONT OF BURNING FOIL

[27] Semenov, N. N., Progress of Physical Science (USSR), 24, 433 (1940), Trans. NACA-TN-1026 (1942).

[28] Frank-Kamenetskii, D. A., Diffusion and Heat Exchange in Chemical Kinetics, Trans. N. Thon, Princeton University Press (1955), page 267.

Assuming burning propagation to be controlled by the rate of heat transfer through the foil, we have[29]

$$\frac{\partial T}{\partial \tau} = \frac{k}{\rho c}\frac{\partial^2 T}{\partial x^2} + \frac{Q}{\rho c} \quad , \tag{6}$$

where

T = temperature
τ = time
x = distance along the foil
k = thermal conductivity of the metal
c = specific heat of the metal
ρ = density of the metal
Q = rate of heat generation,

and, introducing v, the burning velocity, we find for the one-dimensional case

$$\frac{d^2T}{dx^2} - \beta\frac{dT}{dx} + \frac{Q}{k} = 0 \tag{7}$$

where

$$\beta = v\rho c/k \quad .$$

Figure 44

EFFECT OF TEMPERATURE ON HEAT-LOSS OR HEAT-GENERATION RATES

(Uranium foil: width, 0.3 cm; thickness, 0.01 cm)

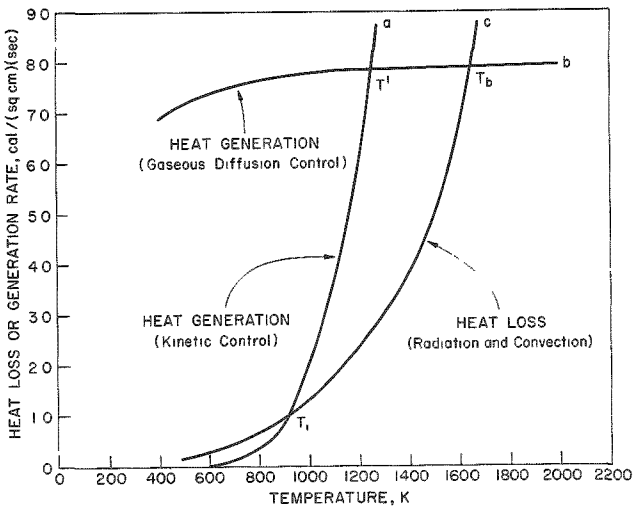

The steady-state rate of reaction in air is controlled by the rate at which oxygen can diffuse to the metal through a nitrogen boundary layer (see ANL-6477, page 168). At moderate temperatures the chemical reaction occurring at the metal is rate controlling. The effect of temperature on these processes which control the rate of heat generation, Q, is shown in Figure 44 for uranium foil 0.3 cm wide and 0.01 cm thick. Curve a gives the rate of heat generation when the reaction rate is controlled by chemical kinetics. This is strongly temperature dependent because of a factor $e^{-E/RT}$. Curve b for heat generation when the gaseous diffusion rate is

[29] Eckert, E. R. G., and Drake, R. M., Jr., Heat and Mass Transfer, McGraw-Hill Book Company, Inc., New York (1959), page 31.

controlling is almost independent of temperature. The third curve, c, represents the rate of heat loss neglecting conduction. If the foil is heated to T_i,* the rate of heat generation due to chemical reaction exceeds the rate of heat loss, and the sample will self-heat to T'. At this temperature the reaction becomes controlled by gas-phase diffusion and continues to self-heat to T_b. At T_b a heat balance is achieved, and burning continues at this temperature. Because the reaction rate, and hence Q, falls so rapidly with temperature below T', we simplify Equation 7 by assuming $Q = 0$ for $T < T'$. Also, since the reaction rate is not very temperature dependent between T' and T_b, we assume for $T' \leq T \leq T_b$ that Q is constant. With the additional requirement of continuity at $x = 0$, equation (7) may be solved:[27]

$$v = \left[\frac{2wq\xi\,\alpha^2}{(T_b - T_a)\,tk}\right]^{1/2} , \qquad (8)$$

where

$\alpha = k/\rho c$, the thermal diffusivity,
w = rate of reaction,
Q = heat of reaction, and

ξ is given by

$$\frac{T' - T_a}{T_b - T_a} = \frac{1 - e^{-\xi}}{\xi} . \qquad (9)$$

Values of T_b and w were taken from theoretical calculations of Mouradian and Baker (see ANL-6477, page 168). Determination of values of T' could be made by finding the temperature at which chemical kinetic-controlled reaction rates equalled gaseous diffusion-controlled rates. The latter was calculated by Mouradian and Baker. Experimental information is available for oxidation rates of both uranium (see ANL-6543, page 170) and zirconium.[30] Since the oxidation rates for both metals, in the required temperature range, are each a function of the amount of oxide present, some choice of that quantity had to be made before T' could be found. The value used for a first approximation was the amount of oxidation needed to generate enough heat to raise the metal temperature from T_a to T_b. With this constant value for the amount of oxide present, and the known equation for oxidation rate[30] (see also ANL-6543, page 173), the temperature was

---

* The ignition temperature T_i shown in Figure 44 is higher than the experimental value of 670 K for this foil because curve a is a plot of the high-temperature rate law and is valid only above 725 K. The low-temperature reaction rate would be greater than that shown here, and a lower ignition temperature would result.

[30] Porte, H. A., Schnizlein, J. G., Vogel, R. C., and Fischer, D. F., J. Electrochem. Soc., 107, 506 (1960).

calculated at which the chemical kinetic reaction rate was equal to the rate of the diffusion-controlled process at T_b. A refinement of this first T' was made by changing the value used for the amount of oxide present to that needed to generate enough heat to raise the metal temperature from T_a to T'. Only a slight change in T' resulted from this iteration.

Values for the other factors in Equation (7) were taken from various sources.[31,32] The numerical values used for a typical case are listed below:

Uranium foil: width = 0.3 cm; thickness = 0.01 cm

$W = 3.04 \times 10^{-5}$ moles/(sq cm)(sec),

$T_b = 1648$ K,

$T' = 1253$ K,

$T_a = 300$ K,

$\xi = 0.76$,

$q = 2.6 \times 10^5$ cal/mole,

$c = 0.0386$ cal/(g)(K),

$\rho = 17.9$ g/cc,

$k = 0.118$ cal/(sec)(cm)(K), and

$v = 0.47$ cm/sec.

The results of these calculations, all for $T_a = 300$ K, are shown in Figures 45, 46, 47, and 48. The solid lines are the theoretical results, and the points are the experimental values. The theoretical results are somewhat low for uranium and somewhat high for zirconium. It seems noteworthy that the theoretical calculations predict the correct trend with regard to foil thickness, foil width, and geometry (relation between foils and wires).

As was mentioned earlier, this work using foils is closely related to the combustion of single pieces of metal scrap. A few experiments were carried out on the combustion of uranium and zirconium turnings. It was found that these turnings burned at rates comparable with those found for foils of similar size. For example, a piece of a uranium turning, L = 0.35 cm and t = 0.025 cm, burned at about 0.40 cm/sec. In comparison, the burning velocity found for uranium foil, L = 0.30 cm and t = 0.031 cm, was 0.30 cm/sec.

---

[31] Katz, J. J., and Rabinowitch, E., The Chemistry of Uranium, McGraw-Hill Book Co., Inc., New York (1951).

[32] Wilkinson, W. D., and Murphy, W. F., Reactor Metallurgy, D. van Nostrand Co., Inc., New York (1958).

Figure 45

EFFECT OF FOIL WIDTH ON PROPAGATION VELOCITY FOR URANIUM FOILS OF VARIOUS THICKNESSES

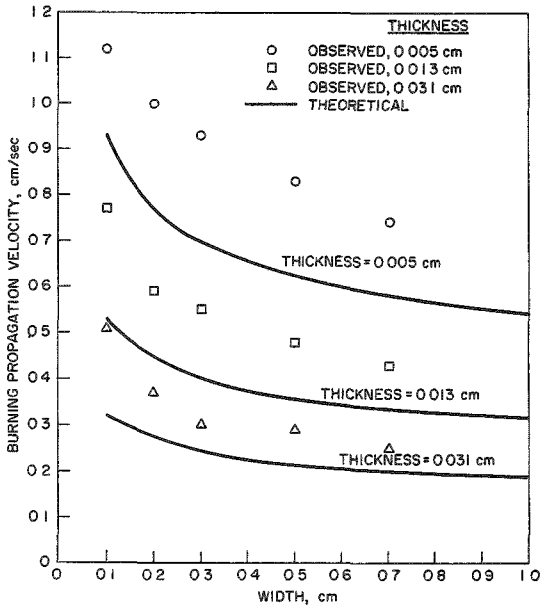

Figure 46

EFFECT OF WIRE DIAMETER OR FOIL THICKNESS ON PROPAGATION VELOCITY FOR URANIUM WIRES AND 0.3 cm WIDE URANIUM FOILS

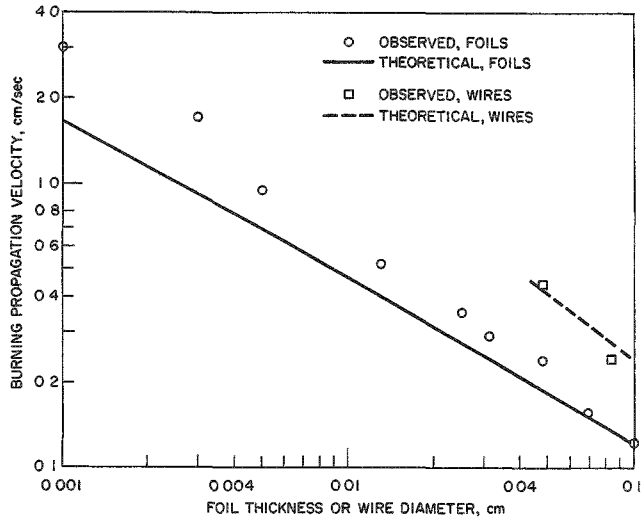

Figure 47

EFFECT OF FOIL WIDTH ON PROPAGATION VELOCITY FOR 0.002 cm THICK ZIRCONIUM FOILS

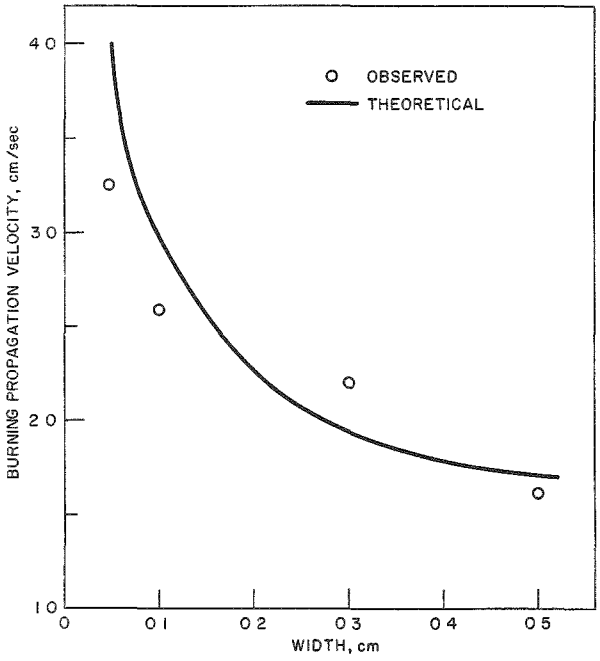

Figure 48

EFFECT OF FOIL THICKNESS ON PROPAGATION VELOCITY FOR 0.06 cm WIDE ZIRCONIUM FOILS

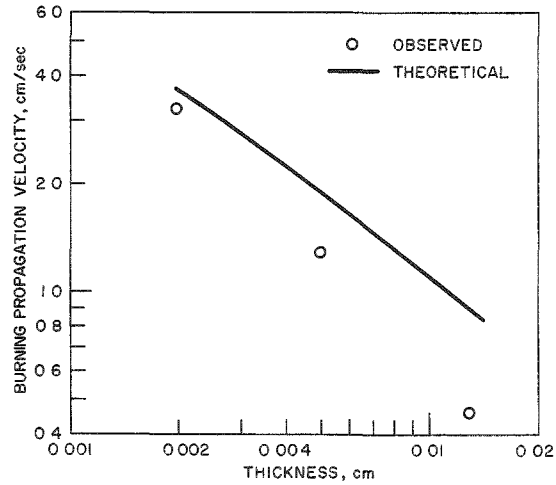

This work, however, is directly applicable only to the combustion of single pieces of metal. Burning of numerous pieces, such as in a scrap pile or a mass of powder, is a problem of a different character. If the aggregate is packed together very tightly, it might behave as a single piece of the same size, but when air flows through the mass it is possible that other effects become important.

Consider a large mass of uranium scrap, in air, which has somehow been raised above the ignition temperature at the center. The effective ambient temperature of neighboring pieces is rapidly raised and ignition will occur. Propagation in the sense discussed above is of lesser importance in these circumstances. Because of the protective nature of uranium oxide above 450 C (see ANL-6543, page 169), the reaction rate may be limited by chemical kinetics in some parts of the mass and by gas diffusion in others. As the mass of metal consumes oxygen at a greater and greater rate, the velocity of air through it will increase, and a forced-convection region occurs, in which higher combustion temperatures may be reached. Quantitative description of these processes would be extremely complex in any but the most idealized case.

3. Zirconium Powder Ignition
(J. G. Schnizlein, J. W. Allen)

Of the metals whose ignition behaviors are being studied (uranium, zirconium, and plutonium), the ignition of zirconium has probably resulted in the most severe incidents. Most of these incidents have been with finely divided metal.

In order to understand the important causative factors and the conditions leading to the hazards of ignition, studies of zirconium powder were undertaken. Variables currently being investigated by means of vacuum- and helium-shielded experiments on spherical powder are specific area, sample size and shape, and exposure to air.

a. Specific Area

Spherical zirconium powder was obtained from Linde Company and carefully separated into various mesh fractions. Aggregates of fine particles were broken apart by shaking in a Wig-L-Bug without an impactor before final sieving (see ANL-6477, page 185). Ignition temperatures have been measured by the helium-shielded method and by a vacuum-shielded method. Although vacuum-shielded experiments initially produced ignition temperatures somewhat lower than helium-shielded experiments (see ANL-6379, page 194), continued exposure to the dry-box atmosphere resulted in very similar ignition temperatures by each method. Further study of the effect of exposure to air will be conducted in the future when a fresh supply of powder is obtained.

The helium- and vacuum-shielded ignition temperatures for 0.3-g samples of three mesh sizes of spherical powder in a 1-cm-diameter copper crucible are presented in Figure 49. Data for single foils (see ANL-6413, page 155) and pertinent data from the literature are also presented for comparison.

Figure 49

ZIRCONIUM IGNITION TEMPERATURES

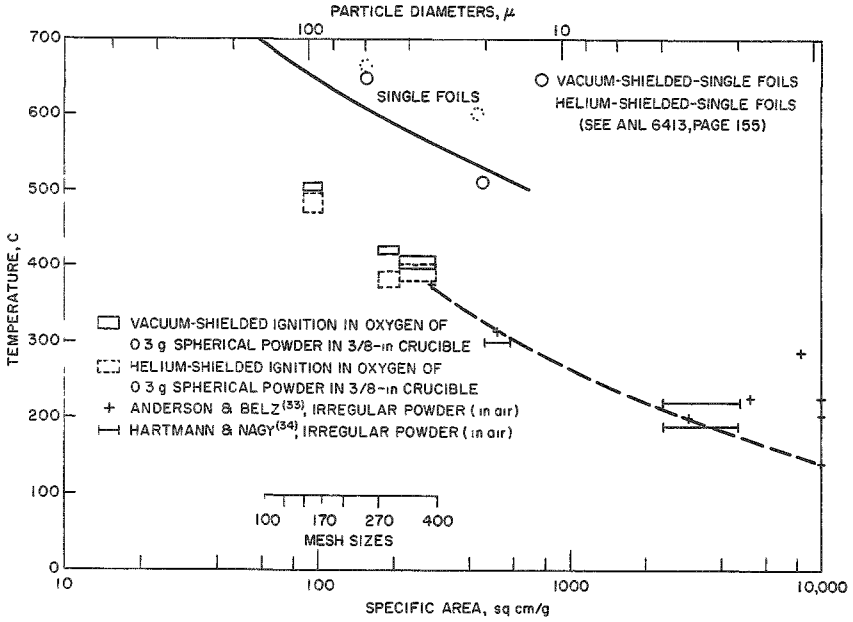

The specific areas of samples used by H. C. Anderson and L. H. Belz[33] were judged from air permeability studies. No special care was taken to avoid contact with air or water prior to their experiments. Although they stated that their particles were irregular and that measured specific areas by BET gave values 3 to 9 times greater than those judged from air-permeability studies, ignition temperatures of the BET-measured samples did not show consistent specific area dependence. I. Hartmann and J. Nagy[34] studied the ignition behavior of several powders. The specific area was judged from reported particle size distributions. They found the ignition temperature to be 30 degrees lower for 2- to 3-μ-diameter powder which had been stored under water than for similar powder received dry.

b. Dependence on Sample Size

Helium-shielded ignition experiments have been completed in oxygen for varied sample weights of both -325 +400 and -140 +170 mesh

[33] Anderson, H. C., and Belz, L. H., J. Electrochem. Soc., 100, 240 (1953).

[34] Hartmann, I., and Nagy, J., NBS-RI 4835 (1951).

powder in a $\frac{1}{4}$-in. copper crucible. Bulk densities for both powders were determined to be 4.0 g/cc. The density could vary about five percent, depending on the degree of packing. The sample weight, depth, nonignition temperatures, and ignition temperatures are presented in Tables 40 and 41.

Table 40

HELIUM-SHIELDED IGNITION EXPERIMENTS ON -325 +400 MESH SPHERICAL ZIRCONIUM POWDER IN 1/4-INCH CRUCIBLES

Bulk Density = 4.00 g/cc

Weight (g)	Depth (cm)	Temperature (C)		Weight (g)	Depth (cm)	Temperature (C)	
		Nonignition	Ignition			Nonignition	Ignition
0.0098	0.0182	440		0.1211	0.133	393	
0.0099		480		0.1199		400	
0.0094		530		0.1197			401
0.0099		585		0.1203			420
0.0099			618				
0.0097			630	0.300	0.275	353	
				0.301		370	
0.0198	0.0336	490		0.300			395
0.0207		516		0.300			415
0.0191			540				
				0.600	0.512	350	
0.0298	0.0456	490		0.600		352	
0.0297			507	0.600			367
0.0301			527	0.600			385
				0.600			385
0.050	0.0712	420					
0.050		420					
0.0516		424					
0.050			432				
0.0491		443					
0.0496		446					
0.050			462				
0.0513			467				

Table 41

HELIUM-SHIELDED IGNITION EXPERIMENTS ON -140 +170 MESH SPHERICAL ZIRCONIUM POWDER IN 1/4-INCH CRUCIBLES

Bulk Density = 4.00 g/cc

Weight (g)	Depth (cm)	Temperature (C)		Weight (g)	Depth (cm)	Temperature (C)	
		Nonignition	Ignition			Nonignition	Ignition
0.0100	0.0182	716		0.0512	0.0712	546	
0.0100			729	0.0498		548	
0.0109			741	0.0504			567
0.0108		750		0.0508			597
0.0104			780				
				0.3004	0.275	472	
0.0205	0.0336	637		0.3002			497
0.0197		650					
0.0202			653				
0.0307	0.0456	584					
0.0304		602					
0.0301			617				

The relationship between logarithm of sample depth and ignition temperature is illustrated in Figure 50. The shape of the curve agrees with the predictions and observations of Anderson and Belz.[33]

Figure 50

HELIUM-SHIELDED IGNITION TEMPERATURES OF VARIED DEPTHS OF SPHERICAL ZIRCONIUM POWDER

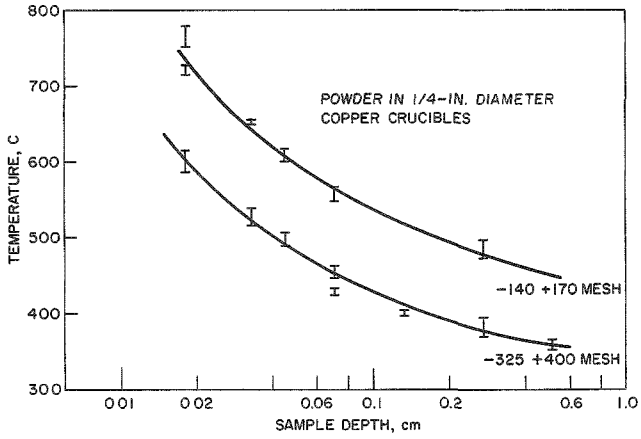

For very small samples it should be noted that ignition temperatures are somewhat higher than those observed for foils of equivalent specific area; that is, a foil with a specific area of 100 sq cm/g would ignite at 650 C, which is the ignition temperature of 0.02 g of -140 +170 mesh powder. This is probably attributable to heat loss to the crucible since lower weight samples are less than 5 particle diameters in depth.

Definition of the effect of increased specific area and the effect of sample size should provide the essential information to predict the temperature at which a particular zirconium powder may be hazardous. Further understanding of the heat transfer process through the powder may make it possible to explain the ignition of zirconium powder solely in terms of fundamental quantities.

B. Metal-Water Reactions
(L. Baker)

1. Isothermal Studies of the Uranium-Steam Reaction by the Volumetric Method
(R. E. Wilson, P. Martin)

A knowledge of the rates of reaction of metals with steam under isothermal conditions is necessary for the prediction of metal-water reactions under the conditions of a reactor accident. The volumetric experiment was designed to study metal-steam reactions. The volume of hydrogen evolved is taken as the measure of the amount of reaction.

The uranium sample was supported by a stainless steel-clad thermocouple, centered in the sample volume. This thermocouple also provided the means of temperature control and measurement. The sample was heated inductively to the desired temperature in flowing steam at a pressure of about one atmosphere. After passing the sample, the steam

was condensed and the hydrogen produced by the metal-steam reaction was collected and measured. A more detailed description of the apparatus and the procedure may be found in the previous Quarterly Report (see ANL-6543, page 185).

The reaction of approximately one-cm cubes of uranium, prepared at Argonne (see ANL-5974, page 146, for typical analysis), with steam was studied over the temperature range from 400 to 1200 C.

Figure 51

HYDROGEN EVOLUTION IN THE REACTION OF STEAM AT 1 ATMOSPHERE WITH URANIUM

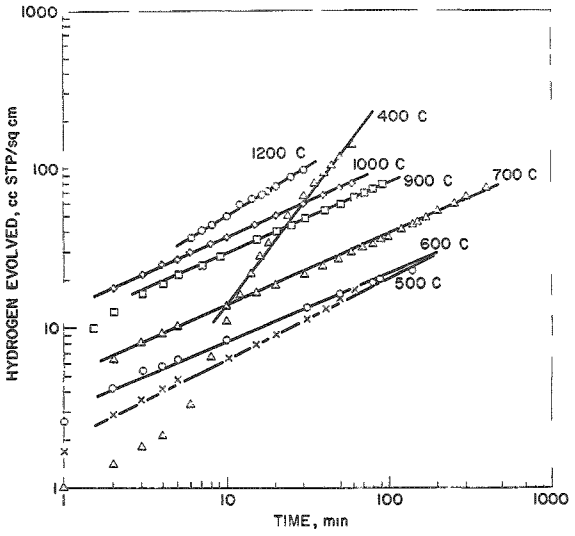

Typical results of an experiment at each of the temperatures studied are shown in Figure 51. At 500 C and above the rate law is nearly parabolic, whereas at 400 C a two-stage linear reaction occurs. The two cases will be discussed separately.

a. Studies at High Temperature

The slope of the lines, shown in the log-log plot in Figure 51, is approximately 0.5 for the runs at 500 C and above. This indicates that the reaction obeys the parabolic rate law, which has the following form:

$$V^2 = kt, \qquad (11)$$

where V is the volume of hydrogen generated, t is time, and k is the parabolic law constant. The constants for the parabolic rate law were obtained by plotting the square of the volume of hydrogen reduced to standard conditions vs time for each run. An example of a plot of the results of two runs obtained at 1000 C is given in Figure 52. The slopes of the straight lines in Figure 52 are the rate constants, and the differences between the slopes of the duplicate runs are an indication of the precision of the experiment.

The parabolic rate law constants obtained from the runs are given in Table 42. The average values and the standard deviations from the mean are also given. The Arrhenius plot, shown in Figure 53, was plotted from the average values given in Table 42. The length of a datum point is equal to the standard deviation at the indicated temperature. From this plot it is evident that a consistent rate law is obtained over the temperature range from 600 to 1200 C, despite the fact that uranium undergoes three phase changes in this range.

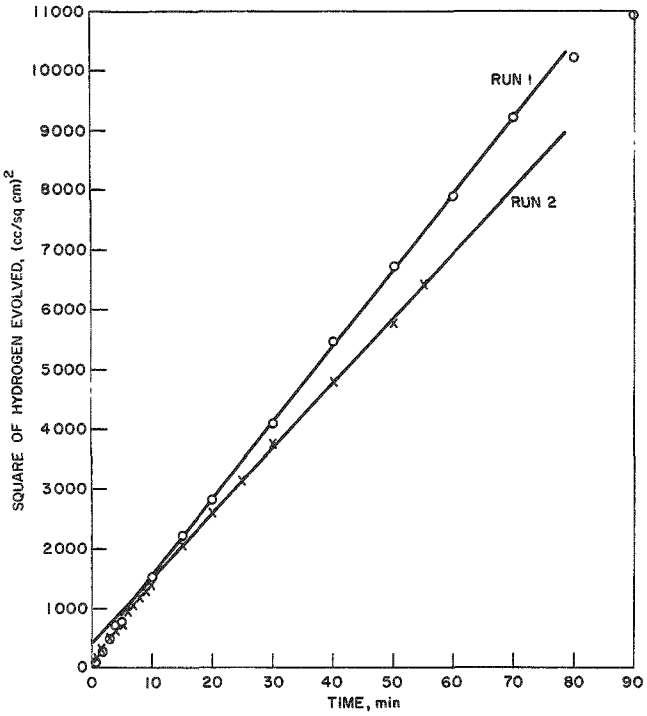

Figure 52

HYDROGEN EVOLUTION IN THE URANIUM-STEAM REACTION AT 1000 C

Table 42

RATE LAW CONSTANTS FOR THE URANIUM-STEAM REACTION

Temperature (C)	Rate Law Constant, k [(cc STP/sq cm)²/min]	Avg. Constant (k)	Standard Deviation	Temperature (C)	Rate Law Constant, k [(cc STP/sq cm)²/min]	Avg. Constant (k)	Standard Deviation
500	5.47			900	84.5		
500	5.05			900	64.7		
500	2.87	4.5	1.1	900	50.9	67	14
600	3.69			1000	131		
600	3.03	3.36	0.33	1000	109	120	11
700	17.4			1200	341		
700	13.7	15.6	1.9	1200	341	341	-

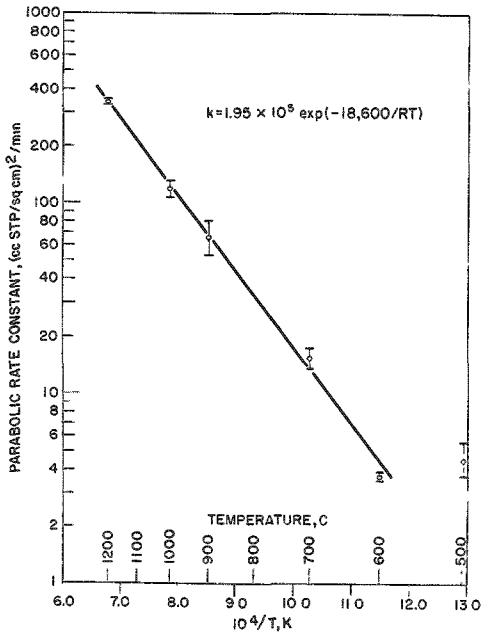

Figure 53

EFFECT OF TEMPERATURE ON THE RATE OF HYDROGEN EVOLUTION FOR THE REACTION OF STEAM WITH URANIUM

The results at 500 C are not consistent with the data at higher temperatures. It was possible to study the reaction with molten metal at 1200 C without modification of the apparatus because the oxide shell served as a satisfactory container for the molten metal.

The oxide formed on the surface of the uranium cubes was adherent and retained the original polish of the metal surface. This oxide showed no tendency to flake off while the metal was at the reaction temperature. However, as the sample cooled at the end of an experiment, the oxide flaked off the sample, with an audible ping, at approximately 300 C. The pieces of oxide which came off were of large size, and the oxide surfaces formed from the original metal remained shiny. A sample of this oxide is shown in Figure 54. This piece of oxide is about one cm square and two mm thick. It is believed that the cracks in the oxide occurred during cooling.

Figure 54

URANIUM OXIDE PLATE PRODUCED BY URANIUM-STEAM REACTION AT 600 C

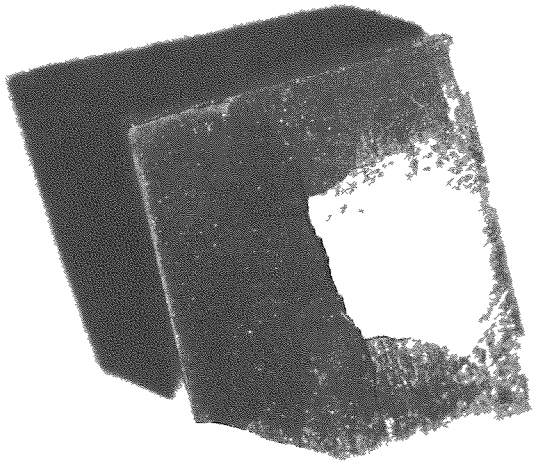

1 cm

The data at 500 C also gives a parabolic plot, although the slope is too high to fit the Arrhenius plot. It is believed that at this temperature there are some transitional effects, in which a linear rate law at 400 C is transformed into the parabolic rate law at temperatures above 600 C.

b. Studies at Low Temperatures

Two experiments were carried out at 400 C. The results of these experiments are shown in Figure 55. The uranium-steam reaction follows the linear rate law at this temperature with a slope of 2.85 ± 0.05 cc of H_2/(sq cm)(min), following an induction period of about 10 min. The difference between the two kinetic curves is due almost entirely to a difference in the length of this induction period.

Figure 55

HYDROGEN EVOLUTION IN THE URANIUM-STEAM REACTION AT 400 C

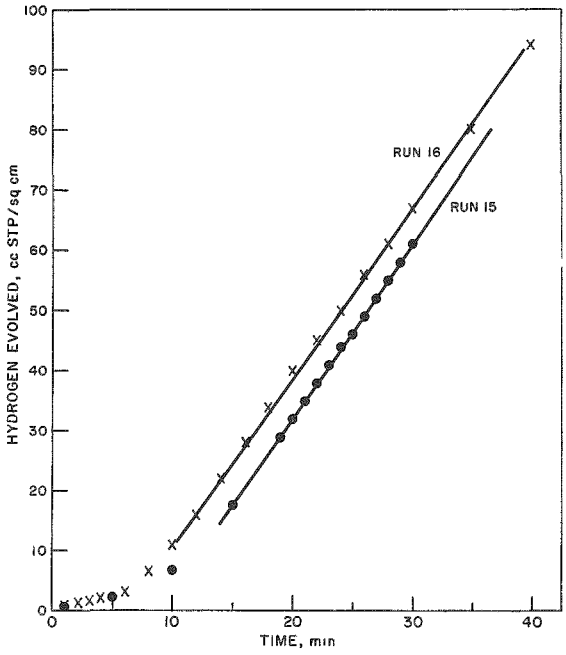

The oxide produced in these experiments was nearly colloidal in character and powdered off the sample continuously. It was evident that the oxide produced at 400 C afforded no protection to the underlying metal. The difference in appearance between the oxide formed at 400 C and that formed at 500 C and higher is very striking and correlates precisely with the differences in kinetic behavior.

c. Comparison with Results of Previous Investigators

Hopkinson[35] reported a linear reaction rate of 2.5 cc of H_2/(sq cm)(min) [reported as 1.8 mg/(sq cm)(min)] at 400 C, which is in good agreement with the value of 2.85 cc H_2/(sq cm)(min) reported above. Hopkinson reported the transition to a parabolic reaction to occur at 880 C in contrast with the 400 to 500 C found in this study. In addition, he reported that the parabolic reaction was followed by a linear reaction after some 120 min. No evidence of such a change was found in this study out to 400 min. The causes of these differences are not presently understood.

The results found for the uranium-steam reaction parallel those reported in previous quarterlies (see ANL-6413, page 160, and ANL-6543, page 168) for the uranium-oxygen reaction. The oxide produced in the reaction with oxygen also changed from a powdery, nonprotective form to a more compact, protective oxide at a temperature of 450 C. It is not likely that the change in the character of the uranium-steam reaction

[35] Hopkinson, B. E., J. Electrochem. Soc., 106, 102 (1959).

is due to hydriding or some other hydrogen reaction because of the very similar change occurring in the reaction with pure oxygen. It is likely that the oxides produced above and below 450 C consist of different phases. Hoekstra, Santoro, and Siegel,[36] in a study of the oxidation of UO_2, found only the compounds UO_2, U_4O_9, and U_3O_8 above 500 C. Below 500 C, a compound designated as $UO_{2.3}$ was identified.

2. Metal-Water Reaction Studies in TREAT*
(R. C. Liimatainen, R. O. Ivins, F. J. Testa, P. Krause)

The study of metal-water reactions initiated by a high-intensity neutron pulse is continuing. The technique consists of exposing fuel specimens immersed in water to a transient in the TREAT reactor. The objectives of this program are:

1) to determine the extent of reaction between the metal and water;

2) to determine the fuel temperature and pressure history during the excursion; and

3) to determine the physical damage that occurs as a result of the transient; this includes metallographic and particle size evaluations.

a. Experiments with Zirconium Plates

A series of three experiments were performed in TREAT. These provided data on the extent of reaction and the behavior during meltdown of an unclad, 89.4 weight percent zirconium, 10.6 weight percent uranium alloy fuel plate. The fuel was 93 percent enriched with uranium-235. The nominal dimensions of the plates were 1 in. x 0.5 in. x 0.1 in. Table 43 summarizes the results of this series of experiments.

In all of these experiments the plates melted during the transients and subsequently solidified in the bottom of the alumina crucible in which they were contained. The thermocouples evidently lost contact with each of the fuel plates during the transients, because the measured peak temperatures were considerably lower than the actual, maximum temperature of the fuel plate as indicated by later observation of melting of the fuel plates. Figure 56 shows a photograph of the melted plate and part of the broken crucible from the most energetic transient.

[36]Hoekstra, H. R., Santoro, A., and Siegel, S., J. Inorg. Nucl. Chem., 18, 166 (1961).

*The cooperation of J. Boland, F. Kirn, and H. Lawroski, of the Idaho Division, for the operation of the TREAT reactor is gratefully acknowledged.

Table 43

SUMMARY OF THE RESULTS OF METAL-WATER MELTDOWN EXPERIMENTS CONDUCTED IN TREAT ON ZIRCONIUM-URANIUM ALLOY FUEL PLATES, UNCLAD

Test Conditions: H_2O at 25 C under 20 psia He pressure

Fuel Plates: Unclad alloy (submerged in H_2O) of 89.4 w/o Zr and 10.6 w/o U, 93 percent enriched; total weight of plate = 5.5 g

	TREAT Transient		
Reactor Pulse	CEN 87	CEN 88	CEN 89
Integrated Power, Mw-sec[a]	251	372	458
Peak Power, Mw	1055	1140	1080
Period, ms	83	79	79
Results			
Measured temp, C	555	220	>1500
Estimated temp, C[b]	1840 (m.p. Zr)	2200	2860
Peak Pressure,[c] psia	90	150	195
Visual observations of fuel after irradiation	Solidified puddle of metal found in bottom of each crucible. Particles fused to autoclave cap in CEN-89.		
Extent of Metal-Water Reaction, Percent of total	5.2	9.5	11.5

[a] Analytical data not yet available to convert to calories per gram of sample.

[b] Based on observation of melting of Zr-U in CEN-87 and estimation in CEN-88 and 89 from increase in energy.

[c] Pressure traces were smooth with no "spikes," pulse, or unusual effects other than radiation effects.

Figure 56

MELTED ZIRCONIUM-URANIUM FUEL PLATE
AND BROKEN ALUMINA CRUCIBLE FROM
TREAT METAL-WATER EXPERIMENT CEN 89

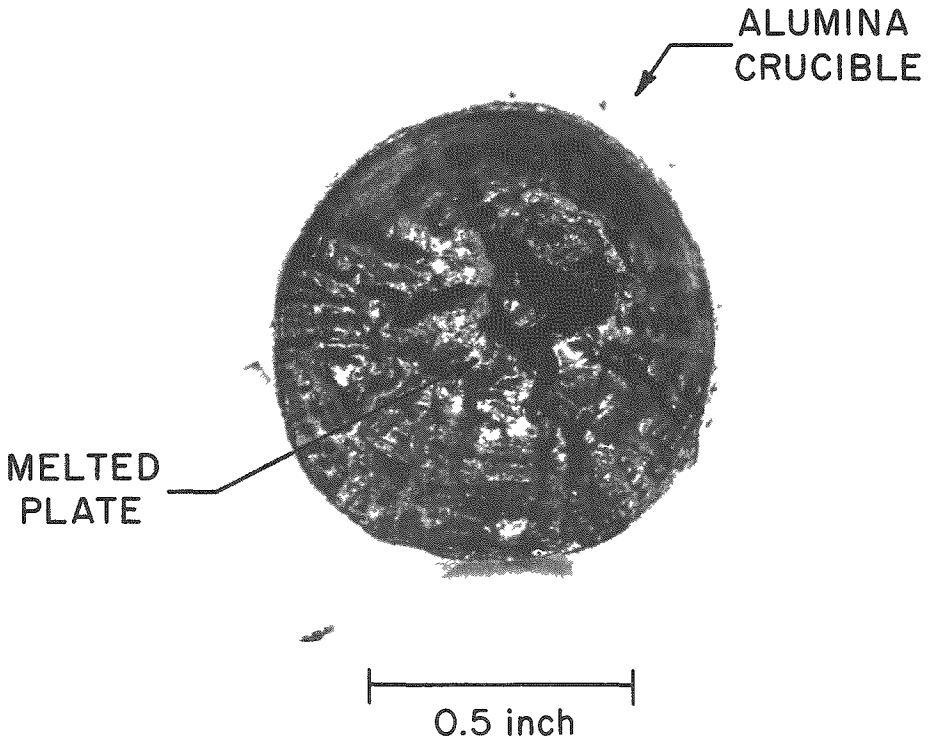

The crucibles in all three experiments were broken, and in Transient CEN-89 molten metal was splattered onto the inner surface of the autoclave where it had solidified and remained. The pressure traces in these experiments were smooth with deflections caused primarily by radiation effects on the transducers.

The results, shown in Table 43, indicate that the extent of metal-water reaction increased with increasing burst energy. This trend is consistent with previous results on other types of fuel elements. Further interpretation awaits analytical results to determine the number of fissions that occurred within the specimens and to compute the energy absorbed by the specimens.

V. ENERGY CONVERSION*

Two methods of converting nuclear energy into electricity are being examined. These methods are the regenerative cell and the thermoelectric effect.

A. Regenerative Emf Cell

(C. E. Crouthamel, M. Foster, C. E. Johnson, R. Heinrich, R. Eppley, S. F. Banaszek)

During this quarterly period the group has been moving into a new laboratory. The work of the group on thermally regenerative emf cell systems (see ANL-6543, page 195) will be resumed when the move is completed. The moving and installation of the following major units is now being carried out: (1) Fused salt-purification system, (2) system for hydrogen-diffusion studies through metals, (3) heating and cooling curve control and recording system associated with an inert atmosphere box-furnace combination, (4) special helium-purification system to recirculate and maintain box atmospheres. The latter unit is serving as an experimental model and, if successful, would be duplicated to serve as a helium-purification unit for a number of inert atmosphere boxes in the division. The objective of this unit is to maintain a box atmosphere of helium with less than 100 ppm by volume of impurities. For a box of 15 to 20 cu ft of volume in typical usage it is estimated that a flow of 2.5 to 5.0 cu ft/min of helium would be required through the purifier. The design and construction of an adequate unit has not been a straightforward problem and is causing delays in the progress of the experimental program.

B. Thermoelectricity Research

(R. K. Edwards, H. M. Feder)

Studies in thermoelectricity are underway to contribute to the technological development of direct conversion of heat energy from nuclear reactors into electrical power by means of the thermocouple effect.

Two limited materials areas are under study. These are liquid thermocouple systems and refractory solid thermocouple materials. The latter are considered to be of particular interest to reactor energy conversion.

1. Liquid Systems

(R. K. Edwards)

The thermoelectric properties of liquid systems are of importance since their study should contribute to the extension of solid state theory to the liquid state. Solid state investigations of the transport properties of

*A summary of this section is given on pages 12 and 13.

binary semiconductors are generally limited to very narrow composition ranges by virtue of narrow ranges of phase stability. Liquid binary systems offer a greater latitude for study of composition dependencies.

From a standpoint of the programmatic objective of efficient energy conversion, the liquid studies are directed toward obtaining systematic data which will lead to correlation and understanding of the factors pertinent to the controlled modification of electronic structures in metallic or semimetallic systems toward more favorable thermoelectric properties. A theoretical analysis by Klemens[37] has suggested that metallic materials might, through alteration of their electronic distributions, yield desirable performance possibilities.

During the past quarter, Seebeck coefficients in the liquid indium-bismuth system were measured for the mean temperature 450 C. The general procedure has been described in a previous quarterly report (see ANL-6477, page 215). Seebeck coefficients relative to platinum were obtained from the ratio of the thermoelectric emf to the difference between the hot and cold junction temperatures. The results are shown in Figure 57, where they are plotted as absolute values after correction for the known contribution of platinum. However, the emphasis of the work is on the systematic composition dependence rather than the absolute values. To this end, a rather large temperature difference (100 C) was maintained in order to increase the relative precision in the set of measurements. This tends to minimize the effect of stray electrical pickup, but it also leads to an "averaged Seebeck coefficient" rather than a true differential.

Figure 57

ABSOLUTE SEEBECK COEFFICIENT FOR THE LIQUID SYSTEM INDIUM-BISMUTH AT 450 C

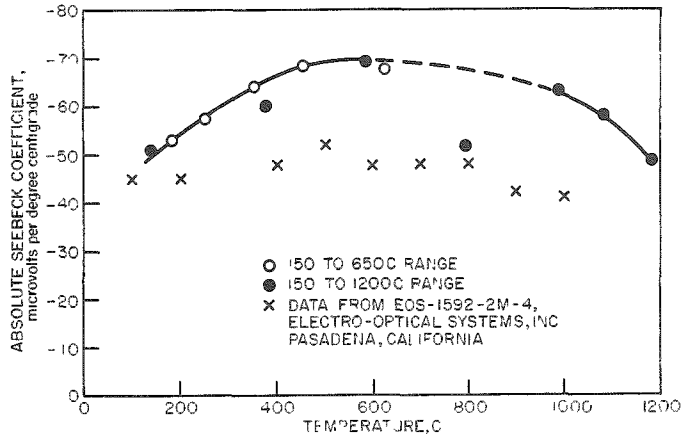

The marked tendency for the data of the indium-bismuth system to show regions of linear behavior is evident. It would be premature to attempt extensive generalizations until more systems have been studied. However, simple comparisons with the isoelectronic indium-antimony system (see ANL-6477, page 214) are interesting. Firstly, the minimum

[37]Klemens, P. G., Theoretical Requirements for Thermoelectric Materials, Westinghouse Research Report 929-8904-R2 (July 12, 1961).

in Figure 57 occurs at the same composition as the pronounced minimum in the indium-antimony system (approximately at In/Sb atom ratio 5/1). Both systems show regions for which the Seebeck coefficient depends linearly on the composition.

2. Refractory Solid Thermocouple Systems
(M. Tetenbaum, F. Mrazek)

For high-temperature use, a refractory broad-band semiconductor is required if thermoelectric properties are to be favorable over a large temperature interval. The lanthanide and actinide sulfide systems are highly refractory and have phases with electron concentrations at the semiconducting range. The uranium and thorium sulfide systems and their solid solutions have been selected for the initial studies.

Measurements of the Seebeck coefficient as a function of temperature have been made with a plate of uranium monosulfide fabricated from a sintered ingot. The material contained approximately 5 weight percent uranium oxysulfide. The lattice parameter of the monosulfide phase was found to be $a_0 = 5.487 \pm 0.005$ Å, which is in agreement with the values obtained by D. Cater (see ANL-6140).

The results of two series of measurements are shown in Figure 58. In the first series, Seebeck coefficients were obtained in the temperature range from 150 to 650 C; in the second series, measurements were made over the temperature range from 150 to 1200 C. The hot and cold junction temperature difference during these measurements was approximately 10 C.

For comparison, measurements obtained by Electro-Optical Systems, Inc.,[38] on a melted uranium monosulfide specimen of undefined composition are included in Figure 58. It should be pointed out that the room-temperature resistivity of their specimen was approximately five times higher than the value found by us.

Room-temperature Hall coefficient measurements[39] were also made with the sintered plate of uranium monosulfide. The results are summarized in Table 44. For comparison, we have included in Table 44 results previously obtained with an arc-melted uranium monosulfide specimen which had yielded a favorable figure-of-merit value. Also included in the table are recent Hall values measured at General Atomic for the promising refractory cerium sulfide system.

[38] Jordan, C. B., High Temperature Semiconducting Compounds for Thermoelectric Power Generation, Bimonthly Progress Report No. 4, June 15-August, 1962, EOS-1592-2M-4, Electro-Optical Systems, Incorporated, Pasadena, California.

[39] We are indebted to Dr. Manual Kanter of the Solid State Science Division for making these measurements possible.

Figure 58

VARIATION OF ABSOLUTE SEEBECK COEFFICIENT WITH TEMPERATURE FOR URANIUM MONOSULFIDE

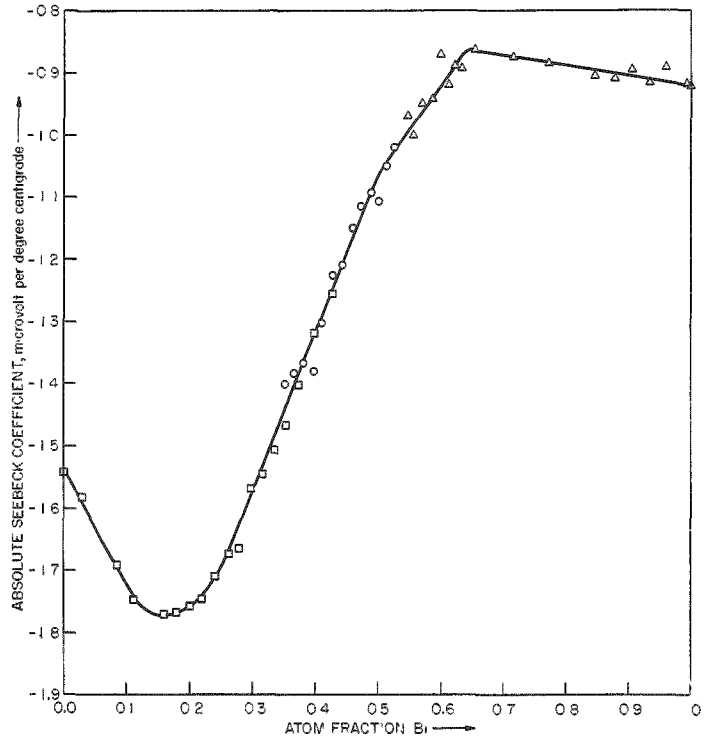

Table 44

ROOM-TEMPERATURE HALL MEASUREMENTS

	US sintered[a]	US arc melted[b]	$CeS_{1.33-1.50}$ melted[c]
Hall Coefficient (cc/coulomb)	6.2×10^{-3}	9×10^{-3}	1.3×10^{-3}
Resistivity (ohm-cm)	530×10^{-6}	200×10^{-6}	455×10^{-6}
Mobility (sq cm/volt-sec)	11.7	45	2.8
Carrier Density (electrons/cc)	1.0×10^{21}	0.7×10^{21}	5×10^{21}

[a] ~5 percent UOS

[b] ~16 percent UOS

[c] Data from General Atomic, division of General Dynamics Corporation, reported in Status Report on Thermoelectricity, NRL Memorandum Report 1241, January 1962, U.S. Naval Research Laboratory, Washington, D. C.

It is apparent from Table 44 that these systems appear to be characterized by high carrier concentrations and low mobilities. The Seebeck coefficients reported for the cerium sulfide system are considerably higher than the values obtained with uranium monosulfide.

VI. DETERMINATION OF NUCLEAR CONSTANTS*
(C. E. Crouthamel)

Knowledge of fast-neutron cross sections is necessary to the fast reactor program. Neutron cross sections are being studied by means of monoenergetic neutrons and by means of the spectra of fast breeder reactors. The monoenergetic-neutron work includes the measurement of capture and total cross sections as a function of neutron energy.

The capture cross sections of many of the rare earth elements are presently unknown in the energy region above 0.17 Mev. Several of these elements have been considered recently as possible materials for reactor control. A brief review of this work was given in ANL-6379, pages 224 to 228. In the present program, neutron-capture cross sections are being measured for several rare earth isotopes, and determination of the total cross section of some of these elements has begun. Determinations of the ratio of the capture-to-fission cross section, alpha, of uranium-233 in EBR-I, Mark III, are reported.

A. Monoenergetic Neutron Cross Sections
(D. C. Stupegia, E. H. Dewell)

1. Neutron Total Cross Section of Dysprosium

Measurements were recently made of the neutron total cross section of dysprosium as a function of neutron energy. The Van de Graaff accelerator and the neutron collimation and detection apparatus of the Physics Division were used in this work.

The neutron total cross section was determined by measuring the attenuation of a well-collimated neutron beam by the sample being studied. The neutron source was the $Li^7(p,n)Be^7$ reaction, and the neutron detector consisted of a large cylindrical tank in which BF_3 neutron counters were immersed in a neutron moderator. Measurements were made between neutron energies of 13 and 210 kev.

Preliminary results up to 97 kev are shown in Figure 59, and from 80 to 210 kev in Figure 60. The standard deviations of the cross sections relative to each other are about ± 1.5 percent. The neutron energy spreads at each point are about ±1.5 kev. Also, the absolute values of the neutron energies are correct within spreads of ± 2 kev. A report on this work is being prepared for publication.

*A summary of this section is given on page 13.

Figure 59

NEUTRON TOTAL CROSS-SECTION
OF DYSPROSIUM
(low range)

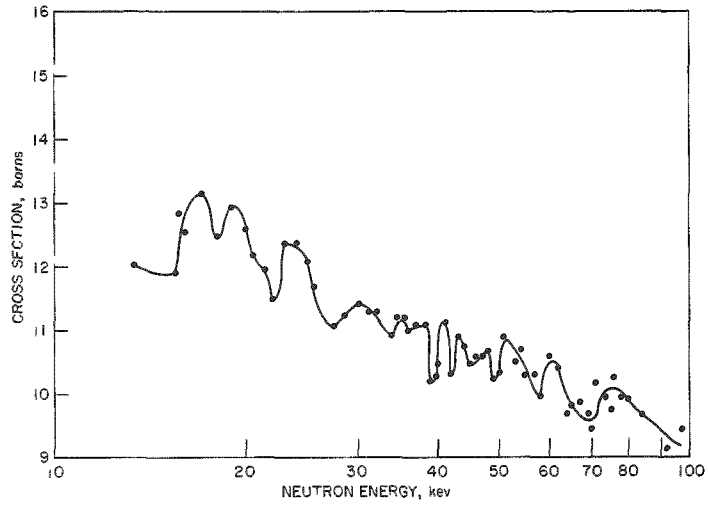

Figure 60

NEUTRON TOTAL CROSS-SECTION OF DYSPROSIUM
(high range)

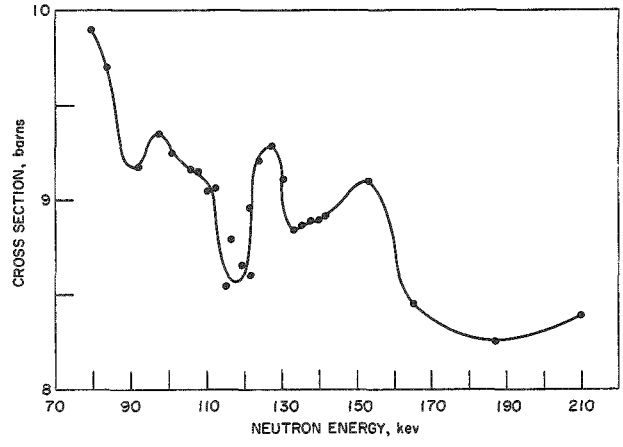

2. Neutron-energy Spreads

The neutrons produced by a Van de Graaff accelerator through the $Li^7(p,n)Be^7$ reaction are monoenergetic at a given angle to the proton beam provided that the lithium-7 target has negligible thickness and provided that the proton beam strikes at a point. In practice, neither of these conditions is met exactly; thus, there is always a spread in the neutron energies seen by any target. Moreover, in work on activation cross sections, it is necessary to keep the irradiated sample close to the neutron source in order to produce sufficient radioactivity for good counting data. This means that the sample may subtend a considerable angle at the neutron source and, since the neutron energy varies almost inversely with the square of the beam angle, this additional factor contributes to the total spread in neutron energies.

The neutron-energy spreads seen by a sample 1.0 cm in diameter placed 2.0 cm from the lithium-7 target have been calculated for proton energies between 2.1 and 3.0 Mev in 0.1-Mev intervals for the cases of lithium targets of proton stopping powers from 5 kev to 45 kev in 5-kev intervals and for a rectangular beam spot, 3.2 x 6.4 mm ($\frac{1}{8}$ in. x $\frac{1}{4}$ in.). The curves for 2.10- to 2.80-Mev protons striking a 4.5-kev target are reproduced as Figure 61. A compilation of all the spectra computed and details of the calculations is in preparation.

Figure 61

VARIATION OF NEUTRON INTENSITY WITH NEUTRON ENERGY FOR VARIOUS PROTON ENERGIES IN THE $Li^7(p,n)Be^7$ REACTION

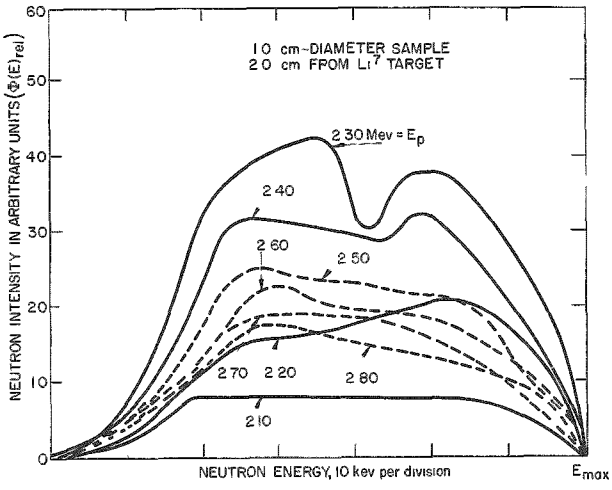

B. Capture and Fission in EBR-I, Mark III

(C. E. Crouthamel, R. R. Heinrich, and G. H. McCloud)

The possibility of a thorium-232-uranium-233 fast reactor breeder cycle has been considered as an alternate breeder cycle for many years. In 1957, the Chemical Engineering Division undertook the task of obtaining the needed data on uranium-233. The proposed experiment was the determination of the fission events by cesium-137 monitoring, which had been previously employed in experiments with uranium-235 and plutonium-239. The number of capture events was to be obtained by determining the uranium-233/uranium-234 mass ratio of the irradiated uranium. Calculations showed that, on an 800,000-kwh exposure in EBR-I, approximately 20 to 40 ppm of uranium-234 would be produced in the uranium-233. This made it necessary to obtain uranium-233 of higher isotopic purity than had hitherto been available. A joint effort was organized with ORNL to isolate protactinuim-233 from irradiated thorium-232. This work resulted in the isolation of about 10 g of uranium-233 of extremely high isotopic purity (uranium-232/uranium-233 = 4×10^{-6}, uranium-234/uranium-233 = $< 4 \times 10^{-6}$). This material was considered suitable for the planned experiment.

The applicability of the thorium-232-uranium-233 cycle is to a large extent dependent upon the ratio of the capture-to-fission cross section of the fertile fuel. If the breeding ratio is defined as the number of fissionable atoms formed per number of fissionable atoms destroyed, this ratio may be expressed in terms of reactor characteristics as follows:

$$R = \frac{\nu - 1 - \alpha - A - \Lambda + F(\nu' - 1)}{1 + \alpha}$$

where

ν = number of neutrons produced per fission in fissionable isotope (uranium-233, uranium-235, or plutonium-239).

ν' = number of neutrons produced per fission in fertile isotope (thorium-232, uranium-238).

α = ratio of capture cross section to fission cross section of fissionable isotope.

F = number* of fertile atoms fissioned.

A = number* of parasitic neutron-capture events.

Λ = number* of neutrons escaping from reactor system.

(*Numbers per fission of primary fissionable isotope.)

From the above equation, the importance of a low alpha value to achieve a high breeding ratio R is apparent. Moreover, the facts that alpha appears twice in the equation and that both times the larger value produces decrease of the breeding ratio make it one of the most important characteristics of the reactor. The value of F, the fissions of thorium-232 as fertile material, will be considerably less than that of uranium-238.

The important result obtained from the Mark III irradiation of uranium-233 was that the value of alpha in the core and inner blanket remained low. The core value of alpha was relatively constant at 0.055 and remained well below 0.1 throughout the inner blanket.

Figure 62 shows alpha as a function of distance from the EBR-I vertical axis along the mid-plane of the reactor. Figure 63 shows the variation along the vertical axis, with alpha being plotted against the distance from the horizontal mid-plane.

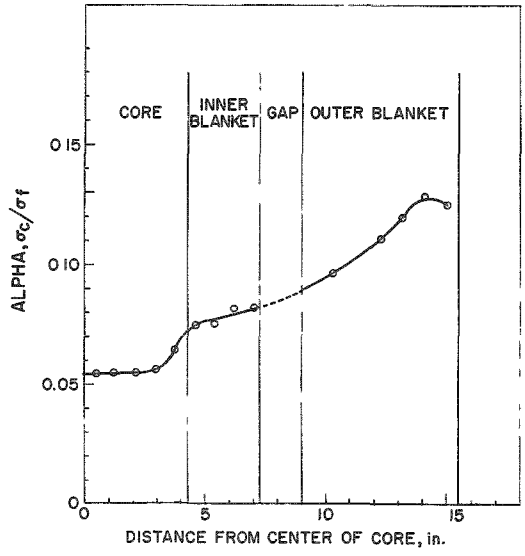

Figure 62

ALPHA FOR URANIUM-233
HORIZONTAL LOADING
IN EBR-I, MARK III

Figure 63

ALPHA FOR URANIUM-233 VERTICAL LOADING IN EBR-I, MARK III

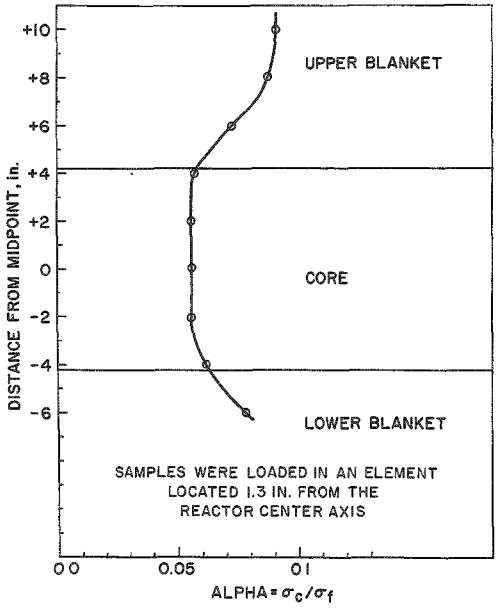

The individual values of the number of capture and fissions per million uranium-233 atoms are listed in Table 45 for the horizontal variation, and in Table 46 for the vertical variation. These values are plotted in Figures 64 and 65, respectively.

The number of captures in uranium-233 was measured by the mass spectrometric determination of uranium-234, and the number of fissions by the assay of the fission product cesium-137. In calculating the number of fissions, the half-life of cesium-137 was taken as 30.0 years, and its fission yield for the fast neutron spectrum as 6.51 percent.

Uranium-235 and plutonium-239 alpha values were previously obtained in experiments in EBR-I, Mark I, and were reported by Kafalas, Levenson, and Stevens.[40] In recent work by this Division, which will be reported in detail in the next quarterly, the core alpha value for uranium-235 was found to be lower than the value reported previously by Kafalas et al. (0.125 as compared with 0.144). Alpha values obtained in the blanket were in agreement with the values of Kafalas.

Table 45

HORIZONTAL VARIATION OF σ_c/σ_f OF URANIUM-233 IN EBR-I, MARK III. MID-PLANE

Pile Position of Sample	Distance from Reactor Axis (in.)	Fissions per 10^6 U^{233} atoms	Captures per 10^6 U^{233} atoms	Alpha (σ_c/σ_f)
core	0.5	1488	81.1 ± 3	0.0545
core	1.25	1422	79.0 ± 2	0.0556
core	2.15	1329	73.3 ± 3	0.0552
core	3.00	1189	66.6 ± 2	0.0560
core	3.80	1018	65.4 ± 3	0.0642
inner blanket	4.60	737.5	55.5 ± 3	0.0753
inner blanket	5.40	637.6	48.4 ± 1	0.0759
inner blanket	6.20	531.0	43.5 ± 3	0.0819
inner blanket	7.00	443.2	36.6 ± 2	0.0826
outer blanket	10.3	234.6	22.6 ± 2	0.0963
outer blanket	12.3	177.5	19.7 ± 3	0.111
outer blanket	13.15	168.3	20.2 ± 2	0.120
outer blanket	14.05	185.1	23.8 ± 1	0.129
outer blanket	15.00	368.5	45.9 ± 2	0.125

[40] Kafalas, P., Levenson, M., and Stevens, C. M., Nuclear Sci. and Eng., 2, 657 (1957).

Table 46

VERTICAL VARIATION OF σ_c/σ_f OF URANIUM-233 ALONG EBR-I, MARK III, AXIS

Pile Position of Sample	Vertical Distance from Mid-Plane (in.)	Fissions per 10^6 U^{233} atoms	Captures per 10^6 U^{233} atoms	Alpha
upper blanket	+9.82	287.9	25.9 ± 0.7	0.0900
upper blanket	+7.85	416.7	36.5 ± 0.8	0.0876
upper blanket	+5.90	652.7	47.3 ± 3	0.0725
core	+3.95	1091	61.7 ± 3	0.0566
core	+2.02	1354	73.6 ± 2	0.0546
core	+0.08	1422	79.0 ± 2	0.0556
core	-1.89	1293	72.2 ± 1	0.0558
core	-3.88	877	55.2 ± 2	0.0615
lower blanket	-5.88	533	41.7 ± 1	0.0782

Figure 64

URANIUM-233 HORIZONTAL LOADING-CAPTURE AND BURN-UP IN EBR-I, MARK III

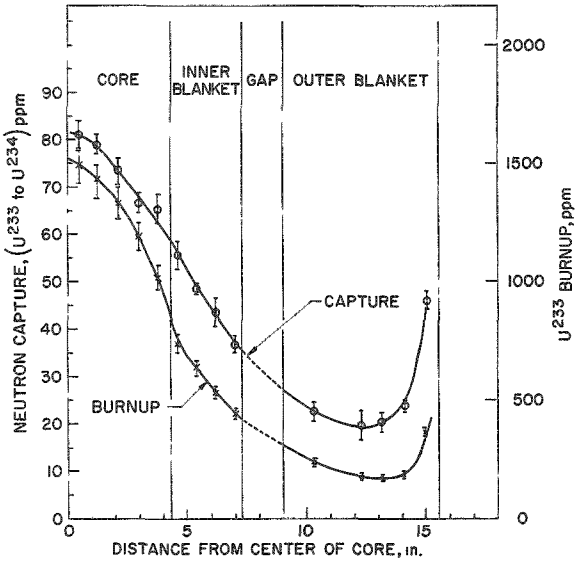

Figure 65

URANIUM-233 VERTICAL LOADING-CAPTURE AND BURNUP IN EBR-I, MARK III

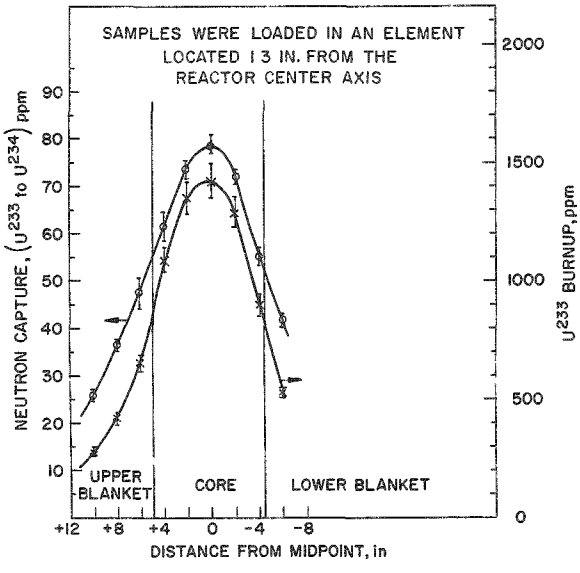

Work is nearing completion on other species irradiated in EBR-I, namely, uranium-238, plutonium-239, and plutonium-240. The study of the (n,2n) reactions in uranium-233 as a function of reactor position is also being completed and will be reported in the next quarter.

VII. ROUTINE OPERATIONS
(H. G. Swope)

A. Waste Processing
(H. G. Swope, J. Harast, K. Bremer, G. Teats and R. Juvinall)

Routine Operations

There were a total of 74,160 gallons of liquid radioactive wastes processed during April, May and June 1962. The volumes processed by the various methods are tabulated below:

Process	Gallons
Evaporation and Concentration	30,159
Filtration	21,520
Ion-Exchange (Cation, only)	21,520
Neutralization of HF Wastes	171
Absorption into Vermiculite	790
Total	74,160

B. High-level Gamma-irradiation Facility
(H. G. Swope, J. Harast, N. Ondracek, B. Kullen, V. Lemke and D. Bryant)

A summary of irradiations performed in Racks M-1 and M-2 for April through June 1962 is given in Table 47.

Table 47

SUMMARY OF IRRADIATIONS PERFORMED IN RACKS M-1 AND M-2 DURING APRIL THROUGH JUNE, 1962

	Rack M-1				Rack M-2		
Month	No. of Samples[a]	No. of Special Dosimetry Samples	Total Urn Units[b] Day	Total Urn Units[b] Night	No. of Urns	No. of Special Dosimetry Urns	Total Urn Units[c]
April	168	8	691	2207	1	4	4
May	62	52	504	1805	1	4	4
June	111	22	693	2423	2	2	11
	341	82	1888	6435	4	10	19

[a] Equivalent to a No. 2 sized can.
[b] 1 urn unit in Rack M-1 = 2×10^6 rad.
[c] 1 urn unit in Rack M-2 = 2×10^5 rad.